Associated Production of Higgs Bosons and Heavy Quarks in Two Photon Collisions at Next-To-Leading Order

Dissertation
zur Erlangung des Doktorgrades
des Departments Physik
der Universität Hamburg

vorgelegt von
Frank Fugel
aus Barßel

Hamburg
2007

Abstract

We consider the process $\gamma\gamma \rightarrow t\bar{t}H$ which can be studied at a future linear e^+e^--collider operated in the two-photon mode. We compute the QCD correction in order to increase the accuracy for the prediction of its cross section.

The associated production of Higgs bosons and heavy quarks in two-photon collisions allows for a further and direct measurement of the respective Yukawa coupling. The precise determination of the Higgs properties is necessary in order to establish the Higgs mechanism of electroweak symmetry breaking.

We evaluate the occurring tensor integrals by means of a recently proposed reduction method. In case of exceptional phase space points, alternative recursion relations are used. These involve expansions in those parameters which become small and would spoil the numerical evaluation. In order to arrive at infrared-finite expressions, which can be numerically integrated over the respective phase space in four dimensions, we apply a subtraction method. The results for the subprocess $\gamma\gamma \rightarrow t\bar{t}H$ are integrated over the spectra of the incoming photons in order to obtain a prediction for the parent process $e^+e^- \rightarrow \gamma\gamma \rightarrow t\bar{t}H$, which can be studied at a linear e^+e^--collider.

The correction for the subprocess as well as for the parent process amounts to about 10% for high energies of the colliding particles. Near threshold, it can reach several tenths of percent. We assess the scheme and scale dependences to be reduced by one order of magnitude. To this end, we convert the on-shell results to those valid in a mixed scheme.

The calculation of the virtual correction suggests that the recursion relations for exceptional phase space points, in particular when the determinant of the kinematical matrix becomes small, are numerically unstable. In those cases, we may set the integrand equal to zero without affecting the desired numerical precision.

It turns out that our results for the QCD correction deviate from those already given in the literature. A further independent calculation is therefore highly desirable.

Zusammenfassung

Wir betrachten den Prozess $\gamma\gamma \to t\bar{t}H$, der an einem zukünftigen linearen e^+e^--Beschleuniger im Zwei-Photon-Modus untersucht werden kann. Wir berechnen die QCD-Korrektur, um die Genauigkeit der Vorhersage für seinen Wirkungsquerschnitt zu erhöhen.

Die assoziierte Produktion von Higgs-Bosonen und schweren Quarks in Zwei-Photon-Stößen erlaubt eine weitere und direkte Messung der entsprechenden Yukawa-Kopplung. Die genaue Bestimmung der Higgs-Eigenschaften ist notwendig zur Etablierung des Higgs-Mechanismus der elektroschwachen Symmetriebrechung.

Zur Auswertung der auftretenden Tensorintegrale verwenden wir eine kürzlich vorgeschlagene Reduktionsmethode. Im Fall von exzeptionellen Impulskonfigurationen werden alternative Rekursionsrelationen benutzt. Hier wird in denjenigen Parametern entwickelt, die klein werden und so die numerische Auswertung instabil machen würden. Um infrarot-endliche Ausdrücke zu erhalten, die numerisch in vier Dimensionen über den jeweiligen Phasenraum integriert werden können, verwenden wir eine Subtraktionsmethode. Die Ergebnisse für den Subprozess $\gamma\gamma \to t\bar{t}H$ werden über die Spektren der einlaufenden Photonen integriert, um eine Vorhersage für den Elternprozess $e^+e^- \to \gamma\gamma \to t\bar{t}H$ zu erhalten, welcher an einem linearen e^+e^--Beschleuniger untersucht werden kann.

Die Korrektur beträgt sowohl für den Subprozess als auch für den Elternprozess ungefähr 10% bei hohen Energien der kollidierenden Teilchen. Nahe an der Schwelle kann sie mehrere zehn Prozent erreichen. Wir schätzen ab, dass die Schemen- und Skalenabhängigkeiten um eine Größenordnung reduziert werden. Hierzu rechnen wir die On-shell-Ergebnisse in solche um, die in einem Misch-Schema gültig sind.

Die Berechnung der virtuellen Korrektur legt nahe, dass die Rekursionsrelationen für exzeptionelle Phasenraumpunkte, insbesondere wenn die Determinante der kinematischen Matrix klein wird, numerisch instabil sind. In solchen Fällen können wir den Integranden gleich Null setzen, ohne dabei die gewünschte numerische Genauigkeit zu verlieren.

Es zeigt sich, dass unsere Ergebnisse für die QCD-Korrektur von denen abweichen, die bereits in der Literatur angegeben sind. Eine weitere unabhängige Rechnung wäre daher sehr wünschenswert.

Contents

Chapter 1

Introduction

The standard model (SM) describes the fundamental interactions between the elementary particles. It has been impressively confirmed by many experiments. Among the particles contained in the SM, there is only one remaining undiscovered. This is the Higgs boson (H), whose mass M_H is a free parameter of the theory.

In order to generate masses for the fermions and gauge bosons without violating the gauge symmetry of the theory, it is spontaneously broken by means of the so-called Higgs mechanism. A complex doublet scalar field is introduced which has a non-vanishing vacuum expectation value. Through electroweak symmetry breaking, three massless Goldstone bosons arise which become the longitudinal degrees of freedom of the massive $W^\pm$ and Z bosons. The fourth degree of freedom is the Higgs boson which remains in the physical spectrum.

The Higgs boson has already been directly searched for at the CERN Large Electron-Positron Collider LEP 2. This led to a lower bound for its mass of $M_H > 114.4$ GeV at 95% confidence level (CL) [1]. But it is also possible to search for indirect effects through quantum corrections involving the Higgs boson. High-precision measurements, especially at LEP and the SLAC Linear Collider SLC, yielded to the value $M_H = \left(76^{+33}_{-24}\right)$ GeV at 68% CL together with an upper limit of $M_H < 144$ GeV at 95% CL [2].

On the other hand, theoretical considerations can also restrict the possible values for the Higgs-boson mass. The vacuum-stability and triviality bounds suggest that it lies between 130 and 180 GeV if the SM is valid up to the grand-unification scale (see, for example, Refs. [3, 4]).

These measurements and considerations clearly show that the SM-Higgs

boson, if existent, should be found at the CERN Large Hadron Collider (LHC), where Higgs bosons with masses up to 1 TeV will be searched for. The LHC will also be able to perform first measurements of SM-Higgs properties. However, a detailed study of the Higgs sector is left to a future linear collider like the International Linear Collider (ILC) [5].

Such a linear e^+e^--collider can also be used to study processes where one or both of the incoming particles are photons (see Ref. [6] and References therein). Laser back-scattering of electron and positron beams produces highly energetic photons in large numbers. The cross section for the considered subprocess is integrated over the photon spectra of the colliding photons in order to get a prediction for the parent process $e^+e^- \to \gamma\gamma \to X$.

In this work, we consider the production of SM-Higgs bosons in association with a top (t) and an anti-top quark $(\bar{t})$, $\gamma\gamma \to t\bar{t}H$. This process allows for a further and direct measurement of the $Ht\bar{t}$ Yukawa coupling. It is therefore important to have an accurate prediction for the cross section of this process. The Yukawa couplings can be significantly different in other models compared to the SM. The measurement of the $Ht\bar{t}$ Yukawa coupling thus also provides a means for discriminating different models [7]. Moreover, it can be used in the determination of the CP properties of the Higgs boson. A recent review on the SM-Higgs boson is given in Ref. [4]. The measurement of the $Ht\bar{t}$ Yukawa coupling through the process $e^+e^- \to t\bar{t}H$ was studied in Refs. [8].

Only for Higgs-boson masses larger than twice the top-quark mass, the $Ht\bar{t}$ Yukawa coupling could be measured in the decay of the Higgs boson into a $t\bar{t}$-pair. For masses favoured experimentally and theoretically, the associated production of Higgs bosons is the only direct way of probing the Yukawa coupling at the LHC as well as at a linear collider like the ILC [7].

Let us now summarise the present status of known results for the associated production of Higgs bosons, including the case of e^+e^--collisions. For completeness, we also list the References for the production of the charged and neutral Higgs bosons of the minimal supersymmetric extension of the SM (MSSM). The leading-order results for the production of Higgs bosons in association with heavy quarks, namely top and bottom quarks, are all known. For $\gamma\gamma$-collisions, the results are specified in Refs. [9], [10], and [11] for the production of SM-, neutral MSSM-, and charged MSSM-Higgs bosons, respectively. In the case of e^+e^--collisions, they are given in Refs. [12]. In Ref. [13], the QCD and electroweak corrections at next-to-leading order (NLO) have been calculated for the SM-Higgs case in $\gamma\gamma$-collisions. For e^+e^--

collisions, the NLO QCD results are all known. Refs. [14] contain the results for the SM-Higgs boson, while Refs. [15] consider the neutral MSSM-Higgs bosons. Within the MSSM, additional QCD corrections arise, which are not due to the exchange or radiation of gluons. These have been evaluated for the neutral Higgs bosons in Refs. [16]. The full QCD results at NLO for the charged Higgs bosons are given in Ref. [17]. Furthermore, the electroweak corrections are known for the associated production of SM-Higgs bosons in e^+e^--collisions. They can be found in Refs. [18]. A recent review on the MSSM-Higgs bosons is given in Ref. [19].

Here, we consider the NLO QCD correction to the process $\gamma\gamma \to t\bar{t}H$. It is due to the exchange of virtual and the radiation of real gluons. While a result for this correction already exists in the literature, an independent calculation is still lacking. However, a confirmation of the result is indispensable for such a complex calculation. Furthermore, this computation is the first step towards a calculation of the missing NLO corrections for the associated production of MSSM-Higgs bosons and heavy quarks in two-photon collisions. Moreover, polarisation effects could be taken into account and the background to this process could be studied in future extensions of this work.

The inclusion of the QCD correction should reduce the theoretical error of the prediction for the cross section. In particular, the scheme and scale dependences are expected to decrease significantly. In order to reduce the occurring tensor integrals, we apply the method recently developed in Refs. [20]. The application of the method in this non-trivial case, which includes massive propagators, allows for a further assessment of its usefulness in realistic NLO computations. Therefore, the present calculation is also of conceptual importance.

This work is organised as follows. We first outline the general setup, introduce the notation, and explain the basic calculational methods. This is done in Chapter 2. The actual calculations are shown in Chapter 3. We discuss the general approach and address the evaluation of the basis integrals. Furthermore, we perform the cancellation of the ultraviolet (UV) as well as of the infrared (IR) divergences. Also diverse calculational details are specified. We conclude this Chapter by discussing the various checks that have been considered. Chapter 4 contains the numerical results of our computation. It also addresses the issue of scheme and scale dependences. Finally, a comparison is drawn with the results specified in the literature. We conclude with a summary in Chapter 5.

Chapter 2

Calculational Methods

In order to calculate the QCD correction to the process $e^+e^- \to \gamma\gamma \to t\bar{t}H$, we have to reduce the occurring tensor integrals to a basis set of known integrals. The method used here is explained in Section 2.2. The virtual correction as well as the real one develop IR singularities which only cancel in the sum of both contributions to the cross section. We apply a subtraction method in order to deal with these singularities, which is described in Section 2.3. Since we consider the process $\gamma\gamma \to t\bar{t}H$, where the two photons are produced via laser back-scattering, we have to integrate its cross section over the spectra of the incoming photons. The respective photon spectrum is discussed in Section 2.4. Before the general methods are outlined, we shall set the notation and discuss the framework of our calculations. This is done in Section 2.1.

2.1 General Setup

The Born level diagrams of the subprocess $\gamma\gamma \to t\bar{t}H$ are depicted in Fig. 2.1. In the six diagrams, the two photons couple to a top quark off which the Higgs boson is radiated. The momenta of the external particles are defined as follows:

$$\gamma(p_1) \ \ \gamma(p_2) \ \to \ t(p_3) \ \ \bar{t}(p_4) \ \ H(p_5)\,. \tag{2.1}$$

Here, the momenta of the two photons are considered incoming while the others are outgoing. Momentum conservation yields the following relation between the five momenta:

$$p_1 + p_2 - p_3 - p_4 - p_5 = 0\,. \tag{2.2}$$
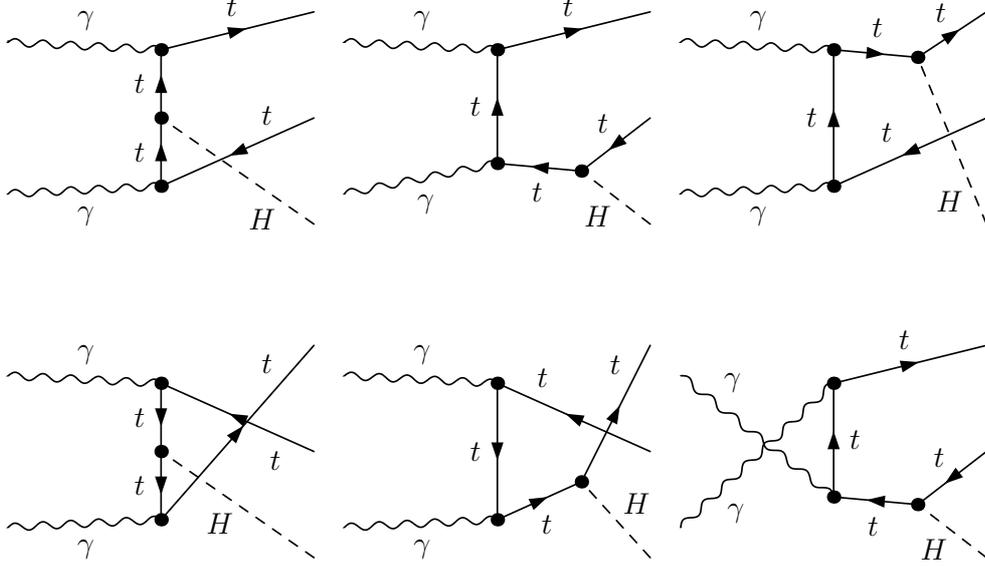
Figure 2.1: Born level diagrams for the subprocess.

The on-shell conditions read:

$$p_1^2 = 0\,, \; p_2^2 = 0\,, \; p_3^2 = m_t^2\,, \; p_4^2 = m_t^2\,, \; p_5^2 = M_H^2\,, \tag{2.3}$$

where m_t and M_H are the masses of the top quark and of the Higgs boson, respectively. Furthermore, we define the kinematical invariants

$$s_{ij} = (p_i + p_j)^2 \; \text{ with } \; i, j \, \epsilon \, \{1, \dots, 4\}\,. \tag{2.4}$$

Exploiting momentum conservation and the on-shell conditions, we get the following relation between the kinematical invariants:

$$s_{13} + s_{14} + s_{23} + s_{24} - s_{12} - s_{34} - 4m_t^2 + M_H^2 = 0\,. \tag{2.5}$$

We call the polarisation vectors of the incoming photons $\epsilon_1(p_1)$ and $\epsilon_2(p_2)$. These are transverse:

$$\epsilon_1(p_1) \cdot p_1 = 0 \; \text{ and } \; \epsilon_2(p_2) \cdot p_2 = 0\,. \tag{2.6}$$

The spinors of the outgoing top and anti-top quarks are denoted as $\bar{u}(p_3)$ and $v(p_4)$, respectively. They obey the Dirac equations

$$\bar{u}(p_3) \cdot \slashed{p}_3 = \bar{u}(p_3) \cdot m_t \; \text{ and } \; \slashed{p}_4 \cdot v(p_4) = -m_t \cdot v(p_4)\,. \tag{2.7}$$

The amplitude of the process has the general form

$$\mathcal{M} = \sum_{i=1}^{16} C_i \, \bar{u}(p_3) \, \Gamma_i \, v(p_4) \,, \tag{2.8}$$

where the Γ_i are 16 independent structures in Dirac space and the C_i their coefficients. We choose the Γ_i as

$$\begin{aligned}
&\Gamma_1 = \mathbf{1}\,, \ \Gamma_2 = \not{p}_1\,, \ \Gamma_3 = \not{p}_2\,, \ \Gamma_4 = \not{p}_1\not{p}_2 - \not{p}_2\not{p}_1\,, \\
&\Gamma_5 = \not{\epsilon}_1\,, \ \Gamma_6 = \not{\epsilon}_1\not{p}_1\,, \ \Gamma_7 = \not{\epsilon}_1\not{p}_2\,, \ \Gamma_8 = \not{\epsilon}_1\not{p}_1\not{p}_2\,, \\
&\Gamma_9 = \not{\epsilon}_2\,, \ \Gamma_{10} = \not{\epsilon}_2\not{p}_2\,, \ \Gamma_{11} = \not{\epsilon}_2\not{p}_1\,, \ \Gamma_{12} = \not{\epsilon}_2\not{p}_2\not{p}_1\,, \\
&\Gamma_{13} = \not{\epsilon}_1\not{\epsilon}_2 - \not{\epsilon}_2\not{\epsilon}_1\,, \ \Gamma_{14} = \not{\epsilon}_2\not{\epsilon}_1\not{p}_1\,, \ \Gamma_{15} = \not{\epsilon}_1\not{\epsilon}_2\not{p}_2\,, \\
&\Gamma_{16} = \not{\epsilon}_1\not{p}_1\not{\epsilon}_2\not{p}_2 + \not{\epsilon}_2\not{p}_2\not{\epsilon}_1\not{p}_1\,.
\end{aligned} \tag{2.9}$$

The momenta p_5 as well as p_3 and p_4 do not show up in these Dirac structures since they can be eliminated by the use of momentum conservation and the Dirac equations, respectively. The coefficients C_i must be of the form

$$\begin{aligned}
C_1 &= U^{(1)}\epsilon_1 \cdot \epsilon_2 + \sum_{j_1,j_2=1}^{4} U^{(1)}_{j_1 j_2} \, p_{j_1} \cdot \epsilon_1 \, p_{j_2} \cdot \epsilon_2\,, \\
C_2 &= U^{(2)}\epsilon_1 \cdot \epsilon_2 + \sum_{j_1,j_2=1}^{4} U^{(2)}_{j_1 j_2} \, p_{j_1} \cdot \epsilon_1 \, p_{j_2} \cdot \epsilon_2\,, \\
C_3 &= U^{(3)}\epsilon_1 \cdot \epsilon_2 + \sum_{j_1,j_2=1}^{4} U^{(3)}_{j_1 j_2} \, p_{j_1} \cdot \epsilon_1 \, p_{j_2} \cdot \epsilon_2\,, \\
C_4 &= U^{(4)}\epsilon_1 \cdot \epsilon_2 + \sum_{j_1,j_2=1}^{4} U^{(4)}_{j_1 j_2} \, p_{j_1} \cdot \epsilon_1 \, p_{j_2} \cdot \epsilon_2\,, \\
C_5 &= \sum_{j=1}^{4} X^{(1)}_j \, p_j \cdot \epsilon_2\,, \\
C_6 &= \sum_{j=1}^{4} X^{(2)}_j \, p_j \cdot \epsilon_2\,, \\
C_7 &= \sum_{j=1}^{4} X^{(3)}_j \, p_j \cdot \epsilon_2\,, \\
C_8 &= \sum_{j=1}^{4} X^{(4)}_j \, p_j \cdot \epsilon_2\,,
\end{aligned}$$

$$
\begin{aligned}
C_9 &= \sum_{j=1}^{4} Y_j^{(1)} \, p_j \cdot \epsilon_1 \,, \\
C_{10} &= \sum_{j=1}^{4} Y_j^{(2)} \, p_j \cdot \epsilon_1 \,, \\
C_{11} &= \sum_{j=1}^{4} Y_j^{(3)} \, p_j \cdot \epsilon_1 \,, \\
C_{12} &= \sum_{j=1}^{4} Y_j^{(4)} \, p_j \cdot \epsilon_1 \,, \\
C_{13} &= Z^{(1)} \,, \\
C_{14} &= Z^{(2)} \,, \\
C_{15} &= Z^{(3)} \,, \\
C_{16} &= Z^{(4)} \,.
\end{aligned}
\tag{2.10}
$$

Again, the momentum p_5 has been eliminated by means of momentum conservation. Note that some of the terms in above sums are equal to zero upon Eqs. (2.6). We are therefore left with 68 different structures. The $U^{(i)}$, $U_{j_1 j_2}^{(i)}$, $X_j^{(i)}$, $Y_j^{(i)}$, and $Z^{(i)}$ are the corresponding coefficients which are, however, not all independent. This leads to different checks on the calculations, as explained in Section 3.5. The coefficients depend on the s_{ij} and on the masses of the external particles. Due to Eq. (2.5) and the on-shell conditions of Eqs. (2.3), only m_t, M_H, and five additional kinematical invariants s_{ij} are independent.

Let us now expand the amplitude in the QCD coupling α_s:

$$
\mathcal{M} = \mathcal{M}_0 + \alpha_s \, \mathcal{M}_1 + \dots \,,
\tag{2.11}
$$

where $\mathcal{M}_0$ and $\mathcal{M}_1$ denote the amplitude at tree level and at NLO QCD, respectively, and the ellipsis represents the residual NLO contributions as well as all contributions beyond NLO. In order to obtain the cross section for the subprocess, we have to integrate the squared amplitude over the respective phase space. The squared amplitude reads, using Eq. (2.11) and truncating the perturbation series after the linear term in α_s:

$$
|\mathcal{M}|^2 = |\mathcal{M}_0|^2 + 2\alpha_s \Re \left(\mathcal{M}_1 \cdot \mathcal{M}_0^* \right) \,.
\tag{2.12}
$$

We consider unpolarised particles in the external state. Therefore, we have to average over the polarisations of the incoming photons and sum over the

spins of the outgoing top and anti-top quarks. Also the colour states of the quarks have to be summed over which leads to an overall factor of $N_C = 3$, the number of colours, for the Born level diagrams.

At NLO QCD, we have to calculate the one-loop diagrams where a virtual gluon (g) is exchanged. Additional contributions arise from the radiation of a real gluon off the top-quark line. If the energy of this gluon is sufficiently small, it cannot be resolved by the detector due to its finite resolution. In this case, the original process and the real radiation process are degenerate and cannot be distinguished. Therefore, we have to take the latter into account. In fact, the virtual correction and the real correction both develop IR divergences which only cancel in the sum of these contributions (see Section 3.3 and below).

The one-loop diagrams contain tensor integrals with up to five external legs. In detail, we encounter 12 diagrams with self-energy corrections, 18 with vertex corrections, 12 box diagrams, and 6 pentagon diagrams. Sample diagrams of each type are depicted in Figs. 2.2, 2.3, 2.4, and 2.5, respectively. Note, that we have not counted those diagrams where the loop does not involve a gluon line. If only quark lines are present in the loop, one gluon is always attached to it. Due to colour conservation, all these contributions are identically zero. In Fig. 2.6, we exemplarily show some of the 24 real correction diagrams. The application of the colour algebra to the diagrams enumerated above always leads to a colour factor of $N_C C_F = 4$, $C_F = 4/3$ being the casimir operator of the fundamental representation of the $SU(3)$ Gauge group.
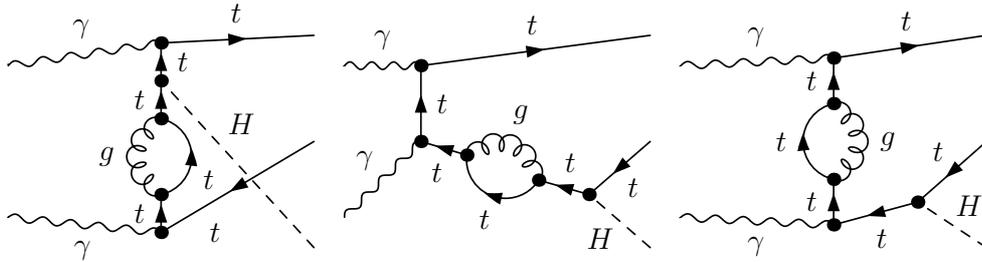
Figure 2.2: Sample diagrams for the subprocess at NLO QCD; self-energy corrections.
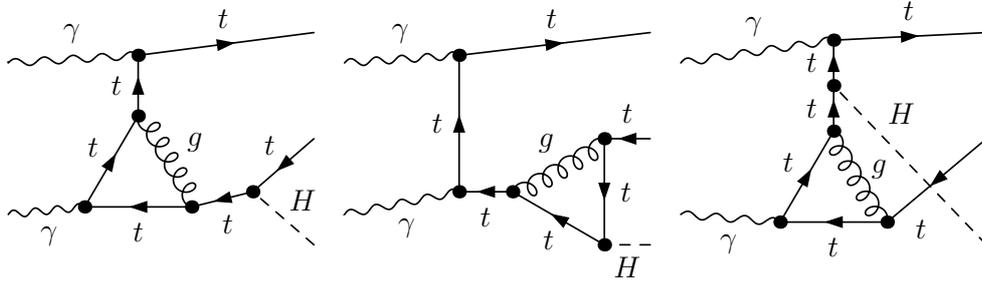
Figure 2.3: Sample diagrams for the subprocess at NLO QCD; vertex corrections.
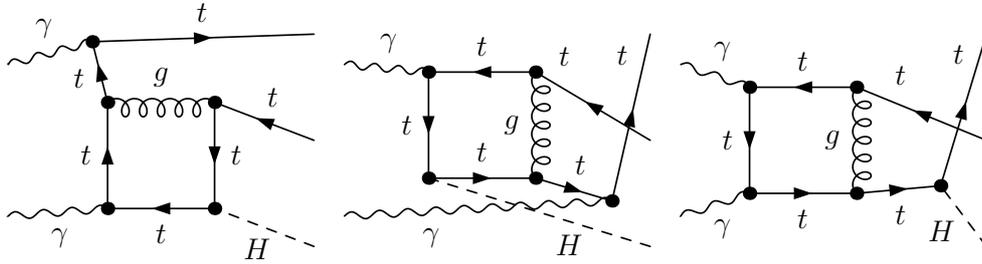
Figure 2.4: Sample diagrams for the subprocess at NLO QCD; box diagrams.
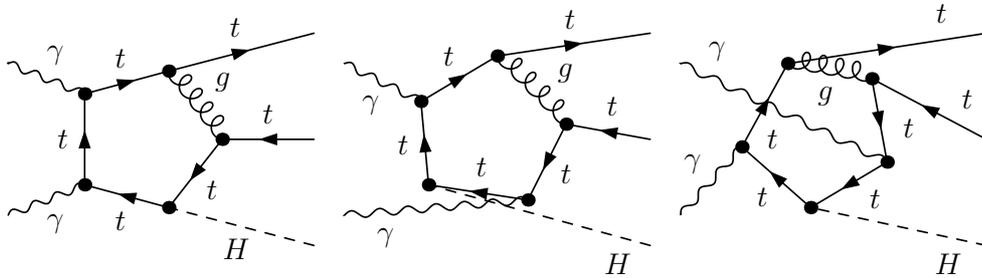
Figure 2.5: Sample diagrams for the subprocess at NLO QCD; pentagon diagrams.

In the case of the real correction diagrams, a gluon appears as a further particle in the final state. We denote its momentum as p_6 and its polarisation
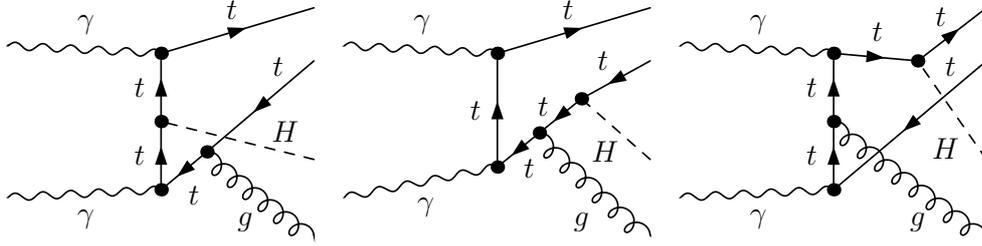
Figure 2.6: Sample diagrams for the real correction to the subprocess at NLO QCD.

vector as $\epsilon_6(p_6)$. They obey:

$$\epsilon_6(p_6) \cdot p_6 = 0 \;\; \text{and} \;\; p_6^2 = 0 \,. \tag{2.13}$$

Momentum conservation for this $2 \to 4$ process reads:

$$p_1 + p_2 - p_3 - p_4 - p_5 - p_6 = 0 \,. \tag{2.14}$$

If we now augment the set of kinematical invariants given in Eq. (2.4) by those involving the momentum p_5 of the external Higgs boson, we can write down the following relation between them:

$$s_{12} - s_{13} - s_{14} - s_{15} - s_{23} - s_{24} - s_{25} + s_{34} + s_{35} + s_{45} + 2m_t^2 + M_H^2 = 0 \,. \tag{2.15}$$

In the case of the real correction, however, we will not make use of a general form for the amplitude like the one of Eqs. (2.8, 2.9, 2.10).

The loop integrals may develop UV divergences when the loop momentum approaches $\pm\infty$. These divergences are removed through renormalisation of the mass and the wavefunctions of the top and anti-top quarks in the diagrams of Fig. 2.1. Also IR divergences can appear in the loop integration. We distinguish the two cases of collinear and soft IR divergences. The collinear divergences show up when an external line with a light-like momentum is attached to two massless propagators. In this case, a singularity is developed when the propagator momenta are collinear to the external momentum. Inspection of our one-loop diagrams reveals that they do not develop collinear divergences. However, they do produce soft IR divergences. These show up when a massless particle is exchanged between two on-shell particles. Here, the singularity appears for integration momenta where the propagator

momentum of the massless particle approaches zero. Examples for such a
configuration are given by the diagrams of Fig. 2.5. Inspection now reveals
that all diagrams involving pentagon integrals develop soft IR divergences
while none of the other diagrams do so. For a detailed treatment of the IR-
singularity structure of one-loop integrals see, for example, Ref. [21]. On the
other hand, also the phase space integration of the real correction diagrams
may produce such divergences. Here, collinear singularities appear when a
massless external particle splits into two massless particles. The divergence
arises in the region of phase space where the two particles become collinear.
Again, in the process under consideration, this is not the case. Soft singu-
larities show up if a massless particle is radiated off an external line. In the
region of phase space where the momentum of the massless particle tends to
zero, the singularity is developed. This is the case, for example, in the first
diagram of Fig. 2.6. Since we only encounter soft IR divergences, we do not
have overlapping IR singularities. Note that also the wavefunction renormal-
isation contributes IR-divergent terms. This is discussed in Section 3.3. The
soft IR divergences are shown to cancel in the sum of the three contributions
in the same Section.

   In order to perform the loop and phase space integrations, we first have
to regularise the integrals. We choose dimensional regularisation, with di-
mension $d = (4 - 2\epsilon)$, for both the UV as well as the IR divergences. Let
us conclude this Section by setting the notation for a generalised N-point
tensor integral of rank m:

$$I_N^{\mu_1\mu_2\cdots\mu_m}(D; \{q_i\}, \{\nu_i\}) = \int \frac{d^D\ell}{i\pi^{D/2}} \frac{\ell^{\mu_1}\ell^{\mu_2}\cdots\ell^{\mu_m}}{d_1^{\nu_1}d_2^{\nu_2}\cdots d_N^{\nu_N}}, \qquad (2.16)$$

with the propagators defined as

$$d_i = (\ell + q_i)^2 - M_i^2 + i0. \qquad (2.17)$$

The μ_j, $j \,\epsilon\, \{1, 2, ..., m\}$, are Lorentz indices, ℓ is the loop momentum, and
$\ell + q_i$ are the momenta of the diverse propagators with masses M_i, with
$i \,\epsilon\, \{1, 2, ..., N\}$. The integral is generalised with regard to the common N-
point functions in respect that the propagators are raised to the integer
powers ν_i and the dimension is given as $D = (n - 2\epsilon)$, n also being an
integer. $i0$ is the common infinitesimal imaginary part. The sum of the
powers of the propagators, ν_i, is denoted as σ.

2.2 Tensor Reduction

We have to compute tensor integrals in order to evaluate the one-loop diagrams. In our case, they can have up to five external legs (see Fig. 2.5) with a maximal rank of $m = 4$. The rank is, however, further reduced to a maximal value of $m = 3$ through the application of the Dirac algebra. We choose to reduce these integrals to a basis set, using the methods worked out in Refs. [20]. Reviews of the different methods for computing tensor integrals are given in Refs. [20, 22].

In the following, we outline the approach of Refs. [20]. Thereby, we restrict ourselves to the case of tensor integrals with $N < 6$ which may develop only soft IR singularities. However, we take into account that the integrands of our tensor integrals contain massive top-quark propagators.

At first, the tensor integrals are reduced to scalar integrals by means of the method developed in Ref. [23]. This way, the tensor N-point integrals are expressed as a sum of scalar N-point integrals with higher dimension and raised powers of the propagators:

$$I_N^{\mu_1\mu_2\cdots\mu_m}\left(D; \{q_i\}, \{1\}\right) =$$
$$\sum_{\lambda, x_1, x_2, \ldots, x_N} \delta_{(2\lambda + \sum_i x_i - m)0} \left(-\frac{1}{2}\right)^\lambda x_1! \, x_2! \, \cdots \, x_N!$$
$$\times \quad \left\{ g^\lambda q_1^{x_1} q_2^{x_2} \cdots q_N^{x_N} \right\}^{\mu_1\mu_2\cdots\mu_m}$$
$$\times \quad I_N\left(D + 2(m - \lambda); \{q_i\}, \{1 + x_i\}\right) . \tag{2.18}$$

$\left\{ g^\lambda q_1^{x_1} q_2^{x_2} \cdots q_N^{x_N} \right\}^{\mu_1\mu_2\cdots\mu_m}$ means that the m Lorentz indices are carried by λ metric tensors and x_i momentum vectors q_i, $i \in \{1, 2, ..., N\}$, in all possible manners. We have, for example,

$$\{q_1 q_2\}^{\mu_1\mu_2} = q_1^{\mu_1} q_2^{\mu_2} + q_1^{\mu_2} q_2^{\mu_1} . \tag{2.19}$$

The generalised scalar integrals produced this way are UV divergent if $\sigma = D/2$. They may be IR divergent if $(\sigma - N + 2) = D/2$. Additional requirements for IR singularities have already been discussed in Section 2.1. Integrals which lie between these boundaries are definitely finite. Fig. 2.7 now shows the scalar integrals as dots in the $(D/2, \sigma - N)$ plane for $N = 2, 3, 4, 5$. We see that the two boundaries are given by the lower and the upper solid line, respectively. Only the six-dimensional self-energy, which is also UV divergent, lies beyond these boundaries. The two lines coincide for two-point
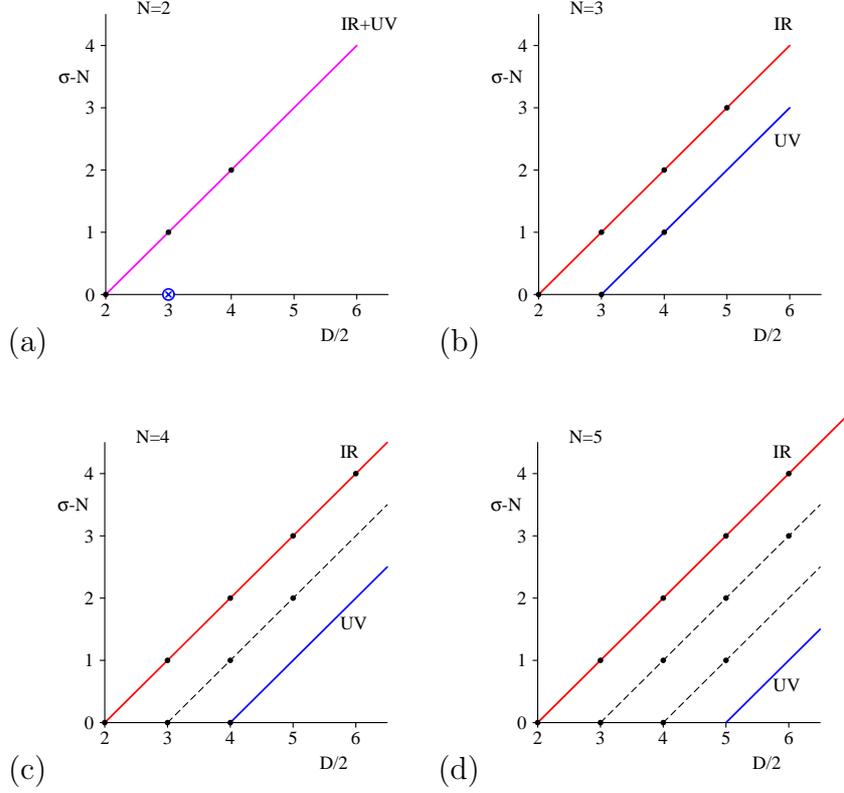
Figure 2.7: The generalised scalar integrals are shown in the $(D/2, \sigma - N)$ plane for the different cases $N = 2, 3, 4, 5$. The Figure has been taken from the first of Refs. [20].

functions. However, in our case, these integrals have at least one massive propagator and are therefore UV but not IR divergent. In Fig. 2.8, the integrals are shown in the (N, σ) plane. This allows to read off all the UV divergent integrals. In our case, we only have

$$\{I_3(6 - 2\epsilon; \{q_i\}, 1, 1, 1), I_2(6 - 2\epsilon; \{q_i\}, 2, 1), I_2(4 - 2\epsilon; \{q_i\}, 1, 1)\}. \quad (2.20)$$

But also in the general case, there is only a small number of UV-divergent integrals. These are extracted and considered as basis integrals.

In contrast, the UV-finite integrals are reduced to a basis set of integrals by means of recursion relations. The latter express an integral through a
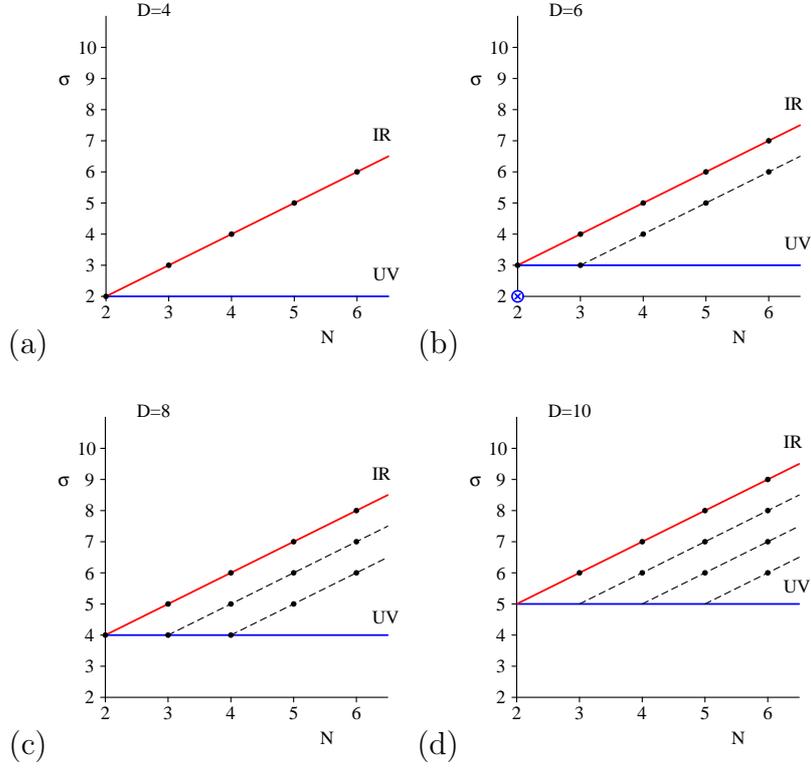
Figure 2.8: The generalised scalar integrals are shown in the (N, σ) plane for the different cases $D = 4, 6, 8, 10$. The Figure has been taken from the first of Refs. [20].

sum of integrals which have a lower dimension and/or smaller propagator powers. Recursion relations can be obtained as follows. The integration by parts identity of Refs. [24] is applied to

$$\int \frac{d^D \ell}{(2\pi)^D} \frac{\partial}{\partial \ell^\mu} \left(\frac{\left(\sum_{i=1}^N y_i \right) \ell^\mu + \left(\sum_{i=1}^N y_i q_i^\mu \right)}{d_1^{\nu_1} d_2^{\nu_2} \cdots d_N^{\nu_N}} \right) , \qquad (2.21)$$

where the $\{y_i\}$ are N arbitrary parameters. We work out the respective relation and apply the dimensional shift identity,

$$I_N(D - 2; \{\nu_k\}) = -\sum_{i=1}^N \nu_i I_N(D; \{\nu_k + \delta_{ik}\}) . \qquad (2.22)$$

Here and in the following, we often suppress the argument $\{q_i\}$ of the generalised scalar integral. We get the following base equation:

$$\sum_{j=1}^{N} \left(\sum_{i=1}^{N} S_{ji} y_i \right) \nu_j I_N(D; \{\nu_l + \delta_{lj}\}) =$$
$$- \sum_{i=1}^{N} y_i I_N(D-2; \{\nu_l - \delta_{li}\}) - \left(D - 1 - \sum_{j=1}^{N} \nu_j \right) \left(\sum_{i=1}^{N} y_i \right) I_N(D; \{\nu_l\}).$$
$$(2.23)$$

Here, we have introduced the kinematical matrix $S_{ij} = (q_i - q_j)^2 - M_i^2 - M_j^2$. For $N \leq 6$, the determinant of S_{ij} is unequal zero and the inverse of S_{ij} exists. We can, therefore, choose the $\{y_i\}$ such that $\sum_{i=1}^{N} S_{ji} y_i = \delta_{jk}$, for any $k \leq N$, is fulfilled. The left-hand side of the base equation then reduces to a single term and yields a useful recursion relation. The desired $\{y_i\}$ read:

$$y_i = S_{ik}^{-1} \text{ for any } k \leq N. \qquad (2.24)$$

The inverse can be numerically calculated, for example, by means of the Singular Value Decomposition technique. If we insert Eq. (2.24) into the base equation, we obtain the basic recursion relation

$$(\nu_k - 1) I_N(D; \{\nu_l\}) =$$
$$- \sum_{i=1}^{N} S_{ki}^{-1} I_N(D-2; \{\nu_l - \delta_{li} - \delta_{lk}\}) - b_k (D - \sigma) I_N(D; \{\nu_l - \delta_{lk}\}),$$
$$(2.25)$$

with $b_i = \sum_j S_{ij}^{-1}$. Summing this equation over k and applying the dimensional shift identity, we get:

$$(D - 1 - \sigma) \, B \, I_N(D; \{\nu_l\}) =$$
$$I_N(D-2; \{\nu_l\}) - \sum_{i=1}^{N} b_i I_N(D-2; \{\nu_l - \delta_{li}\}), \qquad (2.26)$$

respectively

$$I_N(D; \{\nu_l\}) =$$
$$(D + 1 - \sigma) \, B \, I_N(D+2; \{\nu_l\}) + \sum_{i=1}^{N} b_i I_N(D; \{\nu_l - \delta_{li}\}), \quad (2.27)$$

with $B = \sum_i b_i$. Combining Eqs. (2.25) and (2.26), we finally find:

$$
\begin{aligned}
(\nu_k - 1)I_N(D; \{\nu_l\}) = \\
-\frac{b_k}{B}I_N(D - 2; \{\nu_l - \delta_{lk}\}) \\
+\sum_{i=1}^{N}\left(\frac{b_k b_i}{B} - S_{ki}^{-1}\right)I_N(D - 2; \{\nu_l - \delta_{li} - \delta_{lk}\}) \, .
\end{aligned}
\tag{2.28}
$$

Note that above recursion relations can lead to propagator powers equal to zero. In this case, the respective propagator is pinched out and the N-point integral becomes an $(N - 1)$-point integral.

The different recursion relations now shall be exploited in order to systematically reduce the UV-finite integrals to a basis set. The relations are illustrated as arrows in Fig. 2.9. First, Eq. (2.27) is applied to the integrals with $N \neq 3$ and $D = 4$. Then, Eq. (2.25) is used for integrals with $N \neq 3$ and $(\sigma - N + 2) = D/2$. Now, Eqs. (2.26) and (2.28) are subsequently applied respecting $(\sigma - N + 2) < D/2 \leq \sigma$. For triangle integrals with mass and momentum configurations of IR-divergent ones, however, we have $\det(S) = 0$. Thus, these integrals cannot be reduced as above. They are considered as basis integrals.

As can be seen from Fig. 2.9, in the case of triangles and boxes, the recursion relations express finite integrals through UV-divergent ones. Of course, these artificial UV divergences cancel in the sum. This is due to

$$
\sum_{i=1}^{N}\left(\frac{b_k b_i}{B} - S_{ki}^{-1}\right) = 0 \, ,
\tag{2.29}
$$

which is the prefactor of the UV poles appearing on the right-hand side of Eq. (2.28) which produces the artificial UV divergences. However, it is possible to subtract regulator terms from the divergent integrals. These read

$$
R(D, \sigma) = \frac{1}{\epsilon}\frac{(-1)^\sigma}{\Gamma(D - \sigma)} \, ,
\tag{2.30}
$$

with $D = 2\sigma$. Also these regulator terms cancel in the sum due to Eq. (2.29). Furthermore, the regulated integrals still respect Eq. (2.26). Since Eq. (2.28), which produces the artificial divergences, does not contain the dimension as a factor, we do not get additional finite terms from ϵ multiplying a divergent integral. Eq. (2.26), which does contain the dimension as a factor, is now
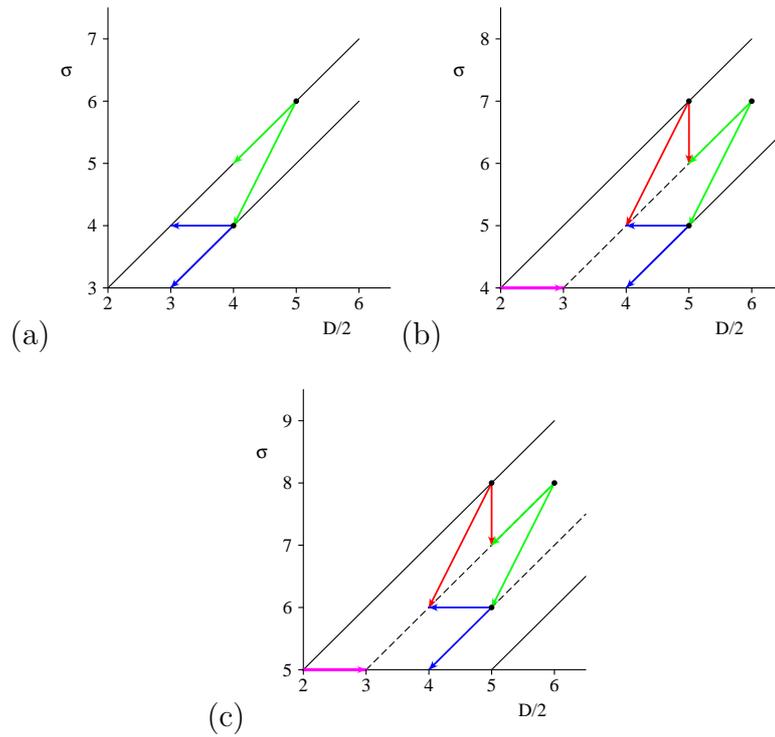
Figure 2.9: The generalised scalar integrals as well as the different recursion relations are shown in the $(D/2, \sigma)$ plane for the different cases $N = 3$ (a), $N = 4$ (b), and $N = 5$ (c). The recursion relations are indicated as arrows. The Figure has been taken from the first of Refs. [20].

only applied to regulated integrals. We also do not get such finite terms from the reduction of IR-divergent pentagon and box integrals. The only integrals which are produced by Eqs. (2.25) and (2.27) together with the dimension as a prefactor are finite.

The result of the procedure outlined above is that the generalised scalar integrals are expressed through a basis set of integrals. Note, however, that this set is overcomplete and therefore not a true basis in the mathematical sense. The basis set consists of the following integrals:

- the IR-divergent triangle integrals which lie on the $D = 2(\sigma - 1)$ line in Fig. 2.9,

- the UV-regularised triangle integrals which have an IR-divergent con-

figuration and lie on the $D = 2\sigma$ line in Fig. 2.9,

- the UV-regularised self-energy integrals which have $D = 2\sigma$,

- the finite four-dimensional triangle integrals with all propagator powers equal to one,

- the finite six-dimensional box integrals with all propagator powers equal to one,

- the finite six-dimensional pentagon integrals with all propagator powers equal to one,

- the UV-divergent integrals which are extracted right from the beginning.

Actually, the six-dimensional pentagon integrals only appear with coefficients of order $\mathcal{O}(\epsilon)$ (see for example [25]). Since these integrals are finite, they thus do not contribute at NLO.

The application of Eqs. (2.25) and (2.27) to the pentagon and box integrals which lie on the respective IR line $(\sigma - N + 2) = D/2$ leads to integrals with pinched propagators. These integrals, however, still lie on an IR line. Eventually, all IR-divergent integrals are expressed through finite integrals and IR-divergent triangles. This way, the IR-singularity structure is contained solely in three-point functions. The expression for the IR-divergent part of an amplitude obtained through the recursion procedure is, however, quite complex. It is therefore not well suited for an analytic cancellation. But it can also be determined without recourse to any recursion relations. It can be directly read off the original tensor integrals. The resulting expression is very compact and can be used for the cancellation of the IR divergences. The generalisation of this method to the massive case can be done with the help of Ref. [21]. Here, we concentrate on the case of integrals which have at most one massless line. Such integrals can only develop soft IR singularities. This is the case for the process considered in this work.

As already mentioned in Section 2.1, the IR singularities only occur for the pentagon integrals. Here, the massless gluon is always exchanged between on-shell top and anti-top quarks. The loop integration develops a soft IR singularity when the momentum of the gluon propagator reaches zero. Then the gluon propagator as well as its neighbouring propagators become singular. In order to extract this singularity in terms of a three-point function, we

just have to pick out these three propagators, which now build the desired triangle, and set the loop momentum in the other two propagators equal to $-q_j$, where j denotes the propagator of the gluon. If the original integral contains loop momenta in the numerator, these can either be integrated over the loop momentum together with the three propagators of the triangle or also set to $-q_j$. Here, $k = \max(m + 3 - N, 0)$ of the loop momenta in the numerator are chosen as part of the triangle integral while the others are substituted. The Lorentz indices of the loop momenta are now assigned in a symmetric way, and the resulting tensor three-point function is reduced by means of Eq. (2.18). The chosen value for the rank of the triangle integrals has the effect that the same generalised IR-divergent triangle integrals occur as in the case of the reduction procedure. This can be seen by inspection of the recursion relations. From the resulting triangle integrals only the IR-divergent ones are kept. These now contain the desired IR-singularity structure. We therefore have:

$$
\begin{aligned}
I_5^{\mu_1\mu_2\cdots\mu_m} \left(d; \{q_i\}, \{1\}\right)\Big|_{IR} = & \\
& \frac{\ell^{\mu_{k+1}}\cdots\ell^{\mu_m}}{d_a d_b}\bigg|_{\ell\to(-q_j)} \\
\times & \sum_{0\leq x\leq k}\sum_{0\leq y\leq (k-x)} x!\, y!\, (k-x-y)!\, \left\{q_{j-1}^x q_j^y q_{j+1}^{k-x-y}\right\}^{[\mu_1\mu_2\cdots\mu_k]} \\
\times & \; I_3\left(d + 2k; q_{j-1}, q_j, q_{j+1}, 1+x, 1+y, 1+k-x-y\right), \qquad (2.31)
\end{aligned}
$$

where $j - 1$ and $j + 1$ denote the neighbouring propagators of the gluon propagator, and a, b label the residual ones. $[\mu_1\mu_2\cdots\mu_k]$ means that k Lorentz indices have to be chosen out of the m in all possible ways while their order does not make a difference. All these different terms are then summed over and divided by their total number. Note that, on the right-hand side of the latter Equation, a triangle integral can still be IR finite depending on the powers of the propagators. As said above, only the IR-divergent ones are kept.

This expression for the IR-singularity structure is very compact in comparison to the one obtained by the reduction procedure. It is therefore better suited for an analytic cancellation of the IR divergences. Of course, it can also be used to account for finite terms that appear through multiplication of IR poles with $\mathcal{O}(\epsilon)$-terms in front of the original integrals. While we now have an analytic expression for the IR-divergent part, the reduction of the amplitude can be performed numerically in four dimensions.

The recursion relations, which have been written down in Eqs. (2.25, 2.26, 2.27, 2.28), are used in order to reduce the generalised scalar integrals to a basis set of integrals. However, for certain configurations in phase space, the B parameter and/or the determinant of the kinematical matrix may become small. The B parameter occurs in denominators of the recursion relations. A small determinant for the kinematical matrix means that the numerical inversion of the matrix becomes unstable. In the case that the respective parameter is exactly zero, it is possible to switch to relations which have been developed for integrals with more than five external legs. However, if it is not exactly zero but very small, the above mentioned recursion relations become numerically unstable. Then, we have to use alternative recursion relations which involve expansions. We refrain from outlining the whole method for treating these so-called exceptional momentum configurations, but only treat the simplest case of a small B parameter while the inversion of the kinematical matrix is stable. This actually means that the determinant of the Gram matrix is small. The latter is defined as follows:

$$G_{ij} = 2 \, q_i \cdot q_j \ \text{ with } \ i, j \, \epsilon \, \{1, \ldots, N-1\} \,, \tag{2.32}$$

where $q_N = 0$ is assumed. The two determinants and the B parameter are related as follows:

$$\det(G) = (-1)^{N-1} \, B \, \det(S) \,. \tag{2.33}$$

From this relation we readily see that a small B parameter implicates a small Gram determinant. In this case, the recursion relations of Eqs. (2.25) and (2.27) are still numerically stable. In opposition, the relations of Eqs. (2.26) and (2.28) contain the B parameter in the denominator. They cannot be used anymore. In this case, Eq. (2.25) is still applied to integrals lying on the respective IR line while Eq. (2.27) is used in all the other cases. The latter relation expresses an integral through a higher-dimensional one and a sum of integrals whose sums of propagator powers are reduced by one. Each of these integrals is again subject to Eq. (2.27) if none of its propagators has been pinched out. Eventually, we will arrive at integrals with a pinched propagator and integrals which have a certain power of the B parameter as a prefactor. This means we get an expansion in the small B parameter which can be truncated when the desired accuracy has been achieved. In practice, we have to scale the B parameter by powers of a typical hard scale of the process in order to get a dimensionless parameter. Here, we choose the mass of the top quark as the hard scale.

Also in the other cases, alternative recursion relations can be set up. In principle, this allows for the reduction of an arbitrary integral within the desired precision. However, the alternative relations involve iterations which slow down the evaluation. Note further that the application of the alternative recursion relations leads outside the UV/IR boundaries shown in Fig. 2.7. Moreover, the nice feature that no $\mathcal{O}(\epsilon)$-terms have to be accounted for during the reduction of an integral is lost. But still, it is possible to numerically evaluate the coefficients of the Laurent expansions of the integrals. It should also be noted, however, that the basis box integral is now chosen to be the four-dimensional one instead of the six-dimensional.

The computation of the virtual part is the bottleneck of NLO calculations. The method of Refs. [20], which has just been indicated, presents, in principle, a possibility to evaluate arbitrary tensor integrals in an efficient way. However, the applicability can only be assessed by computing realistic NLO cross sections. This has already been done for massless internal particles in Refs. [20, 26]. In Ref. [27], the method has partly been employed to a process containing massive particles in the loop. This work allows for a further assessment of its usefulness. It is concerned with a $2 \to 3$ process which includes massive propagators.

2.3   Subtraction Method

As discussed in Section 2.1, the virtual correction and the real correction separately develop IR singularities. Within dimensional regularisation, these manifest themselves as poles in the parameter ϵ. The divergences of the virtual part stem from the loop integration. Those of the real correction arise during the phase space integration with respect to the additionally radiated gluon which then becomes soft. We therefore have two types of contributions, which are integrated over different phase spaces, and the IR singularities only cancel in their sum. This prevents a straightforward numerical integration in four dimensions. If we used a small gluon mass for the IR regularisation instead of dimensional regularisation, the two contributions would separately develop logarithms of this small mass. In the sum of the virtual and real contributions, this would lead to large cancellations which spoil the numerical evaluation.

One way to deal with the IR singularities is given by the method called Phase Space Slicing. Here, the integration over the one-particle phase space

of the gluon is divided into two parts by means of an energy cutoff. If the energy of the gluon is below the cutoff, the eikonal approximation can be used. It is then possible to analytically evaluate this integration. Since it is this part of the phase space which is responsible for the IR singularities, we now have an analytic expression for it. This procedure is universal and always leads to a factorisation of the squared amplitude into the squared Born amplitude times an eikonal factor. On the other hand, the phase space integration for gluon energies above the cutoff can be performed completely numerically in four dimensions. The analytic expression for the IR singularities still has to be integrated over the same phase space as the virtual part. This contribution can therefore be combined with the virtual correction in order to perform the cancellation of the IR divergences analytically. The resulting expression can be numerically integrated in four dimensions. Note that the Phase Space Slicing method can also be used in order to treat collinear singularities. Further cutoffs extract the parts of phase space where the collinear singularities are developed.

In this work, however, we employ a subtraction method. Such methods do not make use of cutoffs and approximations. Therefore, also no tuning of cutoffs has to be performed in order to find regions for their values where the results are stable against variations of them. Furthermore, subtraction methods can automatically avoid double counting in the case of overlapping divergences. Note further that the Phase Space Slicing method leads to small parts in phase space which are not integrated over (see for example Ref. [28]). However, this again only concerns the case of overlapping divergences.

An actual implementation of the subtraction method is given by the Dipole Subtraction Method, which is also used here. It has first been worked out for massless, unpolarised QCD partons, within dimensional regularisation, in Ref. [29]. A generalisation for massive, polarised particles within QED was achieved in Ref. [30]. In this work, mass regulators have been employed as it is common for electroweak calculations. In the case of massive particles, large logarithms can arise due to particles with non-vanishing but very small masses compared to a typical hard scale of the process. These small masses act as collinear regulators. In the sum, such logarithms cancel like the logarithms of true regulator masses. The subtraction method has been set up in a way that also these logarithms are accounted for. In Ref. [31], the results for massive fermions with equal masses have been given for unpolarised QCD partons and dimensional regularisation. However, large logarithms are not treated in this work. Finally, the full generalisation for

massive, unpolarised QCD partons has been obtained in Ref. [32]. Dimensional regularisation is employed and the large logarithms are accounted for. For other implementations of the subtraction method we refer the reader to Ref. [33] and References therein.

In this Section, we outline the Dipole Subtraction Method of Ref. [32]. The top quark and the anti-top quark in the final state are the only external QCD partons at Born level in the process under consideration. The soft IR divergences of the real cross section are due to the splitting of the top quark into a top quark and a soft gluon respectively of the anti-top quark into an anti-top quark and a soft gluon. The treatment of the colour algebra is simple. As already mentioned in Section 2.1, the Born diagrams all receive a colour factor of $N_C = 3$ while the real and virtual correction diagrams lead to a factor of $N_C C_F = 4$. The subtraction terms all involve the squared Born amplitude with an additional colour factor of $C_F = 4/3$. In the following, we will restrict ourselves to this simplest case. The subtraction terms for the virtual and for the real part will be written down explicitly.

Several complications arise in the general case. The colour algebra is more involved. Gluons in the final state demand helicity projections. All possible splittings of the QCD partons have to be taken into account. Initial state radiation takes place and collinear divergences occur. Initial state radiation or final state tagged hadrons lead to leftover singularities which are absorbed into parton distribution functions respectively fragmentation functions. Furthermore, large logarithms due to QCD partons with small but non-vanishing masses occur. These issues are not discussed here. We just like to note that the special treatment of the large logarithms allows to perform the massless limit for processes where the respective small parton mass does not set the hard scale.

The cross section of a process at NLO is built as the sum of the Born cross section and the NLO correction. The latter consists of a virtual and a real contribution. The Born cross section as well as the virtual part are integrated over the phase space of the m external particles of the Born diagrams. The phase space integration of the real part involves $m + 1$ particles since an additional QCD parton is radiated. The situation looks as follows:

$$\sigma = \sigma^{LO} + \sigma^{NLO} = \int_m d\sigma^B + \int_{m+1} d\sigma^R + \int_m d\sigma^V . \qquad (2.34)$$

Within a subtraction method, an auxiliary cross section $d\sigma^A$ is introduced which has the same pointwise singular behaviour in d dimensions as $d\sigma^R$

(adopting dimensional regularisation). $d\sigma^A$ is furthermore chosen simple enough to enable an analytic integration over the one-parton subspace of the additionally radiated parton. The auxiliary cross section is then subtracted from the real contribution and added back to the virtual one:

$$
\begin{aligned}
\sigma^{NLO} &= \int_{m+1} \left[\left(d\sigma^R \right)_{\epsilon=0} - \left(d\sigma^A \right)_{\epsilon=0} \right] \\
&\quad + \int_m \left[d\sigma^V + \int_1 d\sigma^A \right]_{\epsilon=0} .
\end{aligned}
\tag{2.35}
$$

Here, $\int_1 d\sigma^A$ denotes the auxiliary cross section integrated over the one-parton subspace. As we can see, $d\sigma^A$ acts as a local counterterm for $d\sigma^R$ so that the subtracted expression can be integrated numerically in four dimensions. $\int_1 d\sigma^A$, on the other hand, cancels the poles of the virtual term $d\sigma^V$. After this cancellation has been performed (see Section 3.3), the dimension can be set to four also for the subtracted virtual expression. Again, a numerical integration in four dimensions is possible. We therefore obtain two expressions which are well suited for an implementation in a Monte Carlo program. Note that the need for numerical methods is clearly given by the complexity of NLO calculations.

The real cross section $d\sigma^R$ obeys soft and collinear factorisation properties. In the soft and collinear limits, it factorises into the corresponding Born cross section $d\sigma^B$ times a universal singular factor. In this sense, the IR-singularity structure of the real cross section is process independent. This fact can be exploited in order to set up a general prescription for constructing the auxiliary cross section. Here, $d\sigma^A$ is built as the sum of so-called dipoles. These dipoles resemble the real cross section in the singular limits so that the auxiliary cross section indeed has the same pointwise singular behaviour as the real one. We can write symbolically:

$$
d\sigma^A = \sum_{dipoles} d\sigma^B \otimes dV_{dipole} ,
\tag{2.36}
$$

where the differential dipole factors are denoted as dV_{dipole}. In our case, $\otimes$ just means the common product. In general, $\otimes$ involves colour and spin correlations. Each dipole contains two specific partons, an emitter and a spectator. The emitter splits into two partons and leads to IR singularities. The spectator contains information on colour and spin correlations of $d\sigma^R$ and balances momentum conservation. The sum in Eq. (2.36) exhausts all ordered combinations of two external partons appearing at Born level. A

dipole interpolates smoothly between soft and collinear limits. Therefore, double counting is automatically avoided. In addition to the dipole factors, we need a mapping from the $(m+1)$-parton phase space to an m-parton phase space times a 1-parton phase space factor, where the former corresponds to the Born level phase space. This allows to perform the integral of the dipole factors over the 1-parton phase space factor in a process-independent way. Symbolically we can write:

$$\int_{m+1} d\sigma^A = \sum_{dipoles} \int_m d\sigma^B \otimes \int_1 dV_{dipole} = \int_m \left[d\sigma^B \otimes \mathbf{I} \right] \qquad (2.37)$$

$$\text{with } \mathbf{I} = \sum_{dipoles} \int_1 dV_{dipole} \,. \qquad (2.38)$$

The universal factor $\mathbf{I}$ contains all the IR singularities as poles in ϵ. Using Eqs. (2.36) to (2.38), we can specify Eq. (2.35) as

$$\begin{aligned}
\sigma^{NLO} &= \int_{m+1} \left[\left(d\sigma^R \right)_{\epsilon=0} - \left(\sum_{dipoles} d\sigma^B \otimes dV_{dipole} \right)_{\epsilon=0} \right] \\
&+ \int_m \left[d\sigma^V + d\sigma^B \otimes \mathbf{I} \right]_{\epsilon=0} \,.
\end{aligned} \qquad (2.39)$$

Let us now, for completeness, specify the general phase space $d\Phi_m$ in d dimensions:

$$d\Phi_m(p_1, \ldots, p_m; P) = \left[\prod_{i=1}^m \frac{d^d p_i}{(2\pi)^{d-1}} \delta_+(p_i^2 - m_i^2) \right] (2\pi)^d \delta^{(d)}(p_1 + \ldots + p_m - P) \,, \qquad (2.40)$$

with the total incoming momentum P and the on-shell masses m_i of the final state particles with momenta p_i. Here, we have not included the flux factor, which of course has to be taken into account.

The next task in order is the derivation of the dipoles. In the soft IR limit, we can make use of the eikonal approximation with respect to the soft gluon. Colour conservation can be applied in order to obtain the singular behaviour of the real matrix element squared in terms of emitter-spectator terms. This leads to the introduction of colour-correlated amplitudes. However, the colour algebra is trivial in our case. We therefore just write down the result for the process under consideration. It reads:

$$|\mathcal{M}_{m+1}|^2 \longrightarrow$$

$$8\pi\mu^{2\epsilon}\alpha_s C_F \cdot \frac{1}{p_3 \cdot p_6} \left[\frac{p_3 \cdot p_4}{(p_3 + p_4) \cdot p_6} - \frac{m_t^2}{2p_3 \cdot p_6} \right] \cdot |\mathcal{M}_m|^2$$

$$+ \quad 8\pi\mu^{2\epsilon}\alpha_s C_F \cdot \frac{1}{p_4 \cdot p_6} \left[\frac{p_3 \cdot p_4}{(p_3 + p_4) \cdot p_6} - \frac{m_t^2}{2p_4 \cdot p_6} \right] \cdot |\mathcal{M}_m|^2, \quad (2.41)$$

where $\mathcal{M}_{m+1}$ is the real matrix element and $\mathcal{M}_m$ the one at Born level. In writing down a squared matrix element, a summing over colours and spins/polarisations is always understood. Respective expressions can also be given for the collinear limits, which appear in the general case. However, we still need a mapping of the momenta to a new set. This is necessary in order that momentum conservation is given in a factorisable way. In detail, the momenta of the emitter and of the spectator are redefined. These new momenta satisfy their on-shell conditions, and their sum is equal to the sum of the original spectator momentum and the momenta of the partons which result from the respective splitting process. Of course, the limiting behaviour still has to be satisfied. Having the limiting expression and the mapping at hand, the dipoles can be written down and integrated over the one-parton phase space. As already mentioned, one dipole is sufficient to account for both, the soft IR and the collinear singular behaviour, for each emitter-spectator pair.

We will now explicitly write down the relevant subtraction terms and mappings for the process under consideration. The subtraction terms contain two dipoles. Either the top quark is the emitter and the anti-top quark is the spectator or vice versa. The quark/anti-quark splits into a quark/anti-quark and a gluon. The subtraction term for the real part can therefore be written as:

$$d\sigma^A = \mathcal{D}_{63,4} + \mathcal{D}_{64,3}, \quad (2.42)$$

where the $\mathcal{D}_{63,4}$, $\mathcal{D}_{64,3}$ are the dipoles. The numbering of the external particles follows Section 2.1. The explicit expressions for the two dipoles read:

$$\mathcal{D}_{63,4}(p_3, p_4, p_6) = \frac{1}{2p_3 \cdot p_6} V_{63,4} |\tilde{\mathcal{M}}_m|^2, \quad (2.43)$$

with the top quark as the emitter, and

$$\mathcal{D}_{64,3}(p_3, p_4, p_6) = \frac{1}{2p_4 \cdot p_6} V_{64,3} |\tilde{\mathcal{M}}_m|^2, \quad (2.44)$$

where the anti-top quark is the emitter. $\tilde{\mathcal{M}}_m$ is the real matrix element where the gluon and the quark respectively the anti-quark have been substituted by the parent parton of the corresponding splitting process. This emitter parton is assigned the momentum $\tilde{p}_{ij}$. Furthermore, the momentum of the spectator, p_k, has been transformed to $\tilde{p}_k$. The new momenta are calculated as follows:

$$
\begin{aligned}
\tilde{p}_k^\mu = \tilde{p}_4^\mu \quad &= \quad \frac{\sqrt{Q^2(Q^2 - 4m_t^2)}}{\sqrt{Q^2(Q^2 - 4p_6 \cdot p_3 - 4m_t^2) + 4(p_6 \cdot p_3)^2}} \\
&\quad \times \left(p_4^\mu - \frac{m_t^2 + p_6 \cdot p_4 + p_3 \cdot p_4}{2(m_t^2 + p_3 \cdot p_4 + p_3 \cdot p_6 + p_4 \cdot p_6)} \, Q^\mu \right) \\
&\quad + \frac{1}{2} \, Q^\mu \,, \\
\tilde{p}_{ij}^\mu = \tilde{p}_3^\mu \quad &= \quad Q^\mu - \tilde{p}_4^\mu \,,
\end{aligned}
\tag{2.45}
$$

respectively

$$
\begin{aligned}
\tilde{p}_k^\mu = \tilde{p}_3^\mu \quad &= \quad \frac{\sqrt{Q^2(Q^2 - 4m_t^2)}}{\sqrt{Q^2(Q^2 - 4p_6 \cdot p_4 - 4m_t^2) + 4(p_6 \cdot p_4)^2}} \\
&\quad \times \left(p_3^\mu - \frac{m_t^2 + p_6 \cdot p_3 + p_3 \cdot p_4}{2(m_t^2 + p_3 \cdot p_4 + p_3 \cdot p_6 + p_4 \cdot p_6)} \, Q^\mu \right) \\
&\quad + \frac{1}{2} \, Q^\mu \,, \\
\tilde{p}_{ij}^\mu = \tilde{p}_4^\mu \quad &= \quad Q^\mu - \tilde{p}_3^\mu \,.
\end{aligned}
\tag{2.46}
$$

Here, we have introduced

$$
Q = p_3 + p_4 + p_6 \,.
\tag{2.47}
$$

The $V_{6j,k}$, with $\{j,k\} = \{3,4\}$ respectively $\{4,3\}$, are given by:

$$
V_{6j,k} = 8\pi\alpha_s C_F \left\{ \frac{2}{1 - \tilde{z}_j(1 - y_{6j,k})} - \frac{\tilde{v}_{6j,k}}{v_{6j,k}} \cdot \left[1 + \tilde{z}_j + \frac{m_t^2}{k_6 \cdot k_j} \right] \right\} \,.
\tag{2.48}
$$

The variables $\tilde{z}_j$, $y_{6j,k}$, $\tilde{v}_{63,4}$, and $v_{6j,k}$ read

$$
\tilde{z}_3 = 1 - \frac{p_6 \cdot p_4}{p_6 \cdot p_4 + p_3 \cdot p_4} \,,
\tag{2.49}
$$

$$\tilde{z}_4 = 1 - \frac{p_6 \cdot p_3}{p_6 \cdot p_3 + p_3 \cdot p_4} \,, \tag{2.50}$$

$$y_{6j,k} = \frac{p_6 \cdot p_j}{p_6 \cdot p_3 + p_6 \cdot p_4 + p_3 \cdot p_4} \,, \tag{2.51}$$

$$\tilde{v}_{63,4} = \tilde{v}_{64,3} = \frac{\sqrt{Q^2(Q^2 - 4m_t^2)}}{Q^2 - 2m_t^2} \,, \tag{2.52}$$

$$v_{6j,k} = \frac{\sqrt{[1 - y_{6j,k} + 2\mu^2 y_{6j,k}]^2 - 4\mu^2}}{(1 - 2\mu^2)(1 - y_{6j,k})} \;\; \text{with} \;\; \mu^2 = \frac{m_t^2}{Q^2} \,. \tag{2.53}$$

The two integrated subtraction terms coincide so that we get only one term times a factor of two. It reads as follows:

$$d\sigma^B \otimes \mathbf{I} = |\mathcal{M}_m|^2 \cdot \left\{ 2\frac{\alpha_s}{2\pi} \frac{(4\pi)^\epsilon}{\Gamma(1-\epsilon)} \left[C_F \left(\frac{\mu^2}{2p_3 \cdot p_4} \right)^\epsilon \left(\mathcal{V} - \frac{\pi^2}{3} \right) + \Gamma \right.\right.$$
$$\left.\left. + \frac{3}{2} C_F \ln \left(\frac{\mu^2}{2p_3 \cdot p_4} \right) + \frac{3}{2} C_F + \left(\frac{7}{2} - \frac{\pi^2}{6} \right) C_F \right] \right\} \,, \tag{2.54}$$

with

$$\Gamma = C_F \left(\frac{1}{\epsilon} + \frac{1}{2} \ln(\frac{m_t^2}{\mu^2}) - 2 \right) \tag{2.55}$$

and

$$\mathcal{V} = \left\{ \frac{1}{v_{34}} \left[\frac{1}{\epsilon} \ln(\rho) - \frac{1}{2} \ln^2(\rho_{34}^2) - \frac{\pi^2}{6} \right] + \frac{1}{v_{34}} \ln(\rho) \ln \left(\frac{Q_{34}^2}{2p_3 \cdot p_4} \right) \right.$$
$$+ \frac{3}{2} \ln \left(\frac{2p_3 \cdot p_4}{Q_{34}^2} \right) + \frac{1}{v_{34}} \left[\ln(\rho^2) \ln(1 + \rho^2) + 2\text{Li}_2(\rho^2) \right.$$
$$\left. -2\text{Li}_2(1 - \rho_{34}^2) - \frac{\pi^2}{6} \right] + \ln \left(\frac{Q_{34} - m_t}{Q_{34}} \right) - 2 \ln \left(\frac{(Q_{34} - m_t)^2 - m_t^2}{Q_{34}^2} \right)$$
$$\left. - \frac{m_t^2}{p_3 \cdot p_4} \ln \left(\frac{m_t}{Q_{34} - m_t} \right) - \frac{m_t}{Q_{34} - m_t} + \frac{m_t(2m_t - Q_{34})}{p_3 \cdot p_4} + \frac{\pi^2}{2} \right\} \,. \tag{2.56}$$

In the latter expression, we introduced:

$$Q_{34} = \sqrt{Q_{34}^2} \,, \tag{2.57}$$

$$Q_{34}^2 = (p_3 + p_4)^2 = s_{34} \,, \tag{2.58}$$

$$v_{34} = \frac{\sqrt{Q_{34}^2(Q_{34}^2 - 4m_t^2)}}{Q_{34}^2 - 2m_t^2} \,, \tag{2.59}$$

$$\rho = \sqrt{\frac{1 - v_{34}}{1 + v_{34}}} \,, \tag{2.60}$$

$$\rho_{34} = \sqrt{\frac{1 - v_{34} + 2\frac{m_t^2}{Q_{34}^2}/(1 - 2\frac{m_t^2}{Q_{34}^2})}{1 + v_{34} + 2\frac{m_t^2}{Q_{34}^2}/(1 - 2\frac{m_t^2}{Q_{34}^2})}} \,. \tag{2.61}$$

Note that Eqs. (2.43) and (2.44) contain the squared Born matrix element in dependence on the transformed momenta while the original momenta are used in Eq. (2.54).

The ϵ-poles are contained in Eqs. (2.55) and (2.56). In Eq. (2.56), however, it comes with a factor of

$$\frac{1}{v_{34}} \ln(\rho) = \frac{1}{v_{34}} \ln\left(\sqrt{\frac{1 - v_{34}}{1 + v_{34}}}\right) \,. \tag{2.62}$$

For the cancellation of the IR divergences in Section 3.3, it will prove useful to cast this factor into a different form. We define the new variable

$$\tilde{v}_{34} = \sqrt{1 - \frac{4m_t^2}{s_{34}}} \,. \tag{2.63}$$

The following relations between $\tilde{v}_{34}$ and v_{34} can easily be shown to hold:

$$\frac{2}{v_{34}} = \frac{1}{\tilde{v}_{34}} + \tilde{v}_{34} \,, \tag{2.64}$$

$$\sqrt{\frac{1 - v_{34}}{1 + v_{34}}} = \frac{1 - \tilde{v}_{34}}{1 + \tilde{v}_{34}} \,. \tag{2.65}$$

We therefore have:

$$\frac{1}{v_{34}} \ln\left(\sqrt{\frac{1 - v_{34}}{1 + v_{34}}}\right) \cdot \frac{1}{\epsilon} = \frac{1 + \tilde{v}_{34}^2}{2\tilde{v}_{34}} \ln\left(\frac{1 - \tilde{v}_{34}}{1 + \tilde{v}_{34}}\right) \cdot \frac{1}{\epsilon} \,. \tag{2.66}$$

The subtraction terms are now in place. All we need in addition are $d\sigma^V$ in d dimensions, $d\sigma^R$ in 4 dimensions, and $d\sigma^B$ in d and in 4 dimensions. We can then implement Eq. (2.39) in a Monte Carlo program which performs the

numerical integration over the respective phase spaces. Above subtraction terms have also been given explicitly in one of the examples contained in Ref. [32].

A last note is in order. If we are interested in a non-trivial jet observable, the latter has to fulfil the requirement of infrared safety. In general, the jet observable also has to be collinear safe. In order for the large logarithms to cancel, it furthermore has to obey quasi-collinear safety. We refer the reader to Ref. [32] and References therein for a detailed discussion.

2.4 Photon Spectrum

We consider the process $\gamma\gamma \to t\bar{t}H$, which can be studied at a linear collider run in the two-photon mode (see Ref. [6] and References therein). In order to obtain a prediction for the parent process, $e^+e^- \to \gamma\gamma \to t\bar{t}H$, the subprocess has to be integrated over the spectra of the incoming photons:

$$\sigma(s) = \int\limits_{x_l}^{x_u} dx_1 \int\limits_{x_l \cdot \frac{x_u}{x_1}}^{x_u} dx_2 \, F(x_1) \, F(x_2) \, \hat{\sigma}(x_1 x_2 s) \,. \tag{2.67}$$

Here, $\sigma(s)$ is the cross section of the parent process, which depends on the square of the centre-of-momentum-system (CMS) energy, s. $\hat{\sigma}(x_1 x_2 s)$ denotes the cross section of the subprocess, whose CMS energy squared is calculated as $(x_1 x_2 s)$. x_1 and x_2 are the energy fractions of the incident electron and positron carried away by the two back-scattered photons, respectively. Note, however, that one could also use two electron beams in order to build up a photon collider. $F(x)$ denotes the photon spectrum which is discussed in this Section. We have one spectrum for each of the two photons while it is independent of the type of the incident particle. The spectra depend on the energy fractions x_1 and x_2, respectively. The upper limit x_u of both integrations is given by the energy spectrum. The lower limit of the outer integration is:

$$x_l = \frac{(2m_t + M_H)^2}{x_u s} \,. \tag{2.68}$$

This limit results from the need that the CMS energy squared of the subprocess, $(x_1 x_2 s)$, has to be above the threshold for producing the final state particles. For the same reason, the limit of the inner integration is given by a rescaling of this limit by the factor $\frac{x_u}{x_1}$.

In this work, we use the photon spectrum specified in Ref. [6]. This spectrum is a parametrisation which resembles a full simulation. The author also implemented the spectrum in the `Fortran` function `CompAZ`. The arguments of this function are the energy fraction and the beam energy as well as a parameter which controls the output. For the respective value of this parameter, all contributions to the spectrum are taken into account while polarisation is not considered. The function delivers the value of the photon spectrum for the specified energy fraction and beam energy.

However, for comparison with the literature, we also need the spectrum which is obtained by only taking into account direct Compton scattering. This case will be discussed first. We then outline the improvements obtained in Ref. [6].

In order to turn a linear e^+e^--collider into a photon collider, a low-energy laser beam is directed almost head to head onto each incident particle beam. This way, hard photons are copiously produced nearly in the same direction as the original beam. Here, we follow the presentation given in the second of Refs. [9]. The energy of the scattered photon depends on the scattering angle. The portion of photons with largest energy fractions grows with the energies of the incident particle and laser beams. The same applies to the maximum of the energy fraction. But the energy of the laser beam may not be chosen too large if pair creation of back-scattered photons with incident photons shall be avoided. If we only consider unpolarised photons and assume that the number of back-scattered photons produced per electron is one, this completely determines the energy spectrum of the back-scattered photon in direct Compton scattering. It reads:

$$F(x) = \frac{1}{D(\xi)} \left[1 - x + \frac{1}{1 - x} - \frac{4x}{\xi(1 - x)} + \frac{4x^2}{\xi^2(1 - x)^2} \right] , \qquad (2.69)$$

where $D(\xi)$ is given as

$$D(\xi) = \left(1 - \frac{4}{\xi} - \frac{8}{\xi^2} \right) \ln(1 + \xi) + \frac{1}{2} + \frac{8}{\xi} - \frac{1}{2(1 + \xi)^2} , \qquad (2.70)$$

with

$$\xi \simeq 4.8 . \qquad (2.71)$$

The energy spectrum for direct Compton scattering is shown in Fig. 2.10. As already said above, many hard photons are produced. The maximal energy

fraction x_u carried by the photons turns out to be

$$x_u \simeq 0.83 \,. \qquad (2.72)$$

Above this value, the spectrum is set to zero.
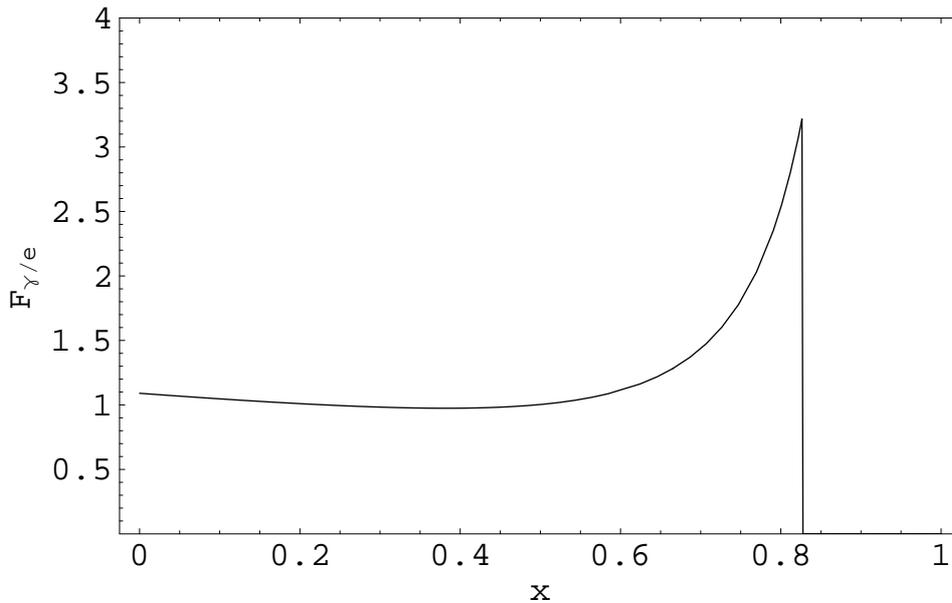
Figure 2.10: Energy spectrum of the back-scattered photon in dependence of the energy fraction of the incident electron respectively positron; here, only direct Compton scattering is taken into account.

The spectrum of Fig. 2.10 will be used for comparison of the Born and NLO results with the literature. As discussed above, it only involves direct Compton scattering. The parameters have been determined by maximisation of the portion of hard photons without making pair creation possible. However, a more realistic description of the photon spectrum has been obtained by a full simulation of the beam. Ref. [6] gives a parametrisation of the resulting spectrum which is convenient to use in numerical programs. The parametrisation is obtained by taking into account the following effects:

- direct Compton scattering,

- nonlinear effects,

- angular correlations,

- electron rescattering,

- scattering of two laser photons.

Nonlinear QED effects are due to the very high density of the laser beam. Angular correlations refer to the wider spread of low-energy photons which leads to a suppression of these. Electron rescattering means that a laser photon may be scattered off an electron which has already been part of a Compton scattering process. Finally, two photons may be scattered off an electron at the same time.

The parametrisation contains 10 free parameters which are determined by a fit to the simulation results. However, only the high-energy part of the spectrum is described by the parametrisation. The overall normalisation is obtained by fitting it to this part of the spectrum. Since we need a CMS energy of the subprocess which is above the threshold value for producing a top quark, an anti-top quark and a Higgs boson, only this high-energy part of the spectrum is relevant and the parametrisation is completely sufficient.

The parametrisation and the full simulation of the photon spectrum are shown in Fig. 2.11 for a beam energy of 250 GeV. As it turns out, the spectrum obtained by full simulation contains a large fraction of low-energy photons. The peak, on the other hand, is less pronounced compared to direct Compton scattering. It is also shifted towards smaller energies. Because of the larger number of low-energy photons, the result for the cross section of $e^+e^- \rightarrow \gamma\gamma \rightarrow t\bar{t}H$ will be considerably smaller if the realistic photon spectrum is used.

The beam energy dependence is also reflected by the parametrisation, and the fit is performed for several beam energies at the same time. This way, the parametrisation can be used for arbitrary energies between 50 GeV and 500 GeV.

It should be noted that energy correlations between the two beams of a photon collider are neglected. However, the fit is performed in a way that the parametrisation describes the high-energy part of the two-photon spectrum, obtained by full simulation, very well. As already pointed out, it is this part of the two-photon spectrum which is needed in our application. We may therefore just use the product of two photon spectra given by `CompAZ`, as it is done in Ref. [6]. Note further that the Photon Collider, which underlies
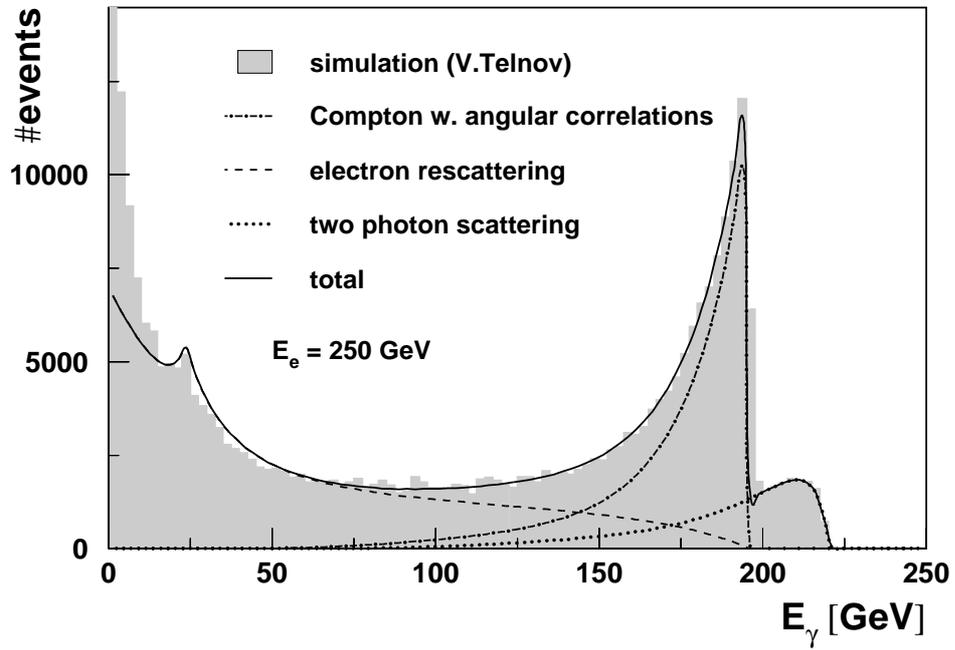
Figure 2.11: Parametrisation of the photon spectrum and the full simulation. The Figure has been taken from Ref. [6].

the full beam simulation, refers to the proposal for TESLA (TeV-Energy Superconducting Linear Accelerator) [34].

Chapter 3

Calculations

This chapter contains the actual calculations. We outline our approach in Section 3.1. In Section 3.2, we explain the evaluation of the basis integrals. The cancellation of the occurring IR and UV divergences is shown in Section 3.3, where also the relevant renormalisation constants are derived. Section 3.4 contains details on the calculations. Finally, we discuss various checks of our calculations in Section 3.5.

3.1   General Approach

The general setup of the process under consideration has been discussed in Section 2.1. We will now give an outline of our actual calculations. We first consider the subprocess $\gamma\gamma \to t\bar{t}H$. The diagrams at Born level and at the NLO level are generated and drawn with the `Mathematica` package `FeynArts` [35]. Sample diagrams have already been shown in Fig. 2.1 respectively in Figs. 2.2, 2.3, 2.4, 2.5, and 2.6. We then use `FeynArts` in order to automatically construct the analytic expressions pertaining to the various diagrams. The `Mathematica` package `FormCalc` [36] transforms these expressions into `Form` [37] code in order to deal with them further. This `Form` code is written to disk before any manipulations are performed by `FormCalc`. It presents the starting point for self-made routines which perform the computation of the cross section.

Born Level

Let us start with the Born level. The automatically generated analytic expressions are further processed by means of a `Form` program. This program first exploits momentum conservation (2.2). Then it simplifies the Dirac structure. To this end, contracted Lorentz indices as well as multiple occurrences of the same slashed momentum are eliminated, and the Dirac equations (2.7) are applied. Here, we also make use of the Dirac algebra which reads:

$$\{\gamma^\mu, \gamma^\nu\} = 2g^{\mu\nu}\,. \tag{3.1}$$

Next, the on-shell conditions (2.3, 2.6) are imposed. The colour algebra is trivial which has already been mentioned in Section 2.1. In a further step, the Dirac structure is brought to the form specified in Eqs. (2.8, 2.9). In principle, one could project out the coefficients of the different structures. However, the general structure is quite complex in our case. We therefore exploit the Dirac algebra of Eq. (3.1) in order to achieve this goal. The scalar products of external momenta are now expressed in terms of the kinematical invariants defined in Eq. (2.4). We also check analytically that the Ward identities are fulfilled (see further Section 3.5). Note that the matrix element for the Born level does not contain the parameter $\epsilon = (4 - d)/2$. Finally, the resulting expression is stored to disk.

In order to have smaller expressions, which are more convenient to deal with, we will usually extract the coefficients $U^{(i)}$, $U^{(i)}_{j_1 j_2}$, $X^{(i)}_j$, $Y^{(i)}_j$, and $Z^{(i)}$ of the 68 structures, which are specified in Eqs. (2.8, 2.9, 2.10). This is also done by means of a `Form` program. The 68 expressions are then stored to disk.

We now want to simplify these expressions and transform them into code which is understandable by `Fortran`. To this end, we first use a `Perl` script to change the output into `Mathematica` code. A `Mathematica` script is then applied which converts the expressions into a simpler form. Afterwards, a `Perl` script is used as an interface between `Mathematica` and `Fortran`. This `Perl` script not only translates the `Mathematica` output to `Fortran` code, but also adds some further `Fortran` code, that turns the expressions into `Fortran` functions. These functions can directly be used in a `Fortran` program for performing the phase space integrations. They can furthermore be pre-compiled and collected in `Fortran` libraries, which is very convenient. The application of the diverse scripts to the different expressions is automatised by means of a makefile.

Real Correction

Now we turn to the real correction. The calculation initially follows the line of the Born calculations. Here, momentum conservation is given by Eq. (2.14), and we use in addition Eqs. (2.13). But instead of bringing the expression to a certain form and extracting the respective coefficients, we directly build the squared and summed matrix element. In contrast to the virtual part, which will be discussed next, the resulting expression stays reasonably small.

The averaging over the polarisations of the initial state photons and the summing over the spins of the final state quarks is done in the common way by exploiting the completeness relations of the quarks,

$$\sum_{Spins} u(p_3)\bar{u}(p_3) = \slashed{p}_3 + m_t \,, \tag{3.2}$$

$$\sum_{Spins} v(p_4)\bar{v}(p_4) = \slashed{p}_4 - m_t \,, \tag{3.3}$$

and using the prescription

$$\sum_{Polarisations} \epsilon_i^\mu \epsilon_i^{*\nu} \longrightarrow -g^{\mu\nu} \ \text{ with } \ i \,\epsilon\, \{1, 2\} \,, \tag{3.4}$$

which leads to the right results due to Ward identities. The summing over the polarisations of the final state gluon can be carried out using the same prescription.

For the real correction, the dimension can be set to four, as explained in Section 2.3. Furthermore, we again employ the on-shell conditions, introduce kinematical invariants and also make use of the relation given in Eq. (2.15). The resulting expression is then stored to disk. As in the case of the Born calculations, it is now treated with `Mathematica` and turned into a `Fortran` function.

Virtual Correction

Finally, we have to deal with the virtual correction. After the trivial colour algebra has been worked out, we cancel squared loop momenta, which may appear in the numerator, against the denominators of the respective terms. Next, we introduce the notation of tensor integrals. The latter include the propagators contained in a loop as well as the loop momenta in the numerator, as specified in Eq. (2.16). The tensor integrals are now reduced

to generalised scalar integrals (see Section 2.2). Again, momentum conservation is applied, the Dirac structure is simplified, the on-shell conditions are employed, the Dirac structure is brought to the general form, and the kinematical invariants are introduced. The resulting expression is stored to disk.

The generalised scalar integrals are to be reduced to a basis set of integrals. The respective method has been outlined in Section 2.2. In the case of non-exceptional phase space points, this reduction can be performed in `Fortran` or already in `Form`. We will follow both paths. The comparison of the numerical results, obtained in these two independent ways, presents a strong check on the calculations. We now explain in turn both approaches.

In the first case, we discard the UV-divergent integrals from the expressions and rename the remaining ones. This way, the main `Fortran` program will recognise that these integrals still have to be reduced. We then extract the coefficients of the 68 structures and write them to disk. Note that the dimension may not be set to four, as pointed out in Section 2.2. Again, we treat the coefficients with `Mathematica` and turn them into `Fortran` functions.

In the second variant, we may set the dimension to four. This has also been argued in Section 2.2. We then apply the diverse recursion relations pertaining to the non-exceptional case. From the resulting expression we separately extract the contributions stemming from the six-dimensional pentagon integrals, the IR-divergent integrals, and the finite part. In each case, the coefficients of the 68 structures are extracted, simplified with `Mathematica`, and turned into `Fortran` functions.

In the case of exceptional phase space configurations, the application of the various recursion relations depends on the actual phase space point. We are thus forced to perform the reduction directly in the main `Fortran` program in such cases.

The UV-divergent generalised scalar integrals are not reduced further but directly extracted. However, here we may not set ϵ to zero. If it occurs as a prefactor of such an integral, we get additional finite terms through the multiplication of ϵ and the $1/\epsilon$-term of the UV-divergent integral. This can conveniently be accounted for by using Eq. (2.30), which gives the coefficients of the $1/\epsilon$-poles of the integrals. The resulting expression is stored, and the 68 coefficients are again simplified and turned into `Fortran` functions.

We also want to directly read off the IR-divergence structure from the original integrals. This way, we get a compact expression for the IR-divergent part of the matrix element. It will be used in the analytic cancellation of the

IR divergences. Furthermore, in the second reduction variant, we use it for taking into account the coefficients of order $\mathcal{O}(\epsilon)$. Above, the tensor integrals have been reduced to generalised scalar integrals. In order to obtain `Fortran` functions which contain the 68 coefficients of the compact expression, we follow the same line. But, in this case, we use Eq. (2.31) for the reduction. The $\mathcal{O}(\epsilon)$-coefficients are taken into account by renaming an integral if it is multiplied by ϵ. The respective factor ϵ is then set to one. The renaming indicates that, instead of the finite part, the coefficient of the $1/\epsilon$-pole of the integral has to be calculated in the main `Fortran` program. Furthermore, we separately tag the terms containing a factor ϵ and those which do not. The first contribution comprises all additional finite terms due to $\mathcal{O}(\epsilon)$-terms. The second one can be used for the cancellation of the IR divergences, which is done in Section 3.3.

In the case where the reduction of the generalised scalar integrals is performed directly within `Fortran`, we generally have to deal with $\mathcal{O}(\epsilon)$-terms. This is done in the same way as above by introducing a new name for a divergent integral multiplied by a factor of ϵ.

Renormalisation

In order to cancel the divergences of UV-nature, we have to renormalise the top-quark mass and its wavefunction. In case of the wavefunction renormalisation, we just have to multiply the Born level matrix element by $Z_V^{1/2} Z_V^{1/2}$ $= Z_V = (1 + \delta Z_V + \ldots)$, where δZ_V is the corresponding renormalisation constant at one-loop order and the ellipsis indicates higher-order terms. One factor $Z_V^{1/2}$ represents the wavefunction renormalisation of the quark while the other belongs to the anti-quark. The terms proportional δZ_V are the desired contributions from wavefunction renormalisation. For the top-quark mass renormalisation, we have to substitute the bare mass by $(m_t + \delta m_t)$ and perform a series expansion in δm_t, where δm_t is the respective renormalisation constant at one-loop order. The linear terms in δm_t are the contributions from the mass renormalisation. The two renormalisation constants are derived in Section 3.3. As we will see in that Section, the wavefunction renormalisation constant contains poles of UV- as well as of IR-nature. However, these can be disentangled so that the cancellation of the divergences can be verified separately for both types. The renormalisation contributions, which have been obtained this way, are now summed up. The further procedure is analogue to the Born calculations.

Squaring and Summing the Matrix Elements

Above, we obtained the coefficients of the 68 structures for the Born level matrix element and for the various contributions of the virtual correction (in the form of `Fortran` functions). However, the cross section is built from the squared matrix element (see Eq. (2.12)). Furthermore, we consider the case of unpolarised external particles. In order to get the squared and summed matrix element, we proceed as follows. First, we take the Born level expression and follow the line of the corresponding calculations up to the point where the coefficients of the 68 structures are extracted. Instead, we multiply this expression in turn with the 68 structures, without any coefficients. Thus, we get 68 expressions, all of which involve the Born matrix element and one of the 68 structures. These structures contain all Dirac matrices and polarisation vectors of an amplitude. The squaring and summing is performed in the same way as for the real correction, separately for each of the 68 expressions. In detail, we revert the order of the Dirac matrices in the Born matrix element, insert the completeness relations for the quarks, apply Eqs. (3.4), and take the trace. The full squared and summed matrix element can now be built up by multiplying each of the expressions by the corresponding coefficient and summing over them. As mentioned above, the coefficients are already available in the form of `Fortran` functions. After the squaring and summing has been performed, the on-shell conditions are applied once more, and contracted external momenta are again substituted by the kinematical invariants. The 68 resulting expressions are then simplified with `Mathematica` and turned into `Fortran` functions.

Note that it is not possible to build up the squared matrix element directly within a `Form` program because of the size of the expressions. Note further that the Born matrix element is a real expression, apart from the spinors and polarisation vectors. The complex conjugations on the right-hand side of Eq. (2.12) therefore only have an effect in Eqs. (3.2,3.3,3.4). The same is true for the matrix element of the real correction.

In order to have a check on this procedure, we also follow a slightly different path. We multiply each of the 68 structures in turn with each of the same 68 structures, without any coefficients. This way, we get a $(68, 68)$-matrix. For each of these matrix elements the squaring and summing is performed as above, and the resulting expressions are turned into `Fortran` functions. Here, we refrain from a simplification with `Mathematica`. The full squared and summed matrix element can now be built up by combining

each of the $(68 \cdot 68)$ expressions with the two corresponding coefficients and summing over these.

Further $\mathcal{O}(\epsilon)$-Induced Terms

As it turns out, the squaring and summing leads to terms which contain the parameter ϵ. These again lead to additional finite terms whenever they combine with the pole-parts of divergent integrals. In the following, we will discuss how these are taken into account. However, we will need the coefficients of the $\mathcal{O}(\epsilon)$-terms of above 68 expressions. Therefore, in above calculation, we separately extract the coefficients of the $\mathcal{O}(\epsilon^0)$-part and of the $\mathcal{O}(\epsilon^1)$-part of the 68 structures and turn them into different `Fortran` functions. Let us call the former b_j^0 and the latter b_j^1, with $j \in \{1, \ldots, 68\}$.

We now discuss the treatment of the above-mentioned $\mathcal{O}(\epsilon)$-terms. As it will turn out in Section 3.3, the UV divergences cancel for each of the coefficients of the 68 structures separately. Therefore, above 68 expressions are always multiplied by a UV-finite coefficient. However, this is not the case for the IR divergences. These only vanish after squaring and summing. In the latter case, the $\mathcal{O}(\epsilon)$-terms have to be taken into account. This is done in a different way for both evaluations of the virtual part. In the case where the reduction is performed within the main `Fortran` program, we add up all different sources of IR divergences and multiply them by the factor ϵ. Then the coefficients of the 68 structures are extracted, simplified with `Mathematica`, and turned into `Fortran` functions. The latter can now be combined with the b_j^1 functions in order to get the additional contributions. The IR divergences stem from three different sources. First, the genuine virtual correction contributes. Second, we have to take into account the IR part of the wavefunction renormalisation. These contributions are obtained as described above. Third, the subtraction term for the virtual part has to be taken into account. It is specified in Eq. (2.54) and the following. Here, we only take the Born matrix element instead of its square in Eq. (2.54).

In the case where the reduction has already been performed within `Form`, we take the compact IR-divergent expression for the contribution from the genuine virtual correction. We only keep the coefficients of the pole-parts of the three different contributions. The pole-parts of the IR-divergent triangles are obtained in Section 3.2. Then we perform the squaring and summing directly within the `Form` program, as in the case of the real correction. The coefficient of the $\mathcal{O}(\epsilon)$-part of the result comprises the desired finite contri-

butions. It is extracted, simplified with `Mathematica`, and turned into a
`Fortran` function.

Subtraction Terms

In Section 2.3, we saw that the virtual and the real corrections cannot directly
be integrated numerically over the respective phase spaces. We therefore
build the subtracted expressions as specified in Eq. (2.39). To this end, we
implement the subtraction terms for the virtual part (2.42 and the following)
and for the real part (2.54 and the following) in `Fortran` functions. In case
of the real expression, we have to take into account that the squared matrix
element occurring in the two contributions (2.43, 2.44) is calculated in each
case for the respective transformed momenta.

Full Squared and Summed Matrix Elements

All the ingredients are now in place, and we can construct the full squared
and summed (subtracted) matrix elements within a `Fortran` program. We
begin with the Born level. Here, we just have to multiply each of the b_j^0
functions with the corresponding coefficient at Born level and sum over the
68 contributions. As a check, we also take the $(68 \cdot 68)$ expressions obtained
above, multiply each by the two corresponding coefficients at Born level, and
sum.

We now turn to the contribution of order $\mathcal{O}(\alpha_s)$. Here, we always use
the b_j^0 functions. The corresponding coefficients are sums of the different
contributions which we obtained above. Furthermore, we have to take into
account the additional finite contributions due to $\mathcal{O}(\epsilon)$-terms which stem
from squaring and summing. However, in the case of non-exceptional phase
space configurations, we have two independent possibilities to evaluate the
virtual part. Let us again first consider the case where the reduction is
performed in the main `Fortran` program.

This variant is also used for exceptional phase space points where the
other one is not applicable. The coefficients contain

- the UV-finite part of the genuine virtual correction,

- the UV-divergent integrals,

- the renormalisation contributions.

The additional finite contributions have also been calculated above. These are combined with the b_j^1 functions instead of the b_j^0 functions. The two resulting expressions are added up to give the full virtual correction.

In the case of the second variant, the reduction has already been performed in a `Form` program. The coefficients are the sums of the following contributions:

- the finite part,

- the IR-divergent part,

- the $\mathcal{O}(\epsilon)$-induced terms of the compact expression for the IR-divergent part,

- the UV-divergent integrals,

- the renormalisation contributions.

Here, the additional finite contributions are comprised by a single `Fortran` function which only has to be added.

The real correction is also contained in a single `Fortran` function. Both the virtual and the real correction can now be combined with the respective subtraction terms.

We like to emphasise that all $\mathcal{O}(\epsilon)$-induced finite terms have properly been taken into account. The cancellation of the UV and IR divergences is, however, postponed to Section 3.3.

As a result of the preceding calculations, we obtain the squared and summed matrix element at Born level as well as the subtracted expressions for the NLO correction. In the main `Fortran` program, we numerically integrate these expressions over the corresponding phase spaces. We need a $(2 \rightarrow 3)$ and a $(2 \rightarrow 4)$ phase space. The former is taken from Version 3.2 of `FormCalc` [36], while the latter stems from Version 5.2 [38]. In the latter Version, an arbitrary phase space can be built up iteratively. The numerical integrations are performed with the Monte Carlo program `Vegas` from the `CUBA` library [39]. The `CUBA` library contains three further programs for numerical integrations. These are used in order to assess the numerical reliability of the integration.

The main `Fortran` program also provides the basis integrals which are the endpoints of the reduction procedure. The calculation of these is postponed to Section 3.2. In order to get a prediction for the parent process, we finally

have to integrate over the photon spectra, as specified in Eq. (2.67). This is done together with the phase space integrations by the Monte Carlo program `Vegas`. Further details on the evaluation of the cross sections will be given in Section 3.4.

3.2 Basis Integrals

The reduction of the generalised scalar integrals finally leads to a number of basis integrals, which have to be provided by the main `Fortran` program. For non-exceptional phase space configurations, these integrals have been listed in Section 2.2. However, it has been mentioned that the recursion relations lead outside the UV/IR boundaries for exceptional phase space configurations. We therefore need the basis self-energy integrals as well as the basis triangle integrals with an IR-divergent configuration for arbitrary dimensions and powers of propagators. Note further that the UV-divergent integrals produced by the reduction procedure are not regularised anymore.

In the case where the reduction is performed directly within the main `Fortran` program, we do not extract the IR-divergent part and the $\mathcal{O}(\epsilon)$-terms are always taken into account. For these reasons, the six-dimensional box integral may be replaced by the four-dimensional one, though the latter can be IR divergent. However, the reduction within `Form` still considers the six-dimensional box integral as the basis integral. If the respective expressions are used, this integral is further reduced by the main `Fortran` program so that we are left with the four-dimensional one also in this case. In Section 2.2, it has also been pointed out that the six-dimensional pentagon integral does not contribute at NLO. This finite integral always occurs with a prefactor of order $\mathcal{O}(\epsilon)$. For the process under consideration, the four-dimensional basis integrals with all propagator powers equal to one can be calculated by means of the program package `LoopTools` [36], which is based on the `FF` package [40]. This will be discussed further below.

Before the reduction is performed, the UV-divergent generalised scalar integrals are extracted. These are considered as basis integrals. In the process under consideration, they are given by (see Eq. (2.20)):

- the four-dimensional self-energy integrals with both propagator powers equal to one,

- the six-dimensional self-energy integrals with one propagator power

equal to one and the other one raised to the value two,

- the six-dimensional triangle integrals with all propagator powers equal to one.

However, we choose to reduce the six-dimensional triangle integrals further down within the main `Fortran` program. Note again that the $\mathcal{O}(\epsilon)$-terms are always accounted for in this reduction.

We are now left with the following integrals which have to be provided by the main `Fortran` program:

- the four-dimensional triangle and box integrals for all powers of propagators equal to one,

- the self-energy integrals for arbitrary dimensions and powers of propagators,

- the triangle integrals with an IR-divergent configuration for arbitrary dimensions and powers of propagators.

Treatment of Divergences

Let us begin with the four-dimensional integrals which do not have raised propagator powers. As mentioned above, we calculate them by means of the program package `LoopTools`. Finite integrals can be calculated without any further considerations. On the other hand, `LoopTools` uses dimensional regularisation in order to deal with UV divergences, while it employs a small mass to regulate IR divergences. The IR divergences thus manifest themselves through logarithms in the small regulator mass. In this work, dimensional regularisation is applied for both types of singularities. However, we only encounter soft IR divergences. In this case, there exists a general prescription which allows to rewrite the result for a mass regulator in terms of dimensional regularisation (see for example Ref. [30]):

$$\ln\left(\lambda^2\right) \longrightarrow \frac{(4\pi\mu^2)^\epsilon \, \Gamma(1+\epsilon)}{\epsilon} + \mathcal{O}(\epsilon)\,, \qquad (3.5)$$

where λ denotes the mass regulator and μ is the dimensional-regularisation scale. If we perform a series expansion on the right-hand side of this prescription and subtract $\ln\left(m_t^2\right)$ on both sides, we find:

$$\ln\left(\frac{\lambda^2}{m_t^2}\right) \longrightarrow \frac{1}{\epsilon} - \gamma_E + \ln(4\pi) + \ln\left(\frac{\mu^2}{m_t^2}\right) + \mathcal{O}(\epsilon)\,, \qquad (3.6)$$

where γ_E is Euler's constant. In any case, `LoopTools` considers the regulator λ as infinitesimally small. It is only kept as an argument for logarithms, otherwise it is set to zero. If we set $\lambda^2 = m_t^2$, the left-hand side of Eq. (3.6) is equal to zero. Accordingly, `LoopTools` returns a result in dimensional regularisation where

$$\frac{1}{\epsilon} - \gamma_E + \ln(4\pi) + \ln\left(\frac{\mu^2}{m_t^2}\right) \tag{3.7}$$

has been set to zero. We know that all poles in ϵ have to cancel out. If we always extract above expression, then also its finite terms have to cancel each other in the end. In conclusion, if we always set $\lambda^2 = m_t^2$ within `LoopTools`, we get a finite result for the respective IR-divergent integral where the pole-part in terms of Eq. (3.7) has been subtracted. The additional finite terms in Eq. (3.7) cancel out together with the $1/\epsilon$-poles. We can therefore use `LoopTools` in order to obtain the finite parts of the IR-divergent four-dimensional integrals, without raised propagator powers, in dimensional regularisation.

However, an integral may be multiplied by the factor ϵ. In this case, the integral is always renamed so that the main program recognises that it has to calculate the coefficient of the respective $1/\epsilon$-pole. These coefficients are directly implemented in the `Fortran` program. The IR-divergent parts of the box integrals are taken from Ref. [41], and the ones for the triangle integrals are extracted from Ref. [42] and compared with Ref. [41]. Also in Ref. [41], a mass regulator is used. The transformation is again performed with Eq. (3.5). Note that an IR-divergent integral is obtained by pinching propagators of a pentagon integral. The resulting integral is IR divergent if the gluon propagator is still present and attached to top-quark propagators which are on-shell. We therefore have one topology for IR-divergent triangle integrals and two different topologies for the divergent boxes. In the case of the box integrals, either one external leg is light-like or all external legs are massive.

We will also need the self-energy integrals, which are UV divergent. `LoopTools` expresses the UV divergences in terms of

$$\Delta = \frac{1}{\epsilon} - \gamma_E + \ln(4\pi)\,. \tag{3.8}$$

It is well-known that the additional finite terms always occur and drop out together with the $1/\epsilon$-pole. We set Δ equal to zero, and we furthermore

choose $\mu^2 = m_t^2$, where μ is the dimensional-regularisation scale introduced by `LoopTools`. This way, the pole-part is subtracted in terms of the same expression as in the case of the IR-divergent integrals (3.7). Again, the pole-terms are needed in order to account for $\mathcal{O}(\epsilon)$-terms. For the self-energy integrals, these are well-known.

Note that we do not have to compute the imaginary parts of the basis integrals. The squared matrix element is built according to Eq. (2.12). The Born level matrix element, which occurs in Eq. (2.12), is real, apart from the spinors and polarisation vectors. The only sources of imaginary contributions to the matrix element at NLO are the basis integrals, again apart from the spinors and polarisation vectors. We sum over all spins and polarisations by means of Eqs. (3.2,3.3,3.4). Hence, the basis integrals deliver the only imaginary contributions within the formula for the squared and summed matrix element. Consequently, they are not needed.

Reduction of Basis Self-Energies

The four-dimensional triangle and box integrals with all propagator powers equal to one are now in place. Furthermore, the respective self-energy integrals have been dealt with. Let us now turn to the self-energy integrals with arbitrary dimensions and powers of propagators. These can be further reduced to four-dimensional self-energy and tadpole integrals with propagator powers equal to one. The calculation of the tadpoles is trivial while the self-energies are already in place. Let us now discuss the reduction procedure.

We apply the integration by parts identity of Refs. [24] for the two differential operators

$$\frac{\partial}{\partial \ell_\mu}(\ell)^\mu \quad \text{and} \quad \frac{\partial}{\partial \ell_\mu}(\ell + q_1)^\mu \tag{3.9}$$

to the generalised scalar self-energy integrals. In addition, we apply Eq. (2.22) which relates integrals of different dimensions. We thus get three relations, which can be used in order to reduce these integrals to the master integrals. The reduction can be done completely automatically by means of the program `AIR` of Ref. [43].

In order to keep the expressions for the diverse integrals compact, we proceed as follows. The complexity of an integral is given by $s = (\sigma + (n-4)/2)$, where σ was the sum of the propagator powers and $n = (D + 2\epsilon)$. For $n = 4$ and all propagator powers equal to one or to zero, the respective integral is a

master integral. If we now raise s by one, we get the next-complicated integrals. These are reduced to the master integrals through `AIR`. We then again raise s by one and reduce the corresponding integrals. This time, however, all the integrals are considered as master integrals which have already been reduced, so that the reduction ends at them. This procedure is repeated up to the value $s = 18$. All integrals with a value of s up to $s = 18$ are now successively expressed through simpler ones, down to the true master integrals. This way, the expressions indeed remain very compact.

Special Cases for Basis Self-Energies

However, there occur special cases for the self-energy integrals which have to be treated separately. If one propagator is massless and the propagator momentum squared is equal to m_t^2 respectively if both propagators are massive and the momentum squared is zero, we get zeros in denominators of above expressions. But these special cases are simple enough to be provided in closed form. This is done in the following. The integrals read:

$$I_1 = \int \frac{d^D \ell}{(2\pi)^D} \frac{1}{[\ell^2]^\alpha \, [\ell^2 - 2\ell \cdot q_1]^\beta} \quad \text{with} \quad q_1^2 = m_t^2 \,, \tag{3.10}$$

$$I_2 = \int \frac{d^D \ell}{(2\pi)^D} \frac{1}{[\ell^2 - m_t^2]^\alpha \, [\ell^2 - 2\ell \cdot q_1 - m_t^2]^\beta} \quad \text{with} \quad q_1^2 = 0 \,. \tag{3.11}$$

We use the Feynman parametrisation in order to evaluate the integrals, which is given by:

$$\frac{1}{a^\alpha b^\beta} = \frac{\Gamma(\alpha + \beta)}{\Gamma(\alpha)\Gamma(\beta)} \int_0^1 dx \, \frac{x^{\beta-1}(1-x)^{\alpha-1}}{[a + (b-a)x]^{\alpha+\beta}} \,, \tag{3.12}$$

where a and b can be chosen as the two propagators of Eq. (3.10) or Eq. (3.11). In the first case, this leads to:

$$\begin{aligned} I_1 \quad &= \quad \frac{\Gamma(\alpha + \beta - D/2)}{\Gamma(\alpha)\Gamma(\beta)} \cdot \frac{i(-1)^{\alpha+\beta}}{(4\pi)^{D/2}} \cdot \\ & \int_0^1 dx \, x^{(D-2\alpha-\beta-1)} (1-x)^{(\alpha-1)} \left(m_t^2 \right)^{(D/2 - \alpha - \beta)} \,, \end{aligned} \tag{3.13}$$

where the integration over the loop momentum has been performed in the common way. Using the well-known result for the Beta-function,

$$\int_0^1 dt \, t^{(x-1)} (1-t)^{(y-1)} = \frac{\Gamma(x)\Gamma(y)}{\Gamma(x+y)} \,, \tag{3.14}$$

we get:

$$
\begin{aligned}
I_1 \;=\; & \frac{i}{16\pi^2} \cdot \frac{1}{(4\pi)^{-\epsilon}} \cdot (-1)^{(\alpha+\beta)} \cdot \left(m_t^2\right)^{(D/2-\alpha-\beta)} \cdot \\
& \frac{\Gamma(\alpha+\beta-D/2)\Gamma(D-2\alpha-\beta)}{\Gamma(D-\alpha-\beta)\Gamma(\beta)} \; .
\end{aligned}
\tag{3.15}
$$

The second case can be treated in the same way. This leads to:

$$
I_2 = \frac{i}{16\pi^2} \cdot \frac{1}{(4\pi)^{-\epsilon}} \cdot (-1)^{(\alpha+\beta)} \cdot \left(m_t^2\right)^{(D/2-\alpha-\beta)} \cdot \frac{\Gamma(\alpha+\beta-D/2)}{\Gamma(\alpha+\beta)} \; .
\tag{3.16}
$$

Note that the special case of both propagators being massive and the squared momentum being equal to $4m_t^2$ is not provided. However, we do not encounter problems during the numerical evaluations. Note further that above reduction procedure is performed separately for the two cases of only one propagator being massive or both. This is again necessary to avoid zeros in denominators.

Reduction of Basis Triangles

Finally, we need the generalised triangle integrals with an IR-divergent configuration. We encounter only one such topology. Such integrals cannot be reduced further by means of the recursion relations which pertain to non-exceptional momentum configurations. The determinant of the kinematical matrix is always zero so that it cannot be inverted. However, the determinant of the Gram matrix may only tend to zero for exceptional momentum configurations. We treat these cases by the alternative recursion relations within the main `Fortran` program. For non-exceptional phase space points, we may either reduce them further within `Fortran` or by means of the program `AIR`. However, since the determinant of the kinematical matrix is always zero, we choose to use `AIR` up to the value $s = 14$. Only when the recursion relations for the exceptional momentum configurations lead to integrals with a higher value for s, these are first reduced further within `Fortran`.

For the reduction of the triangle integrals within `AIR`, we need Eq. (2.22) and, in addition, the three relations which are obtained by applying the integration by parts identity of Refs. [24] for the three differential operators

$$
\frac{\partial}{\partial \ell_\mu}(\ell)^\mu \,, \quad \frac{\partial}{\partial \ell_\mu}(\ell+q_1)^\mu \,, \quad \frac{\partial}{\partial \ell_\mu}(\ell+q_2)^\mu
\tag{3.17}
$$

to the generalised scalar triangle integrals.

In conclusion, arbitrary generalised triangle integrals with an IR-divergent configuration can, in principle, be evaluated. However, the self-energy integrals are only available up to $s = 18$. This sets a limit on the number of iterations in the case of exceptional momentum configurations. The more iterations are performed the larger values for s appear in the reduction.

Details on the Implementation

When we use `AIR`, an integral is automatically expressed in terms of the simpler ones. However, also the successive preparation of the list with master integrals and the invocation of `AIR` are done completely automatically by means of a `Perl` and a shell script. The resulting expressions are written to disk by the `Maple` program `AIR`. These are now expanded within `Mathematica` and turned into `Form`-readable code. The `Form` program performs a series expansion in ϵ. Afterwards, it is checked whether the reductions within `AIR` have introduced $1/\epsilon$-terms as prefactors of integrals. As it turns out, this is not the case so that the only $1/\epsilon$-terms stem from the integrals themselves. For this reason, the master integrals only have to be known up to and including contributions of order $\mathcal{O}(\epsilon^0)$. The resulting expressions are simplified with `Mathematica` and turned into `Fortran` functions. All this is done automatically by means of makefiles and `Perl` scripts.

In addition, interface functions are produced. The arguments of these specify the powers of the propagators, the dimension, and the desired coefficient of the Laurent expansion of the integral which is to be evaluated. We have two such interface functions for the self-energy integrals since the case with one propagator being massless is treated separately. One further interface function is needed for the triangle integrals. In the main `Fortran` program, such a function is called with arguments which correspond to the desired integral. The interface function then calls the respective function which contains the reduction of the integral to simpler integrals. The reduction now proceeds without the need for further interface functions. Finally, the master integrals are reached, which have to be provided by the main `Fortran` program. The use of an interface function is more convenient than collecting all the expressions of the reductions in one function. The `Fortran` functions which contain the reductions as well as the interface functions are now precompiled and collected in libraries.

Calculation of $1/\epsilon$-Poles

We can also use above expressions in order to calculate the coefficients of the $1/\epsilon$-poles of the basis triangle integrals. Instead of turning them into `Fortran` functions, we transform them into `Form` code. A `Form` program is now applied which inserts only the divergent parts of the integrals. We start with the simplest integrals, which are expressed through master integrals. The master integrals are replaced by their pole parts. We then proceed with the next-complicated integrals. Finally, we obtain explicit expressions for the divergences of the basis triangle integrals. Since we only insert the pole parts, also these expressions remain compact. They can be used as a means of checking the results and for the cancellation of the divergences. The procedure is again automatised with the help of a makefile. Furthermore, when the integrals for a certain value of s have been treated, they are simplified by `Mathematica`, the connections again being made by Perl scripts.

However, only two IR-divergent integrals occur in the expressions for the IR-divergent part of the virtual correction. These are given by

- the four-dimensional integral with an IR-divergent configuration and all propagator powers equal to one,

- the six-dimensional integral with an IR-divergent configuration and only the massless propagator raised to the power two.

If a different propagator is raised to the power two while the others have power one, the integral is finite, though it has an IR-divergent configuration. It turns out that the divergent part of the second integral is the same as for the first one except for the sign. As said above, we take the real part of the pole term from Ref. [42] and check it against Ref. [41]. We get:

$$
\begin{aligned}
I_3^{IR}(4 - 2\epsilon; \{q_i\}, 1, 1, 1)\Big|_{pole,\,real} &= \\
-I_3^{IR}(6 - 2\epsilon; \{q_i\}, 1, 1, 2)\Big|_{pole,\,real} &= \frac{1}{\epsilon} \cdot \frac{1}{s_{34}\,\beta_{12}} \ln\left(\frac{1 - \beta_{12}}{1 + \beta_{12}}\right),\ (3.18)
\end{aligned}
$$

with

$$
\beta_{12} = \sqrt{1 - \frac{4m_t^2}{s_{34}}}\,. \tag{3.19}
$$

The superscript IR means that the integral has the mass and momentum configuration of an IR-divergent triangle integral. In the second row of Eq. (3.18), the raised propagator belongs to the gluon.

The variable β_{12} is equal to $\tilde{v}_{34}$ of Eq. (2.63). Thus, the logarithm which appears in Eq. (3.18) is the same as the one of the subtraction term for the virtual part (see Eq. (2.66)). This is important for the cancellation of the IR divergences, which is shown in Section 3.3.

3.3 Cancellation of Divergences

In this Section, we discuss the cancellation of the UV and IR divergences. But at first, we have to calculate the relevant renormalisation constants.

Renormalisation Constants

It has already been mentioned in Section 3.1 that the wavefunctions of the top and anti-top quarks as well as the top-quark mass have to be renormalised. We need only one wavefunction renormalisation constant since left- and right-handed particles are not distinguished within QCD. We compare the general expressions for the renormalisation constants with Ref. [44].

Note that the top quark is an unstable particle. Unstable particles have complex self-energy amplitudes so that their resummed propagators have complex poles. In that case, the renormalisation conditions are more complicated (see, for instance, Refs. [45]). However, the self-energy amplitude of the top quark is real to the order considered in this work. We can therefore restrict ourselves to the case of stable particles. For the same reason, we are not concerned with finite width effects.

We define the amputated one-particle-irreducible self-energy of the top quark as:

$$i\Sigma(q) = i\slashed{q}\Sigma_V(q^2) + im_t^0\Sigma_S(q^2)\,, \tag{3.20}$$

with the bare mass of the top quark denoted as m_t^0 and the external momentum as q. The bare mass m_t^0 and the bare field ψ_t^0 are expressed through renormalised parameters and counterterms according to:

$$
\begin{aligned}
m_t^0 &= m_t + \delta m_t\,, \\
\psi_t^0 &= \psi_t\sqrt{Z_V} = \psi_t\left(1 + \frac{1}{2}\delta Z_V\right)\,.
\end{aligned} \tag{3.21}
$$

δm_t and δZ_V are the renormalisation constants at one-loop order as introduced in Section 3.1. We now sum up the Dyson series with respect to the top-quark propagator. The application of renormalisation conditions

will then give the general expressions for the renormalisation constants. We have:

$$
\begin{aligned}
S^{-1}(q) &= \frac{i}{\slashed{q} - m_t^0} \cdot \sum_{n=0}^{\infty} \left(\frac{i(i\slashed{q}\Sigma_V(q^2) + im_t^0\Sigma_S(q^2))}{\slashed{q} - m_t^0} \right)^n \\
&= \frac{i}{\slashed{q} - m_t^0} \cdot \sum_{n=0}^{\infty} \left(-\frac{(\slashed{q}\Sigma_V(q^2) + m_t^0\Sigma_S(q^2))}{\slashed{q} - m_t^0} \right)^n \\
&= \frac{i}{\slashed{q} - m_t^0} \cdot \frac{1}{1 + \frac{\slashed{q}\Sigma_V(q^2)+m_t^0\Sigma_S(q^2)}{\slashed{q}-m_t^0}} \\
&= \frac{i}{\slashed{q} - m_t^0 + \slashed{q}\Sigma_V(q^2) + m_t^0\Sigma_S(q^2)} \,.
\end{aligned}
\tag{3.22}
$$

We now demand that the renormalised mass is identical to the pole of the propagator including all radiative corrections:

$$
S(q) \cdot u(q)|_{q^2=m_t^2} \overset{!}{=} 0 \,.
\tag{3.23}
$$

Using Eqs. (3.22, 3.21) and the Dirac equation for the top-quark spinor,

$$
\slashed{q} \cdot u(q) = m_t \cdot u(q) \,,
\tag{3.24}
$$

this leads to:

$$
\begin{aligned}
&\left(\slashed{q} - m_t^0 + \slashed{q}\Sigma_V(q^2) + m_t^0\Sigma_S(q^2) \right) \cdot u(q)|_{q^2=m_t^2} = \\
&\left(\slashed{q} - m_t - \delta m_t + \slashed{q}\Sigma_V(q^2) + m_t\Sigma_S(q^2) + \delta m_t\Sigma_S(q^2) \right) \cdot u(q)|_{q^2=m_t^2} = \\
&\left(-\delta m_t + m_t\Sigma_V(q^2) + m_t\Sigma_S(q^2) + \delta m_t\Sigma_S(q^2) \right) \cdot u(q)|_{q^2=m_t^2} \overset{!}{=} 0 \,.
\end{aligned}
\tag{3.25}
$$

The renormalisation constant for the top-quark mass is therefore given by:

$$
\delta m_t = \frac{m_t \left(\Sigma_V(m_t^2) + \Sigma_S(m_t^2) \right)}{1 - \Sigma_S(m_t^2)} \,.
\tag{3.26}
$$

Since we only need δm_t at order $\mathcal{O}(\alpha_s)$, this expression simplifies to

$$
\delta m_t = m_t \left(\Sigma_V(m_t^2) + \Sigma_S(m_t^2) \right) \,,
\tag{3.27}
$$

where $\Sigma_V(m_t^2)$ and $\Sigma_S(m_t^2)$ have to be evaluated at the one-loop order in α_s. The wavefunction renormalisation constant is obtained as the residue of the propagator at its pole. Using Eqs. (3.22, 3.21, 3.26), we find:

$$\frac{i}{\not{q} - m_t^0 + \not{q}\Sigma_V(q^2) + m_t^0\Sigma_S(q^2)} =$$
$$\frac{i}{\not{q} - m_t - \delta m_t + \not{q}\Sigma_V(q^2) + m_t\Sigma_S(q^2) + \delta m_t\Sigma_S(q^2)} =$$
$$\frac{i}{\not{q} - m_t - m_t f(m_t^2) + \not{q}\Sigma_V(q^2) + m_t\Sigma_S(q^2) + m_t f(m_t^2)\Sigma_S(q^2)} \sim$$
$$\frac{i}{\not{q} - m_t} \cdot \frac{1}{1 + \Sigma_V(m_t^2) + 2m_t^2\Sigma_V'(m_t^2) + 2m_t^2\Sigma_S'(m_t^2) + 2m_t^2 f(m_t^2)\Sigma_S'(m_t^2)},$$
$$(3.28)$$

with

$$f(m_t^2) = \frac{\delta m_t}{m_t} = \frac{\Sigma_V(m_t^2) + \Sigma_S(m_t^2)}{1 - \Sigma_S(m_t^2)},$$
$$\Sigma_V'(m_t^2) = \frac{\partial}{\partial q^2}\Sigma_V(q^2)\big|_{q^2 = m_t^2},$$
$$\Sigma_S'(m_t^2) = \frac{\partial}{\partial q^2}\Sigma_S(q^2)\big|_{q^2 = m_t^2}. \qquad (3.29)$$

We can now read off the wavefunction renormalisation constant from the last line of Eq. (3.28):

$$Z_V = \frac{1}{1 + \Sigma_V(m_t^2) + 2m_t^2\Sigma_V'(m_t^2) + 2m_t^2\Sigma_S'(m_t^2) + 2m_t^2 f(m_t^2)\Sigma_S'(m_t^2)}. \qquad (3.30)$$

Expanding this expression in α_s up to and including order $\mathcal{O}(\alpha_s)$, we get:

$$Z_V = 1 - \Sigma_V(m_t^2) - 2m_t^2\Sigma_V'(m_t^2) - 2m_t^2\Sigma_S'(m_t^2), \qquad (3.31)$$

where $\Sigma_V(m_t^2)$, $\Sigma_S(m_t^2)$, and their derivatives are again only needed at order $\mathcal{O}(\alpha_s)$. The results for these expressions are obtained through evaluation of the self-energy diagram with a virtual gluon (see Fig. 3.1). They read:

$$\Sigma_V(m_t^2) = \frac{\alpha_s}{4\pi}C_F \cdot \left(\Delta + \ln\left(\frac{\mu^2}{m_t^2}\right) + 2\right),$$
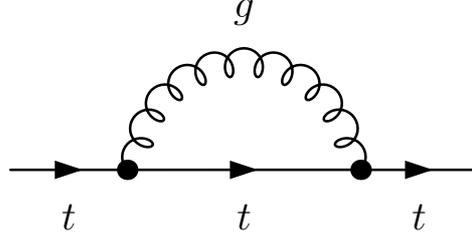
Figure 3.1: Top-quark self-energy at order $\mathcal{O}(\alpha_s)$.

$$
\begin{aligned}
\Sigma_S(m_t^2) &= \frac{\alpha_s}{4\pi} C_F \cdot \left(-4\Delta - 4\ln\left(\frac{\mu^2}{m_t^2}\right) - 6 \right) , \\
\Sigma_V'(m_t^2) &= \frac{\alpha_s}{4\pi} C_F \cdot \left(-\frac{1}{m_t^2}\ln\left(\frac{\lambda^2}{m_t^2}\right) - \frac{3}{m_t^2} \right) , \\
\Sigma_S'(m_t^2) &= \frac{\alpha_s}{4\pi} C_F \cdot \left(\frac{2}{m_t^2}\ln\left(\frac{\lambda^2}{m_t^2}\right) + \frac{4}{m_t^2} \right) .
\end{aligned}
\tag{3.32}
$$

Δ is defined in Eq. (3.8). Here and in the following, we truncate the ϵ-expansion after the terms of order $\mathcal{O}(\epsilon^0)$. In order to disentangle the poles of UV- and of IR-nature, we chose a mass regulator in order to regularise the IR divergences. The results can be transformed into the results of dimensional regularisation by means of Eq. (3.5). In the following, we will write Δ_{UV} for UV poles and Δ_{IR} for IR poles. We thus get the results for the renormalisation constants where the different types of divergences are distinguished:

$$
\begin{aligned}
\delta m_t &= m_t \cdot \frac{\alpha_s}{4\pi} C_F \cdot \left(-3\Delta_{UV} - 3\ln\left(\frac{\mu^2}{m_t^2}\right) - 4 \right) , \\
\delta Z_V &= \frac{\alpha_s}{4\pi} C_F \cdot \left(-\Delta_{UV} - \ln\left(\frac{\mu^2}{m_t^2}\right) - 2\Delta_{IR} - 2\ln\left(\frac{\mu^2}{m_t^2}\right) - 4 \right) .
\end{aligned}
\tag{3.33}
$$

Here, we have employed the on-shell scheme. The renormalisation constant for the top-quark mass in the modified minimal-subtraction ($\overline{\text{MS}}$) scheme is obtained from the on-shell expression by extracting the term containing Δ_{UV}:

$$
\delta m_t^{\overline{\text{MS}}} = m_t^{\overline{\text{MS}}} \cdot \frac{\alpha_s}{4\pi} C_F \cdot \left(-3\Delta_{UV} \right) ,
\tag{3.34}
$$

with $m_t^{\overline{\text{MS}}}$ denoting the respective $\overline{\text{MS}}$ mass.

Mixed Scheme

The residual error due to the truncation of the perturbative series in α_s after the NLO terms can be assessed by performing the calculations in different schemes and at different renormalisation scales. We can, for example, compare the results for an on-shell renormalised top-quark mass to those obtained in the $\overline{\text{MS}}$ scheme. In the latter scheme, the renormalisation scale for the $\overline{\text{MS}}$ mass can be varied. However, we always employ the on-shell conditions (2.3) for the top and the anti-top quark in order to simplify the expressions. This prevents from a simple change to the $\overline{\text{MS}}$ scheme. We thus consider a mixed scheme where the top-quark mass occurring in the Yukawa couplings is renormalised $\overline{\text{MS}}$ while the one stemming from the propagators is kept on-shell. We vary the renormalisation scale from $m_t/2$ to $2m_t$, where m_t is a typical hard scale of the process. This is done in Section 4.2. For our numerical analysis in Section 4.1, we always employ the on-shell scheme.

The mixed scheme is advantageous since the on-shell results can readily be converted to it. First, we have to rescale the Born as well as the NLO results:

$$\mathcal{M} \longrightarrow \mathcal{M} \cdot \frac{m_t^{\overline{\text{MS}}}}{m_t} \,. \tag{3.35}$$

This way, the top-quark mass of the Yukawa coupling is converted to the $\overline{\text{MS}}$ scheme. Second, we have to take into account that the renormalisation contributions to Eq. (2.12) have been calculated in the on-shell scheme. But since the Born matrix element is proportional to the Yukawa coupling, we just have to add the term

$$-2 \cdot |\mathcal{M}_0|^2 \cdot \left(\frac{\delta m_t}{m_t} - \frac{\delta m_t^{\overline{\text{MS}}}}{m_t^{\overline{\text{MS}}}} \right) = +2 \frac{\alpha_s}{4\pi} C_F \cdot |\mathcal{M}_0|^2 \cdot \left(3 \ln \left(\frac{\mu^2}{m_t^2} \right) + 4 \right) \,. \tag{3.36}$$

Running mass and coupling

The renormalisation scale is explicitly introduced by the contributions of Eq. (3.36). Furthermore, the top-quark mass which appears in the Yukawa coupling is now defined in the $\overline{\text{MS}}$ scheme. We therefore need the running top-quark mass at the respective renormalisation scale. The running mass

up to and including the order $\mathcal{O}(\alpha_s)$ is obtained as follows (see, for example, Ref. [46]). We first calculate $\alpha_s^{(5)}(m_t)$ with five active flavours at lowest order:

$$\frac{1}{\alpha_s^{(5)}(m_t)} = \frac{1}{\alpha_s^{(5)}(M_Z)} + \frac{\beta_0^{(5)}}{\pi} \ln\left(\frac{m_t^2}{M_Z^2}\right).$$ (3.37)

We now perform the matching with six active flavours at the scale m_t:

$$\alpha_s^{(6)}(m_t) = \alpha_s^{(5)}(m_t).$$ (3.38)

$\alpha_s^{(6)}(\mu)$ is then obtained with six active flavours according to:

$$\frac{1}{\alpha_s^{(6)}(\mu)} = \frac{1}{\alpha_s^{(6)}(m_t)} + \frac{\beta_0^{(6)}}{\pi} \ln\left(\frac{\mu^2}{m_t^2}\right).$$ (3.39)

Having the running strong coupling at hand, we can evaluate the running top-quark mass in the $\overline{\text{MS}}$ scheme:

$$m_t^{\overline{\text{MS}},(6)} = m_t \left(1 - \frac{\alpha_s^{(6)}(m_t)}{\pi} C_F\right) \left(\frac{\alpha_s^{(6)}(\mu)}{\alpha_s^{(6)}(m_t)}\right)^{\gamma_0/\beta_0^{(6)}}.$$ (3.40)

The upper index in parentheses always denotes the number of active quark flavours. In above formulas, we need the first coefficient of the Callan-Symanzik beta function for five and six active flavours as well as the first coefficient of the quark-mass anomalous dimension:

$$\begin{aligned}
\beta_0^{(5)} &= \frac{1}{4}\left(\frac{11}{3}C_A - \frac{20}{3}T_F\right) = \frac{23}{12}, \\
\beta_0^{(6)} &= \frac{1}{4}\left(\frac{11}{3}C_A - \frac{24}{3}T_F\right) = \frac{7}{4}, \\
\gamma_0 &= \frac{3}{4}C_F = 1,
\end{aligned}$$ (3.41)

with $C_A = N_C = 3$ and $T_F = 1/2$.

The strong coupling α_s is only introduced at NLO. For this reason, its value is not fixed but can be chosen arbitrarily. This is due to the fact that the contributions to the running of the strong coupling are of order $\mathcal{O}(\alpha_s)$. We choose to use $\alpha_s(M_Z)$ for our numerical evaluations in Section 4.1. In order to get an idea about the uncertainty induced by the running of the strong coupling, we will also vary the scale for α_s from $m_t/2$ to $2m_t$ at the one-loop level. This is done in Section 4.2.

UV and IR divergences

Let us now come to the cancellation of the divergences. In Section 3.1, we have constructed the renormalisation contributions. The relevant renormalisation constants have been derived above (3.33, 3.34). It turns out that the wavefunction renormalisation constant does not only contain UV but also IR singularities. They have been disentangled in the explicit expressions so that the two types of divergences can be treated separately. Actually, in the expressions for the renormalisation contributions, we do not insert the results but introduce two variables for the top-quark mass and wavefunction renormalisation constants, respectively. In the main `Fortran` program, we assign these variables the finite parts of the constants. For the cancellation of the divergences, we can use the `Form` expressions where we insert the relevant divergent parts.

We first discuss the cancellation of the UV divergences. The UV-divergent generalised scalar integrals are extracted from the beginning. They have already been listed in Section 3.2. The pole parts are given by Eq. (2.30). Adding the renormalisation contributions, inserting the UV-divergent parts for the integrals as well as for the renormalisation constants, and simplifying the resulting expression, we find that the UV poles cancel for each of the 68 structures of Eqs. (2.8, 2.9, 2.10) separately.

Let us now come to the case of IR divergences. The soft IR singularities have to cancel out in the sum of the virtual and the real contributions due to the Bloch-Nordsieck theorem [47]. For the IR-divergent part of the amplitude, we use the compact analytic expression which has been derived in Section 3.1. The pole-parts for the divergent integrals have been obtained in Eq. (3.18). Below Eq. (3.18), it has been noted that the logarithm appearing in these expressions is the same as the one of the subtraction term for the virtual part. The latter is given in Eqs. (2.54 and the following) and has to be added. Finally, we need the renormalisation contributions where we insert the IR-divergent part of the wavefunction renormalisation. These contributions cancel against those of the subtraction term which are not proportional to the above mentioned logarithm. This cancellation takes place for each of the 68 structures separately. However, this is not true for the remaining IR singularities. However, the contributions from the divergent integrals cancel against the residual ones from the subtraction term after the squaring and summing of the matrix element and some simplifications have been performed. The cancellation of the IR singularities is also checked numerically

within the main `Fortran` program. Furthermore, it is checked numerically that the divergent part of the compact expression is equal to the IR part of the expression obtained by application of the recursion relations.

3.4 Details of the Implementation

We have outlined our approach in Section 3.1. Here, we give details on the actual calculations within the main `Fortran` program.

As has been said in Section 3.1, the matrix element is evaluated through reduction of the occurring tensor integrals. This reduction is performed in two independent ways. In the first case, it is done by `Form` routines. The resulting expressions are turned into `Fortran` functions and can directly be used within the main `Fortran` program. Second, the tensor integrals are only reduced to generalised scalar integrals through `Form` routines. The reduction to the basis set of integrals is then performed directly within the main `Fortran` program. In case an exceptional momentum configuration has been detected, the reduction is always performed by the `Fortran` program. However, the recursion relations pertaining to the cases, where the determinant of the kinematical matrix becomes small, do not give reliable results. This is obvious from the fact that the NLO correction becomes much larger than the tree result for these momentum configurations. But it turns out that such phase space configurations only appear a few times during the phase space integration. It is thus not problematic to set the integrand identically to zero for these cases. On the other hand, we include the case that only the determinant of the Gram matrix becomes small. This happens for about 1% of the phase space points. However, setting the integrand to zero also for small Gram determinants does not alter the results up to the desired precision.

We choose to perform the numerical phase space integration with an accuracy of 0.1% with respect to the Born result. To this end, we set the relative accuracy, which is to be achieved by the numerical integration program, to 0.05% for the calculation of the Born cross section, to 0.2% for the virtual part and to 0.2% for the real correction. The virtual and the real correction are added to the Born cross section to give the NLO prediction. The individual integration errors are added quadratically. For our numerical evaluations, we always use the Monte Carlo program `Vegas` from the `CUBA` library [39]. We furthermore restrict the number of phase space points to be

evaluated for the calculation of the virtual part to 64000. These settings always lead to a resulting integration error for the NLO prediction below 0.1%. The number of phase space points which have to be computed in order to reach the desired accuracy for the Born result and for the real correction can exceed 200000 and 100000, respectively.

The real correction has to be computed by an independent integration since the phase space involves four final state particles in opposition to the three final state particles in case of the Born level and the virtual correction. However, also the Born cross section and the virtual correction should be integrated in separate runs of the integration routine. The reason is the following. The Born expressions are evaluated fast for the individual phase space points while the computation of the NLO expressions is time-consuming. But we do not need to evaluate the NLO correction with the same relative accuracy as the Born result since its value is smaller. Integrating the NLO correction in a separate run with less accuracy thus saves a large amount of computing time without spoiling the desired accuracy of the NLO prediction.

Optimisations

Since the calculation of the NLO part is very time-consuming, it is mandatory to optimise the evaluation. This is done differently for the two independent implementations of the reduction procedure. We first discuss the case the reduction is performed within `Form`. The recursion relations involve the inverse of the kinematical matrix and its sums. These objects are transformed to `Fortran` functions. In the actual calculations, the same inverse kinematical matrix and its sums can occur many times. Calculating the respective function for each occurrence is, therefore, an obvious waste of time. For this reason, we substitute these functions in the NLO expressions by `Fortran` variables. The variables are assigned the respective functions which now only have to be calculated once. This is done completely automatically by means of a makefile and a `Perl` script.

In case the reduction is performed within the main `Fortran` program, we store an integral once it has been evaluated. However, we only do so for non-exceptional phase space configurations. The reduction procedure for exceptional phase space points involves iterations of the recursion relations. The same integral can appear at different stages of such expansions so that the iteration depth for it can vary.

The procedure looks as follows. When an integral is to be calculated, it is

first checked whether it has already been evaluated before. In this case, the result is just taken from the storage. Otherwise, it still has to be calculated and stored. In order to store the result, the integral with its parameters is translated into a code number which uniquely specifies the integral. This number is stored in a vector while its result is stored at the same position in a different vector. In order to find out if an integral has already been computed, the vectors with the code numbers are searched for the corresponding number. If the code number could be found, the result for the integral can be taken from the respective result vector at the corresponding position. This procedure leads to a small amount of memory which has to be allocated. Also the number of necessary initialisations is small in this way.

Using the expressions obtained through reduction within `Form` does not turn out to be faster than performing the reduction directly within the main `Fortran` program. Therefore, we choose to always reduce the generalised scalar integrals within the `Fortran` program for the numerical evaluations. The `Form` expressions are used as a check on the reduction in case of non-exceptional phase space configurations.

Controlling the Computation

The real correction involves an additional final-state gluon. When it is soft, it cannot be resolved by the detector due to its finite resolution. However, when the energy of the gluon is large enough, a $(2 \to 4)$ event is detected. If one is only interested in events where three final state particles are observed, one has to apply a cut on the energy of the additional gluon. This can be done by simply setting a preprocessor variable to the desired value. However, the subtraction term for the real correction is still integrated over the full one-parton phase space of the gluon. This is necessary since its contribution has to cancel against the one stemming from the subtraction term for the virtual part. It is also possible to apply a lower cut on the energy of the gluon. This prevents the phase space integration from developing an IR singularity. We can then set the subtraction term for the real part identically to zero in order to solely compute the genuine real correction. The result can be compared against an independent calculation, as it is done in Section 3.5.

There are further possibilities to control the main `Fortran` program. This is always done by means of preprocessor variables which are collected in a single file. The first option is to calculate either the subprocess or the parent process. In the latter case, we have to choose between direct Compton

scattering and the photon spectrum given by `CompAZ` [6] (see Section 2.4). For our numerical evaluations in Section 4.1, we always use `CompAZ`. Section 4.3 contains a comparison with the literature. The results for the parent process which are specified in the literature have been obtained for direct Compton scattering. We therefore use the respective photon spectrum for the comparison.

The CMS energy of the subprocess respectively of the parent process is specified through an energy range and a step value. Furthermore, the Higgs mass has to be given as well as the residual numerical parameters. Different values for the parameters are chosen for our numerical analysis and the comparison with the literature.

In order to assess the residual error due to the truncation of the perturbation series, we transform the on-shell results into a mixed scheme (see Section 3.3). However, this is only done for the subprocess, and only for a specified energy. Furthermore, the renormalisation scale for the running top-quark mass has to be given, which is varied from half its value to twice its value. We choose the on-shell top-quark mass in our evaluations. The scheme and scale dependences are discussed in Section 4.2.

We also have to specify the threshold in the detection of exceptional momentum configurations. In order to detect such an exceptional phase space point, we first have to compute the Eigenvalues of the kinematical matrix pertaining to the respective integral. The smallest Eigenvalue is then compared to the threshold value. If it is smaller, also the Eigenvalues of the Gram matrix have to be calculated and compared to the threshold value. The appropriate recursion relation can then be chosen. The existence of at least one small Eigenvalue means that the determinant of the matrix is small. In this case, the inversion of the matrix becomes numerically unstable. Recursion relations which use the inverse of such a matrix are, therefore, also numerically unreliable. However, when the inverse of the kinematical matrix can be computed reliably because its determinant is not small, we still have to check the B parameter which occurs in denominators of the recursion relations. If it is small compared to the threshold value, the recursion relations for small Gram determinants are chosen. The relation of the Gram determinant and the B parameter is given by Eq. (2.33). However, as has been explained above, we set the integrand to zero for the cases of a small determinant of the kinematical matrix. Note that it is preferable to compare the smallest Eigenvalue instead of the determinant of the respective matrix to a threshold value. This is due to the fact that the exceptional recursion relations for

small determinants of the kinematical matrix rely on the existence of a small Eigenvalue of the kinematical matrix respectively of the Gram matrix.

Furthermore, the treatment of exceptional phase space points involves expansions in small parameters (see Section 2.2). An expansion is terminated when the prefactor of an integral is smaller than a certain value. This iteration depth is also specified by a preprocessor variable.

In our numerical analysis, we choose for the threshold and for the iteration depth the same value of 10^{-6}. As has been mentioned in Section 2.2, a parameter always has to be turned into a dimensionless quantity before it can be compared to the specified value for the threshold respectively for the iteration depth. To this end, it is scaled by powers of the top-quark mass, which is a typical hard scale of the process. If we choose a smaller threshold value, the numerical precision gets worse. Larger threshold values lead to more phase space points which are treated as exceptional cases. This slows down the computation. Furthermore, the iterations now involve larger expansion parameters. The reduction then leads to basis integrals with higher powers of propagators and larger dimensions, which are not provided anymore. The same applies to much smaller values of the depth. Still, the value of 10^{-6}, which is specified for the threshold as well as for the depth, seems to be a reasonable choice.

The inversion of matrices is done by means of the Singular Value Decomposition. In addition, we have to compute the Eigenvalues and Eigenvectors of real and symmetric matrices. These are needed in order to detect and treat the exceptional momentum configurations. We calculate them with the Jacobi method. The numerical algorithms for the two methods have been taken from [48].

Uncertainties

Let us now discuss the sources of uncertainties for the prediction of the cross section. The truncation of the perturbation series after the NLO term induces an error. As has been said above, one can assess this uncertainty by comparing results for different renormalisation schemes. And if the result in a specific scheme depends on the renormalisation scale, as it is the case in the $\overline{\text{MS}}$ scheme, the scale can be varied around a typical scale of the process. Such comparisons are performed in Section 4.2.

We only consider the NLO QCD correction in this work. However, in case of the process $e^+e^- \to t\bar{t}H$, the electroweak correction turns out to be of

equal importance for large values of the CMS energy [18]. This contribution to the cross section should, therefore, also be provided.

In Section 2.4, we have seen that the two-photon spectrum of the photon collider is obtained from a fit to a beam simulation. The resulting spectrum has to be compared to measurements in order to investigate its accuracy. Second, e^+e^--collisions can still take place in the photon collider. If the energy of the laser photons is above a threshold value, e^+e^--pair-creation in the scattering of backscattered photons and laser photons occurs [34]. Choosing the laser wavelength sufficiently large can avoid the pair creation. This is desired since pair creation lowers the luminosity of two-photon collisions. However, the actual luminosity of e^+e^--collisions depends on the parameters of the photon collider. Such e^+e^--collisions can lead to the same final states as they appear in the signal and background processes in two-photon collisions. For a thorough estimation of the uncertainty for the cross section prediction, these issues should be taken into account.

In a detailed study of the possibility to measure the top-quark Yukawa coupling, one has to include the relevant background processes. Such studies have already been performed for the case of e^+e^--collisions in Refs. [8]. For Higgs-boson masses below 140 GeV, the Higgs-boson decay into a pair of a bottom and an anti-bottom quark is important. Above this value, the decay into a W^+W^--pair has to be considered. The main background comes from the production of a $t\bar{t}$-pair. Through radiation of a gluon which subsequently decays into a pair of a bottom and an anti-bottom quark, the signal can be mimicked (for the QCD correction see [49]). However, a detailed study for a measurement of the top-quark Yukawa coupling in two-photon collisions is not the aim of this work.

A final point is to be discussed. The Higgs-boson energy is maximal when the top quark and the anti-top quark are collinear. The $t\bar{t}$-system then moves opposite to the Higgs direction, while the relative velocity $v_{t\bar{t}}$ between the quarks is small. In this endpoint region of the Higgs energy, Coulomb singularities arise which are proportional $(\alpha_s/v_{t\bar{t}})^n$. In addition, logarithmic divergences proportional $(\alpha_s \ln (v_{t\bar{t}}))^n$ show up. Such enhanced contributions spoil the fixed-order perturbative approach. In Refs. [50], this issue has been addressed for the process $e^+e^- \rightarrow t\bar{t}H$. The authors applied a non-relativistic effective theory in order to sum both of these contributions to all orders. Such corrections become the more important the larger the portion of phase space is, where the $t\bar{t}$-system is non-relativistic. This portion increases for lower CMS energies and larger Higgs masses. As it turned out, for the

process considered in those papers, the deviation from the pure fixed-order approach at NLO amounts to several percent at a CMS energy of 600 GeV. For smaller energies, where the corrections become large, the size of the cross section decreases since we get close to the threshold. If the corrections are of a comparable size for the process $e^+e^- \rightarrow \gamma\gamma \rightarrow t\bar{t}H$, we can roughly estimate the respective uncertainty, away from the threshold, to be at the percent level. Note that the subprocess is integrated over the photon spectra so that its cross section is calculated for energies between the threshold and the maximal energy. One could also avoid these additional corrections by imposing a cut on the Higgs-boson energy or on the invariant mass of the $t\bar{t}$-system. However, we do not encounter any problems in integrating the NLO expressions over the full phase space without special treatment of the endpoint region of the Higgs-boson energy. Still, the corrections stemming from this region then have to be taken into account for an estimate of the residual error on the prediction of the cross section.

3.5   Checks

The preceding Sections have shown that the calculation of the cross section for $e^+e^- \rightarrow \gamma\gamma \rightarrow t\bar{t}H$ is nontrivial. It is, therefore, highly desirable to have strong checks. These should cover as many parts of the calculation as possible. Let us now discuss the various checks which have been applied in this work.

Born Level

First of all, we recalculated the Born results of Ref. [13]. This presents a good check on the automated generation of the `Fortran` functions which contain the matrix element. Furthermore, the $(2 \rightarrow 3)$ phase space is involved in this calculation. Moreover, the squaring and summing of the matrix element is checked in this way. This is also done by following two slightly different ways for the computation (see Section 3.1). In addition, we recalculated the Born results completely automatically with `FormCalc`.

Real Correction

In Section 3.4, we mentioned the possibility to apply a lower cut on the energy of the additionally radiated gluon in case of the real correction. The

lower cut allows to perform the phase space integration solely for the genuine real correction without the need for a subtraction term. The IR divergences stem from the integration region where the gluon becomes soft, which is excluded in this way. The result has been compared to a completely automated calculation using Version 5.2 of `FormCalc`. When no lower cut is applied, the subtraction terms have to be added to the genuine real correction in order to avoid the occurrence of IR divergences in the phase space integration. Thus, the observed convergence of the integration of the subtracted matrix element, without a lower cut, constitutes another check. Multiplication of the subtraction terms with a factor different from one leads to an integral which does not converge anymore. We could furthermore compare the derived subtraction terms for the real as well as for the virtual part with results stated in the literature [32].

Virtual Correction

The most complex part is the calculation of the virtual correction. The following checks are all concerned with this part of the computation. The first thing to note is, that it is indispensable to automate the evaluation as much as possible. This was always done, as already mentioned in the preceding Sections. `FeynArts` was used in order to automatically construct the analytic expressions pertaining to the various diagrams. These were transformed into `Form` expressions with `FormCalc`. We used `Form` to treat the expressions further, and simplifications were performed with `Mathematica`. Basis integrals were reduced further by means of the program `AIR`. The connections between the different packages were made by means of makefiles, `Perl` scripts, and shell scripts. The transformation of the resulting expressions into `Fortran` functions has also been done in a completely automated way.

In order to check the reduction procedure, we implemented the tensor reduction in two independent ways. For non-exceptional phase space points, we could compare the respective results. This is a very strong check that the tensor reduction has been implemented correctly. In both cases, we optimised the evaluation. This speeds up the computation considerably and is thus mandatory. The results are still in agreement for the two independent implementations and also agree with a calculation without optimisation. The $\mathcal{O}(\epsilon)$-terms have also been taken into account in different ways. This way, it is also checked that these additional finite terms are included correctly.

In Section 3.3, we showed the cancellation of the UV as well as of the

IR singularities. These cancellations present further checks on the calculation. Furthermore, we derived the IR divergences in two different ways. We could directly read them off the original tensor integrals and obtain them through reduction. We numerically compared the IR-divergent terms and found agreement. In addition, we can exploit Bose symmetry and Gauge invariance in order to check our expressions. Let us start with the Bose-symmetry property of the matrix element.

Bose Symmetry

The general form of the matrix element for the Born level as well as for the virtual contribution is specified in Eqs. (2.8, 2.9, 2.10). It involves the coefficients C_i respectively $U^{(i)}$, $U^{(i)}_{j_1j_2}$, $X^{(i)}_j$, $Y^{(i)}_j$, and $Z^{(i)}$. They depend, amongst others, on the momenta and polarisation vectors of the external photons. In the following, this will be indicated by four arguments. The first two arguments of the coefficients are the momenta of the first and second photon, while the other two are the polarisation vectors of these, respectively.

The amplitude of the process under consideration obeys Bose symmetry with respect to the two external photons. If we simultaneously interchange the momenta and the polarisation vectors of the two photons, the value of the amplitude must not change. This leads to ten Bose symmetry relations between the coefficients C_i:

$$
\begin{aligned}
C_1(p_1, p_2, \epsilon_1, \epsilon_2) &= C_1(p_2, p_1, \epsilon_2, \epsilon_1)\,, \\
C_2(p_1, p_2, \epsilon_1, \epsilon_2) &= C_3(p_2, p_1, \epsilon_2, \epsilon_1)\,, \\
C_4(p_1, p_2, \epsilon_1, \epsilon_2) &= -C_4(p_2, p_1, \epsilon_2, \epsilon_1)\,, \\
C_5(p_1, p_2, \epsilon_1, \epsilon_2) &= C_9(p_2, p_1, \epsilon_2, \epsilon_1)\,, \\
C_6(p_1, p_2, \epsilon_1, \epsilon_2) &= C_{10}(p_2, p_1, \epsilon_2, \epsilon_1)\,, \\
C_7(p_1, p_2, \epsilon_1, \epsilon_2) &= C_{11}(p_2, p_1, \epsilon_2, \epsilon_1)\,, \\
C_8(p_1, p_2, \epsilon_1, \epsilon_2) &= C_{12}(p_2, p_1, \epsilon_2, \epsilon_1)\,, \\
C_{13}(p_1, p_2, \epsilon_1, \epsilon_2) &= -C_{13}(p_2, p_1, \epsilon_2, \epsilon_1)\,, \\
C_{14}(p_1, p_2, \epsilon_1, \epsilon_2) &= C_{15}(p_2, p_1, \epsilon_2, \epsilon_1)\,, \\
C_{16}(p_1, p_2, \epsilon_1, \epsilon_2) &= C_{16}(p_2, p_1, \epsilon_2, \epsilon_1)\,.
\end{aligned}
\tag{3.42}
$$

If we express the C_i as in Eq. (2.10), the coefficients $U^{(i)}$, $U^{(i)}_{j_1j_2}$, $X^{(i)}_j$, $Y^{(i)}_j$, and $Z^{(i)}$ are introduced. Above relations imply for these coefficients the following

relations:

$$U^{(1)}(p_1, p_2) - U^{(1)}(p_2, p_1) = 0\,, \quad U_{21}^{(1)}(p_1, p_2) - U_{21}^{(1)}(p_2, p_1) = 0\,,$$
$$U_{23}^{(1)}(p_1, p_2) - U_{31}^{(1)}(p_2, p_1) = 0\,, \quad U_{24}^{(1)}(p_1, p_2) - U_{41}^{(1)}(p_2, p_1) = 0\,,$$
$$U_{31}^{(1)}(p_1, p_2) - U_{23}^{(1)}(p_2, p_1) = 0\,, \quad U_{33}^{(1)}(p_1, p_2) - U_{33}^{(1)}(p_2, p_1) = 0\,,$$
$$U_{34}^{(1)}(p_1, p_2) - U_{43}^{(1)}(p_2, p_1) = 0\,, \quad U_{41}^{(1)}(p_1, p_2) - U_{24}^{(1)}(p_2, p_1) = 0\,,$$
$$U_{43}^{(1)}(p_1, p_2) - U_{34}^{(1)}(p_2, p_1) = 0\,, \quad U_{44}^{(1)}(p_1, p_2) - U_{44}^{(1)}(p_2, p_1) = 0\,,$$
$$U^{(2)}(p_1, p_2) - U^{(3)}(p_2, p_1) = 0\,, \quad U_{21}^{(2)}(p_1, p_2) - U_{21}^{(3)}(p_2, p_1) = 0\,,$$
$$U_{23}^{(2)}(p_1, p_2) - U_{31}^{(3)}(p_2, p_1) = 0\,, \quad U_{24}^{(2)}(p_1, p_2) - U_{41}^{(3)}(p_2, p_1) = 0\,,$$
$$U_{31}^{(2)}(p_1, p_2) - U_{23}^{(3)}(p_2, p_1) = 0\,, \quad U_{33}^{(2)}(p_1, p_2) - U_{33}^{(3)}(p_2, p_1) = 0\,,$$
$$U_{34}^{(2)}(p_1, p_2) - U_{43}^{(3)}(p_2, p_1) = 0\,, \quad U_{41}^{(2)}(p_1, p_2) - U_{24}^{(3)}(p_2, p_1) = 0\,,$$
$$U_{43}^{(2)}(p_1, p_2) - U_{34}^{(3)}(p_2, p_1) = 0\,, \quad U_{44}^{(2)}(p_1, p_2) - U_{44}^{(3)}(p_2, p_1) = 0\,,$$
$$U^{(3)}(p_1, p_2) - U^{(2)}(p_2, p_1) = 0\,, \quad U_{21}^{(3)}(p_1, p_2) - U_{21}^{(2)}(p_2, p_1) = 0\,,$$
$$U_{23}^{(3)}(p_1, p_2) - U_{31}^{(2)}(p_2, p_1) = 0\,, \quad U_{24}^{(3)}(p_1, p_2) - U_{41}^{(2)}(p_2, p_1) = 0\,,$$
$$U_{31}^{(3)}(p_1, p_2) - U_{23}^{(2)}(p_2, p_1) = 0\,, \quad U_{33}^{(3)}(p_1, p_2) - U_{33}^{(2)}(p_2, p_1) = 0\,,$$
$$U_{34}^{(3)}(p_1, p_2) - U_{43}^{(2)}(p_2, p_1) = 0\,, \quad U_{41}^{(3)}(p_1, p_2) - U_{24}^{(2)}(p_2, p_1) = 0\,,$$
$$U_{43}^{(3)}(p_1, p_2) - U_{34}^{(2)}(p_2, p_1) = 0\,, \quad U_{44}^{(3)}(p_1, p_2) - U_{44}^{(2)}(p_2, p_1) = 0\,,$$
$$U^{(4)}(p_1, p_2) + U^{(4)}(p_2, p_1) = 0\,, \quad U_{21}^{(4)}(p_1, p_2) + U_{21}^{(4)}(p_2, p_1) = 0\,,$$
$$U_{23}^{(4)}(p_1, p_2) + U_{31}^{(4)}(p_2, p_1) = 0\,, \quad U_{24}^{(4)}(p_1, p_2) + U_{41}^{(4)}(p_2, p_1) = 0\,,$$
$$U_{31}^{(4)}(p_1, p_2) + U_{23}^{(4)}(p_2, p_1) = 0\,, \quad U_{33}^{(4)}(p_1, p_2) + U_{33}^{(4)}(p_2, p_1) = 0\,,$$
$$U_{34}^{(4)}(p_1, p_2) + U_{43}^{(4)}(p_2, p_1) = 0\,, \quad U_{41}^{(4)}(p_1, p_2) + U_{24}^{(4)}(p_2, p_1) = 0\,,$$
$$U_{43}^{(4)}(p_1, p_2) + U_{34}^{(4)}(p_2, p_1) = 0\,, \quad U_{44}^{(4)}(p_1, p_2) + U_{44}^{(4)}(p_2, p_1) = 0\,,$$
$$X_{01}^{(1)}(p_1, p_2) - Y_{02}^{(1)}(p_2, p_1) = 0\,, \quad X_{03}^{(1)}(p_1, p_2) - Y_{03}^{(1)}(p_2, p_1) = 0\,,$$
$$X_{04}^{(1)}(p_1, p_2) - Y_{04}^{(1)}(p_2, p_1) = 0\,, \quad X_{02}^{(2)}(p_1, p_2) - Y_{02}^{(2)}(p_2, p_1) = 0\,,$$
$$X_{03}^{(2)}(p_1, p_2) - Y_{03}^{(2)}(p_2, p_1) = 0\,, \quad X_{04}^{(2)}(p_1, p_2) - Y_{04}^{(2)}(p_2, p_1) = 0\,,$$
$$X_{01}^{(3)}(p_1, p_2) - Y_{02}^{(3)}(p_2, p_1) = 0\,, \quad X_{03}^{(3)}(p_1, p_2) - Y_{03}^{(3)}(p_2, p_1) = 0\,,$$
$$X_{04}^{(3)}(p_1, p_2) - Y_{04}^{(3)}(p_2, p_1) = 0\,, \quad X_{01}^{(4)}(p_1, p_2) - Y_{02}^{(4)}(p_2, p_1) = 0\,,$$
$$X_{03}^{(4)}(p_1, p_2) - Y_{03}^{(4)}(p_2, p_1) = 0\,, \quad X_{04}^{(4)}(p_1, p_2) - Y_{04}^{(4)}(p_2, p_1) = 0\,,$$
$$Y_{02}^{(1)}(p_1, p_2) - X_{01}^{(1)}(p_2, p_1) = 0\,, \quad Y_{03}^{(1)}(p_1, p_2) - X_{03}^{(1)}(p_2, p_1) = 0\,,$$
$$Y_{04}^{(1)}(p_1, p_2) - X_{04}^{(1)}(p_2, p_1) = 0\,, \quad Y_{02}^{(2)}(p_1, p_2) - X_{01}^{(2)}(p_2, p_1) = 0\,,$$

$$Y_{03}^{(2)}(p_1, p_2) - X_{03}^{(2)}(p_2, p_1) = 0 \,, \quad Y_{04}^{(2)}(p_1, p_2) - X_{04}^{(2)}(p_2, p_1) = 0 \,,$$
$$Y_{02}^{(3)}(p_1, p_2) - X_{01}^{(3)}(p_2, p_1) = 0 \,, \quad Y_{03}^{(3)}(p_1, p_2) - X_{03}^{(3)}(p_2, p_1) = 0 \,,$$
$$Y_{04}^{(3)}(p_1, p_2) - X_{04}^{(3)}(p_2, p_1) = 0 \,, \quad Y_{02}^{(4)}(p_1, p_2) - X_{01}^{(4)}(p_2, p_1) = 0 \,,$$
$$Y_{03}^{(4)}(p_1, p_2) - X_{03}^{(4)}(p_2, p_1) = 0 \,, \quad Y_{04}^{(4)}(p_1, p_2) - X_{04}^{(4)}(p_2, p_1) = 0 \,,$$
$$Z^{(1)}(p_1, p_2) + Z^{(1)}(p_2, p_1) = 0 \,, \quad Z^{(2)}(p_1, p_2) - Z^{(3)}(p_2, p_1) = 0 \,,$$
$$Z^{(3)}(p_1, p_2) - Z^{(2)}(p_2, p_1) = 0 \,, \quad Z^{(4)}(p_1, p_2) - Z^{(4)}(p_2, p_1) = 0 \,.$$

$$(3.43)$$

We checked these relations numerically within the main `Fortran` program for the Born level as well as for the virtual part. In case of the Born results, the relations are fulfilled within machine precision. The situation looks different for the virtual contribution. For non-exceptional cases, we still observe the validity of above relations within several orders of magnitude up to machine precision. However, for phase space points where the Gram determinant becomes small, they are only poorly fulfilled. The respective recursion relations, therefore, do not seem to lead to results with high accuracy. Still, since these phase space configurations only occur for about 1% of all phase space points, this should not spoil the desired accuracy of our calculation. Furthermore, we showed that the results do not change within this precision if we set the integrand identically to zero in such cases.

Gauge Invariance

Gauge invariance gives rise to further conditions called Ward identities. If we substitute the polarisation vector of one of the two photons by its momentum, the result for the amplitude has to be zero. These identities again translate into relations for the coefficients $U^{(i)}$, $U_{j_1 j_2}^{(i)}$, $X_j^{(i)}$, $Y_j^{(i)}$, and $Z^{(i)}$. The substitution $\epsilon_1 \to p_1$ leads to:

$$U^{(1)} + U_{21}^{(1)} \cdot \frac{s_{12}}{2} + U_{31}^{(1)} \cdot \frac{(s_{13} - m_t^2)}{2} + U_{41}^{(1)} \cdot \frac{(s_{14} - m_t^2)}{2} +$$
$$X_{01}^{(3)} \cdot \frac{s_{12}}{2} + 2 Z^{(1)} = 0 \,,$$
$$U_{23}^{(1)} \cdot \frac{s_{12}}{2} + U_{33}^{(1)} \cdot \frac{(s_{13} - m_t^2)}{2} + U_{43}^{(1)} \cdot \frac{(s_{14} - m_t^2)}{2} + X_{03}^{(3)} \cdot \frac{s_{12}}{2} = 0 \,,$$
$$U_{24}^{(1)} \cdot \frac{s_{12}}{2} + U_{34}^{(1)} \cdot \frac{(s_{13} - m_t^2)}{2} + U_{44}^{(1)} \cdot \frac{(s_{14} - m_t^2)}{2} + X_{04}^{(3)} \cdot \frac{s_{12}}{2} = 0 \,,$$

$$U^{(2)} + U_{21}^{(2)} \cdot \frac{s_{12}}{2} + U_{31}^{(2)} \cdot \frac{(s_{13} - m_t^2)}{2} + U_{41}^{(2)} \cdot \frac{(s_{14} - m_t^2)}{2} + X_{01}^{(1)} = 0 \,,$$

$$U_{23}^{(2)} \cdot \frac{s_{12}}{2} + U_{33}^{(2)} \cdot \frac{(s_{13} - m_t^2)}{2} + U_{43}^{(2)} \cdot \frac{(s_{14} - m_t^2)}{2} + X_{03}^{(1)} = 0 \,,$$

$$U_{24}^{(2)} \cdot \frac{s_{12}}{2} + U_{34}^{(2)} \cdot \frac{(s_{13} - m_t^2)}{2} + U_{44}^{(2)} \cdot \frac{(s_{14} - m_t^2)}{2} + X_{04}^{(1)} = 0 \,,$$

$$U^{(3)} + U_{21}^{(3)} \cdot \frac{s_{12}}{2} + U_{31}^{(3)} \cdot \frac{(s_{13} - m_t^2)}{2} + U_{41}^{(3)} \cdot \frac{(s_{14} - m_t^2)}{2} + 2Z^{(3)} = 0 \,,$$

$$U_{23}^{(3)} \cdot \frac{s_{12}}{2} + U_{33}^{(3)} \cdot \frac{(s_{13} - m_t^2)}{2} + U_{43}^{(3)} \cdot \frac{(s_{14} - m_t^2)}{2} = 0 \,,$$

$$U_{24}^{(3)} \cdot \frac{s_{12}}{2} + U_{34}^{(3)} \cdot \frac{(s_{13} - m_t^2)}{2} + U_{44}^{(3)} \cdot \frac{(s_{14} - m_t^2)}{2} = 0 \,,$$

$$U^{(4)} + U_{21}^{(4)} \cdot \frac{s_{12}}{2} + U_{31}^{(4)} \cdot \frac{(s_{13} - m_t^2)}{2} + U_{41}^{(4)} \cdot \frac{(s_{14} - m_t^2)}{2} + \frac{X_{01}^{(3)}}{2} = 0 \,,$$

$$U_{23}^{(4)} \cdot \frac{s_{12}}{2} + U_{33}^{(4)} \cdot \frac{(s_{13} - m_t^2)}{2} + U_{43}^{(4)} \cdot \frac{(s_{14} - m_t^2)}{2} + \frac{X_{03}^{(3)}}{2} = 0 \,,$$

$$U_{24}^{(4)} \cdot \frac{s_{12}}{2} + U_{34}^{(4)} \cdot \frac{(s_{13} - m_t^2)}{2} + U_{44}^{(4)} \cdot \frac{(s_{14} - m_t^2)}{2} + \frac{X_{04}^{(3)}}{2} = 0 \,,$$

$$Y_{02}^{(1)} \cdot \frac{s_{12}}{2} + Y_{03}^{(1)} \cdot \frac{(s_{13} - m_t^2)}{2} + Y_{04}^{(1)} \cdot \frac{(s_{14} - m_t^2)}{2} - s_{12}Z^{(3)} = 0 \,,$$

$$Y_{02}^{(2)} \cdot \frac{s_{12}}{2} + Y_{03}^{(2)} \cdot \frac{(s_{13} - m_t^2)}{2} + Y_{04}^{(2)} \cdot \frac{(s_{14} - m_t^2)}{2} = 0 \,,$$

$$Y_{02}^{(3)} \cdot \frac{s_{12}}{2} + Y_{03}^{(3)} \cdot \frac{(s_{13} - m_t^2)}{2} + Y_{04}^{(3)} \cdot \frac{(s_{14} - m_t^2)}{2} - 2Z^{(1)} = 0 \,,$$

$$Y_{02}^{(4)} \cdot \frac{s_{12}}{2} + Y_{03}^{(4)} \cdot \frac{(s_{13} - m_t^2)}{2} + Y_{04}^{(4)} \cdot \frac{(s_{14} - m_t^2)}{2} + Z^{(3)} = 0 \,. \qquad (3.44)$$

$\epsilon_2 \to p_2$ results in the following relations:

$$U^{(1)} + U_{21}^{(1)} \cdot \frac{s_{12}}{2} + U_{23}^{(1)} \cdot \frac{(s_{23} - m_t^2)}{2} + U_{24}^{(1)} \cdot \frac{(s_{24} - m_t^2)}{2} +$$
$$\frac{s_{12}}{2} Y_{02}^{(3)} - 2Z^{(1)} = 0 \,,$$

$$U_{31}^{(1)} \cdot \frac{s_{12}}{2} + U_{33}^{(1)} \cdot \frac{(s_{23} - m_t^2)}{2} + U_{34}^{(1)} \cdot \frac{(s_{24} - m_t^2)}{2} + \frac{s_{12}}{2} Y_{03}^{(3)} = 0 \,,$$

$$U_{41}^{(1)} \cdot \frac{s_{12}}{2} + U_{43}^{(1)} \cdot \frac{(s_{23} - m_t^2)}{2} + U_{44}^{(1)} \cdot \frac{(s_{24} - m_t^2)}{2} + \frac{s_{12}}{2} Y_{04}^{(3)} = 0 \,,$$

$$U^{(2)} + U^{(2)}_{21} \cdot \frac{s_{12}}{2} + U^{(2)}_{23} \cdot \frac{(s_{23} - m_t^2)}{2} + U^{(2)}_{24} \cdot \frac{(s_{24} - m_t^2)}{2} + Z^{(3)} = 0 \,,$$

$$U^{(2)}_{31} \cdot \frac{s_{12}}{2} + U^{(2)}_{33} \cdot \frac{(s_{23} - m_t^2)}{2} + U^{(2)}_{34} \cdot \frac{(s_{24} - m_t^2)}{2} = 0 \,,$$

$$U^{(2)}_{41} \cdot \frac{s_{12}}{2} + U^{(2)}_{43} \cdot \frac{(s_{23} - m_t^2)}{2} + U^{(2)}_{44} \cdot \frac{(s_{24} - m_t^2)}{2} = 0 \,,$$

$$U^{(3)} + U^{(3)}_{21} \cdot \frac{s_{12}}{2} + U^{(3)}_{23} \cdot \frac{(s_{23} - m_t^2)}{2} + U^{(3)}_{24} \cdot \frac{(s_{24} - m_t^2)}{2} + Y^{(1)}_{02} = 0 \,,$$

$$U^{(3)}_{31} \cdot \frac{s_{12}}{2} + U^{(3)}_{33} \cdot \frac{(s_{23} - m_t^2)}{2} + U^{(3)}_{34} \cdot \frac{(s_{24} - m_t^2)}{2} + Y^{(1)}_{03} = 0 \,,$$

$$U^{(3)}_{41} \cdot \frac{s_{12}}{2} + U^{(3)}_{43} \cdot \frac{(s_{23} - m_t^2)}{2} + U^{(3)}_{44} \cdot \frac{(s_{24} - m_t^2)}{2} + Y^{(1)}_{04} = 0 \,,$$

$$U^{(4)} + U^{(4)}_{21} \cdot \frac{s_{12}}{2} + U^{(4)}_{23} \cdot \frac{(s_{23} - m_t^2)}{2} + U^{(4)}_{24} \cdot \frac{(s_{24} - m_t^2)}{2} - \frac{1}{2} Y^{(3)}_{02} = 0 \,,$$

$$U^{(4)}_{31} \cdot \frac{s_{12}}{2} + U^{(4)}_{33} \cdot \frac{(s_{23} - m_t^2)}{2} + U^{(4)}_{34} \cdot \frac{(s_{24} - m_t^2)}{2} - \frac{1}{2} Y^{(3)}_{03} = 0 \,,$$

$$U^{(4)}_{41} \cdot \frac{s_{12}}{2} + U^{(4)}_{43} \cdot \frac{(s_{23} - m_t^2)}{2} + U^{(4)}_{44} \cdot \frac{(s_{24} - m_t^2)}{2} - \frac{1}{2} Y^{(3)}_{04} = 0 \,,$$

$$X^{(1)}_{01} \cdot \frac{s_{12}}{2} + X^{(1)}_{03} \cdot \frac{(s_{23} - m_t^2)}{2} + X^{(1)}_{04} \cdot \frac{(s_{24} - m_t^2)}{2} - s_{12} Z^{(3)} = 0 \,,$$

$$X^{(2)}_{01} \cdot \frac{s_{12}}{2} + X^{(2)}_{03} \cdot \frac{(s_{23} - m_t^2)}{2} + X^{(2)}_{04} \cdot \frac{(s_{24} - m_t^2)}{2} = 0 \,,$$

$$X^{(3)}_{01} \cdot \frac{s_{12}}{2} + X^{(3)}_{03} \cdot \frac{(s_{23} - m_t^2)}{2} + X^{(3)}_{04} \cdot \frac{(s_{24} - m_t^2)}{2} + 2 Z^{(1)} = 0 \,,$$

$$X^{(4)}_{01} \cdot \frac{s_{12}}{2} + X^{(4)}_{03} \cdot \frac{(s_{23} - m_t^2)}{2} + X^{(4)}_{04} \cdot \frac{(s_{24} - m_t^2)}{2} + Z^{(3)} = 0 \,. \quad (3.45)$$

We checked these conditions numerically for the Born level as well as for the virtual contribution. At Born level, the Ward identities have also been checked analytically within `Form` (see Section 3.1). Again, the Born expressions fulfil the relations within machine precision. In case of the virtual part, we only observe a validity of above relations within an accuracy of about two orders of magnitude. This is already true for non-exceptional phase space configurations, while it is even worse for exceptional ones. However, this accuracy should still be sufficient to achieve the desired overall precision for the cross section at NLO. The reason for the poor accuracy could lie in cancellations between terms within a recursion relation. Such cancellations lead to a loss of precision. The reasoning is the same as for the case of exceptional

momentum configurations. Within `Fortran`, the error is always relative to the respective term. If the addition of two terms leads to a result which is smaller than the individual terms, the relative accuracy of the result is obviously worse than the ones for the individual terms. The reduction of an integral usually involves the repeated application of recursion relations. A loss of accuracy can happen in each step of the reduction so that the precision is successively reduced. In the calculation of more complex processes, such cancellations could necessitate a more advanced implementation of the recursion relations which avoid these. They could also render the reduction method inapplicable. In Section 3.4, we varied the threshold for the detection of exceptional momentum configurations. Furthermore, we checked the integration by using in turn the different integration routines of the `CUBA` library. These investigations also support the conclusion that the desired accuracy is indeed achieved. Still, an independently obtained result is desirable in order to thoroughly check the result and its precision for such a calculation. We compare our cross section prediction with a result already specified in the literature in Section 4.3.

Further Checks

As has just been mentioned, we have checked that the different integration routines of the `CUBA` library lead to the same results within the specified precision for the phase space integration of the virtual correction. This is a good way to test the reliability of the Monte Carlo integration.

In addition to above checks, we compared the values for various master integrals with independent calculations performed by Gudrun Heinrich. These were partly done also with `LoopTools` and partly with different methods. Furthermore, we compared the results for the reduction of sample tensor integrals with those obtained by Gudrun Heinrich using a different reduction method [25]. These comparisons constitute a check on the reduction of the tensor integrals to generalised scalar integrals, their transformation into `Fortran` functions, the subsequent reduction to the basis integrals, and the evaluation of the latter.

Conclusion

In conclusion, we applied several strong checks which cover various parts of the calculation. Still, it is desirable to have an independently obtained result

for such a complex calculation. This way, one can also check thoroughly whether the desired accuracy for the result has been achieved. We observe that the Gauge invariance relations are only poorly fulfilled. The reason could be due to cancellations among different terms within a recursion relation. In case of more complex processes, this may call for an improved implementation or even prevent from applying the reduction method. However, this has to be investigated in more detail before a thorough conclusion can be drawn. For our results, we expect that the desired precision has been reached.

Chapter 4

Numerical Evaluation

In this Chapter, we finally specify our numerical results. The cross sections at LO and NLO are given in Section 4.1. We then discuss the scheme and scale dependence of these cross sections in Section 4.2. A comparison with the results given in the literature is drawn in Section 4.3.

4.1 Numerical Results

In this Section, we give the numerical results for the cross section at Born level and at NLO. The numerical values for the diverse parameters have been taken from Ref. [51]. Specifically, we express the vacuum expectation value v of the Higgs field through Fermi's constant $G_F = 1.16637 \times 10^{-5}$ GeV^{-2} according to the Born relation $1/v = 2^{1/4}G_F^{1/2}$. The electric charge e of the electron is expressed in terms of the fine-structure constant $\alpha = 7.297352568 \times 10^{-3}$ via the relation $\alpha = e^2/(4\pi)$. At NLO, we need the value for the strong coupling constant. We choose the mass of the Z boson, $M_Z = 91.1876$ GeV, for the scale of the running coupling. Its value reads $\alpha_s(M_Z) = 0.1176$. We also need the on-shell mass of the top quark, $m_t = 174.2$ GeV, which has been taken from Ref. [52].

The Higgs-boson mass is a free parameter of the theory. However, direct searches, high precision measurements, and theoretical considerations impose restrictions on its value. This has already been discussed in the introduction. We assume the Higgs-boson mass to be equal to $M_H = 130$ GeV. The CMS energy is varied up to the value of 1000 GeV, which is an option for the ILC [53].
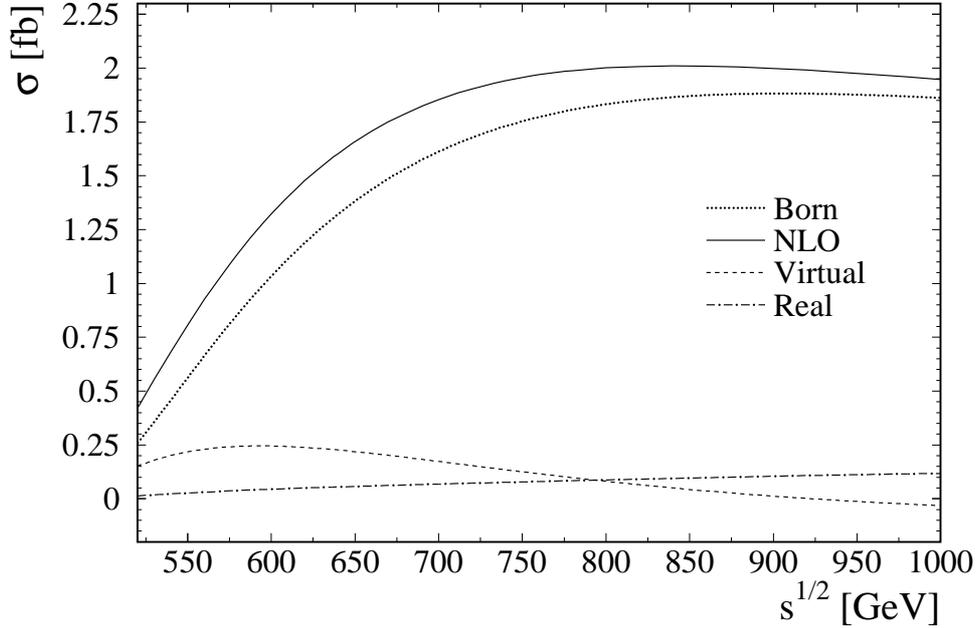
Figure 4.1: Cross section of the subprocess $\gamma\gamma \to t\bar{t}H$ in dependence of its CMS energy; the Higgs mass is 130 GeV.

In Fig. 4.1, we show the cross section of the subprocess in dependence of its CMS energy. The threshold for the subprocess is equal to 478.4 GeV. The CMS energy is varied from 520 GeV to 1000 GeV. We see that the Born level cross section, which is given by the dotted lines, increases rapidly to values above 1 fb. The maximum is reached at a CMS energy of 900 GeV, where its value amounts to 1.88 fb. It then falls off slowly.

Also the NLO prediction for the cross section of the subprocess is given in Fig. 4.1. It is shown as a solid curve. The NLO correction increases the Born result by about 64% at a CMS energy of 520 GeV. This large relative correction may be due to the gluonic Coulomb correction near threshold (see Section 3.4). For larger values of the CMS energy, the relative correction decreases. We find 28% at 600 GeV, 15% at 700 GeV, 9.2% at 800 GeV, 6.2% at 900 GeV, and 4.6% at 1000 GeV. For large CMS energies, we thus

find rather small relative corrections to the Born level result.

The NLO correction to the Born result consists of a virtual and a real part. However, these cannot be integrated separately over the respective phase spaces since both develop IR singularities, which only cancel in the sum of both contributions. We therefore considered subtracted cross sections (see Section 2.3). The individual contributions of these are also shown in Fig. 4.1. The virtual part is given by the dashed curve, while the dashed-dotted curve belongs to the real part. The virtual contribution is dominant at low values for the CMS energy. For larger values, the real part becomes important, while the virtual part gets small. Near 1000 GeV, the virtual contribution becomes negative. Still, for the whole energy range considered here, the total NLO correction is positive.

Fig. 4.2 contains the cross section of the parent process. This is obtained by integrating the cross section of the subprocess over the spectra of the incoming photons. For the latter, we choose the `CompAZ` spectrum (see Section 2.4). The threshold is higher in this case since the back-scattered photons cannot be as energetic as the incoming electrons or positrons. The CMS energy is varied from 700 GeV to 1000 GeV. The Born and the NLO prediction as well as the individual contributions from the virtual and the real part are shown as in Fig. 4.1. Since the NLO correction always increases the Born result for the subprocess, also the cross section of the parent process is larger for the NLO prediction for the whole considered energy range. The relative correction amounts to about 40% at 700 GeV, 24% at 800 GeV, 16% at 900 GeV, and 12% at 1000 GeV. For large values of the CMS energy, the relative correction is thus moderate. The increase of the relative correction towards energies near threshold can obviously be explained by the fact that the relative correction for the subprocess is larger at smaller energies.

At low CMS energies, the virtual part gives the dominant contribution to the NLO correction, while the real contribution is small. With higher energies, the importance of the real part grows. At 1000 GeV, the two contributions are of comparable size. The virtual and the real part are both positive throughout the considered energy range.

4.2 Scheme and Scale Dependence

In Section 3.3, we have discussed the possibility to transform the on-shell results of Section 4.1 into results which are valid in a mixed scheme. In the
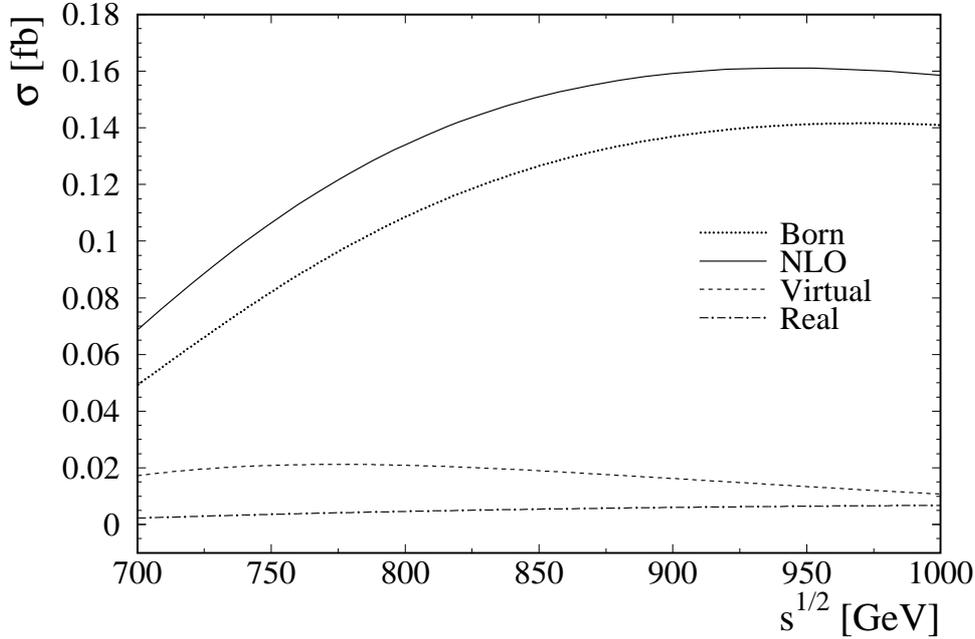
Figure 4.2: Cross section of the parent process $e^+e^- \to \gamma\gamma \to t\bar{t}H$ in dependence of its CMS energy; the Higgs mass is 130 GeV.

latter, the top-quark mass occurring in the Yukawa coupling is renormalised in the $\overline{\text{MS}}$ scheme, while those of the propagators are kept on-shell. We vary the renormalisation scale from 0.5 till 2 times the on-shell top-quark mass, for a CMS energy of 800 GeV. This is done only for the cross section of the subprocess. The result is shown in Fig. 4.3. Again, the Born cross section is given by a dotted curve and the NLO prediction by a solid one.

From the Figure, it is obvious that the scale dependence is strongly reduced. At Born level, the variation of the prediction relative to the central value amounts to 19.0%. This scale dependence is reduced by more than one order of magnitude to 1.6% for the NLO prediction.

The scale dependence can be used as a means to assess the residual error due to truncation of the perturbation series. We observe a reduction of the scale dependence of more than one order of magnitude in going from the Born
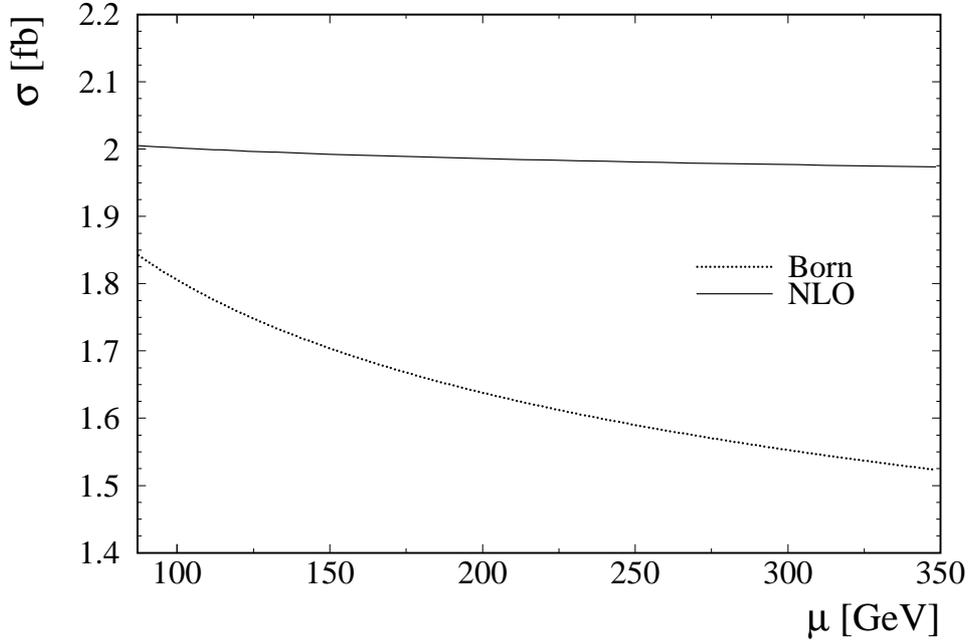
Figure 4.3: Cross section of the subprocess $\gamma\gamma \to t\bar{t}H$ in dependence of the renormalisation scale, which is varied from $0.5\,m_t$ to $2\,m_t$; the CMS energy of the subprocess is 800 GeV; the Higgs mass is 130 GeV.

level to NLO. This supports the conclusion that the uncertainty is reduced to the percent level for CMS energies away from threshold. By the same token, also the residual error for the case of the parent process should be of the order of a few percent if we stay away from the threshold. However, one should keep in mind that only the top-quark mass occurring in the Yukawa coupling is affected by the scale variation within the mixed scheme.

In Fig. 4.4, we also show the scale variation of the cross section for the subprocess. However, we choose the parameters as in Ref. [13] and a Higgs-boson mass of 150 GeV. These values are also adopted in Section 4.3 for a comparison with the results stated in the literature. For this set of parameters, we observe a scale reduction from 18.9% to 3.7%, which is slightly less than an order of magnitude.
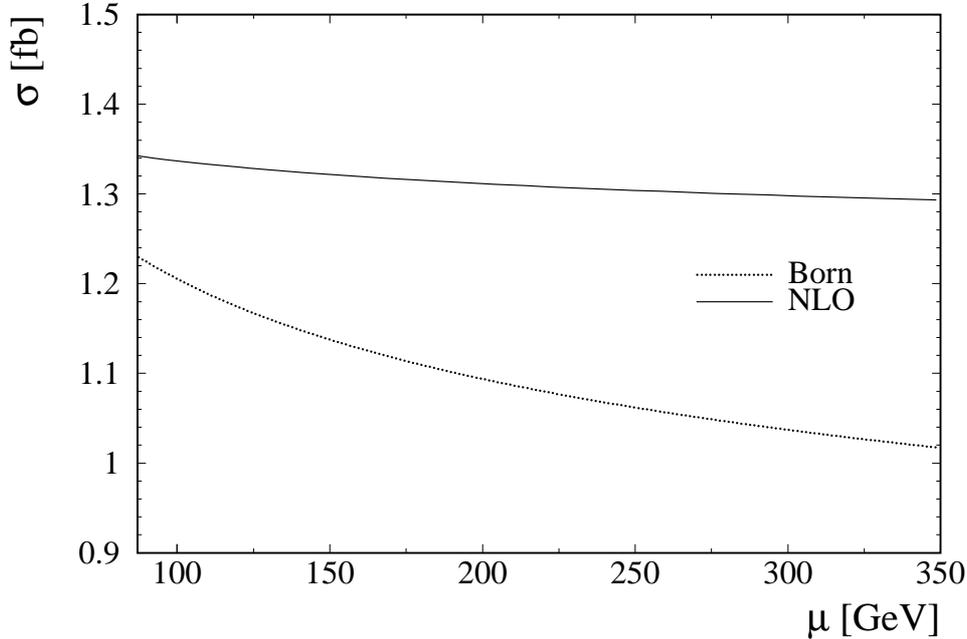
Figure 4.4: Cross section of the subprocess $\gamma\gamma \to t\bar{t}H$ in dependence of the renormalisation scale, which is varied from $0.5\,m_t$ to $2\,m_t$; the CMS energy of the subprocess is 800 GeV; the Higgs mass is 150 GeV; the numerical values for the remaining parameters are chosen as in [13].

We also have mentioned in Section 3.3, that the strong coupling only is introduced at NLO. Its value is thus not fixed. In order to get an idea about the uncertainty induced by the running of the strong coupling, we now vary the scale for the running coupling. This can be done by means of the `Mathematica` package `RunDec` [54]. If we evolve the coupling at the one-loop order with six active flavours, we get $\alpha_s(m_t/2) = 0.1174$ and $\alpha_s(2m_t) = 0.0993$. The relative variation with respect to the central value thus amounts to 16.6%. In Section 4.1, we saw that the NLO correction to the Born level amounts to about 10% away from threshold. The NLO correction is proportional to the running coupling. We may thus also assess the uncertainty due to the scale dependence of α_s to be at the percent level.

However, in the numerical evaluations in Section 4.1, the running coupling has been taken at the scale M_Z.

Let us now compare the Born and the NLO results for the two schemes. In case of the mixed scheme, we take the results for the scale of the running top-quark mass being the on-shell mass of the top quark. Again, we only consider the subprocess and a CMS energy of 800 GeV. The scheme dependence drops down from 9.6% to 0.62% if we go from the Born level to NLO. This is again more than one order of magnitude, which gives further support to our error estimate.

As we have just said, the NLO correction is about 10% away from threshold. This may also suggest a residual error of the order of a few percent. All error estimations thus point to a residual uncertainty of several percent.

4.3 Comparison with Literature

In this Section, we compare our results to those specified in the literature. Let us begin with the cross section at Born level. In Ref. [13], the following values for the numerical parameters are chosen: $\alpha = 1/137.03599976$, $M_W = 80.423$ GeV, $M_Z = 91.1876$ GeV. The electric charge is expressed as in Section 4.1 through α. The vacuum expectation value of the Higgs boson is replaced via the Born relation $1/v = e/(2s_W M_W)$. This relation contains the sine of the weak mixing angle s_W, which is calculated as $s_W = \sqrt{1 - c_W^2}$. c_W is the cosine of the weak mixing angle and obtained as $c_W = M_W/M_Z$.

The Born results have already been calculated in Refs. [9]. In Ref. [13], different results were found. We agree with the results specified in the latter publication. In particular, we could reproduce Table 3 of Ref. [13]. The Table contains results for the cross section of the parent process at Born level. They are specified for diverse values of the top-quark mass, the Higgs-boson mass, and the CMS energy. Also the results of Refs. [9] are shown in this Table for comparison. Our results are collected in Table 4.1. We chose a relative accuracy of 0.1%. The numbers in parentheses give the first digit of the respective result which lies beyond this accuracy. The numbers agree with those of Ref. [13] within the specified accuracy. However, variation of the input parameters does not seem to resolve above mentioned discrepancy.

In Fig. 4.5, we show the cross section for the subprocess in dependence of its CMS energy. Again, the Born and the NLO prediction as well as the

m_t [GeV]	M_H [GeV]	$\sqrt{s}$ [GeV]	σ [fb]
120	60	500	0.390(8)
		1000	2.18(6)
		2000	2.39(1)
150	60	1000	2.74(0)
		2000	3.42(1)
	140	1000	0.311(7)
		2000	0.805(8)
180	140	1000	0.341(2)
		2000	1.05(5)

Table 4.1: Cross section of the parent process $e^+e^- \rightarrow \gamma\gamma \rightarrow t\bar{t}H$ at Born level for diverse values of the top-quark mass, the Higgs-boson mass, and the CMS energy.

individual contributions from the virtual and the real part are plotted as in Fig. 4.1. We also choose the same range for the CMS energy. For the input parameters, we use the numerical values as given above and, in addition, a top-quark mass of 174.3 GeV and a Higgs-boson mass of 150 GeV. For the cross section at NLO, we furthermore need the running coupling α_s. In Ref. [13], the strong coupling is evaluated at the two-loop level with five active flavours and $\alpha_s(M_Z) = 0.117186$. The renormalisation scale is taken to be $(2m_t + M_H)/2$. Using `RunDec`, we find the value $\alpha_s(m_t + M_H/2) = 0.101891$. The resulting cross section at Born level and at NLO can be compared to Fig. 4.6, which has been taken from Ref. [13].

Fig. 4.6 contains the Born and the NLO prediction for the subprocess, which have been obtained in Ref. [13]. They are shown for three different values of the Higgs-boson mass. The dashed curves show the results for $M_H = 150$ GeV. As we can see, the NLO results of Fig. 4.5 and Fig. 4.6 do not agree. The NLO correction specified in Ref. [13] is positive for small CMS energies and becomes negative for larger ones. The change in sign occurs for CMS energies below 1000 GeV. We thus have a qualitatively different result from that obtained in this work. In Fig. 4.5, the NLO correction is always positive within the considered CMS energy range, which extends to the value 1000 GeV.

For completeness, we also show the results for the parent process in Figs. 4.7 and 4.8. The assignments are the same as in Fig. 4.1 and in
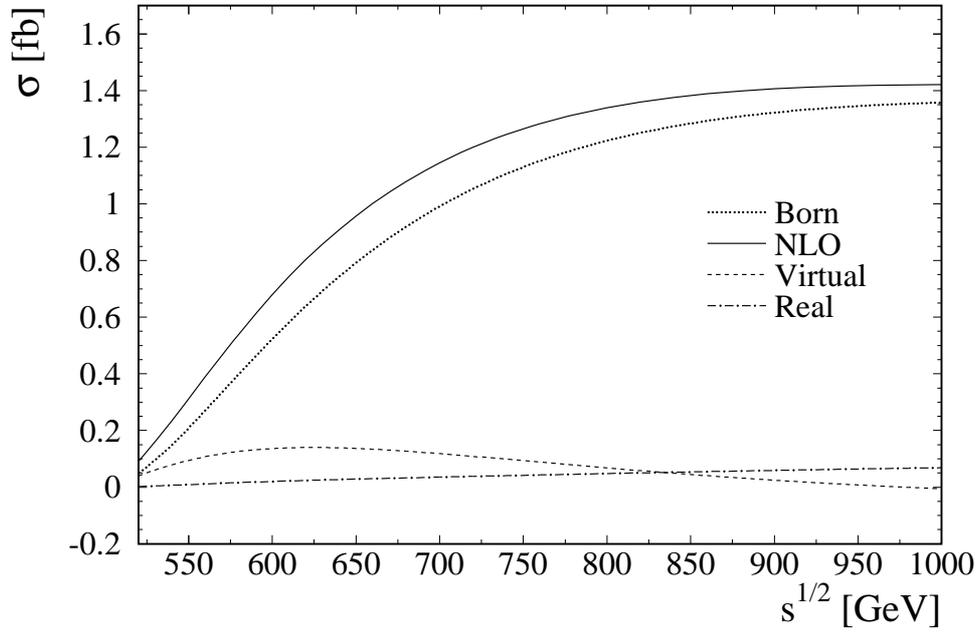
Figure 4.5: Cross section of the subprocess $\gamma\gamma \rightarrow t\bar{t}H$ in dependence of its CMS energy; the Higgs mass is 150 GeV; the numerical values for the remaining parameters are chosen as in [13].

Fig. 4.6, respectively. In Ref. [13], the photon spectrum refers to direct Compton scattering (see Section 2.4). We thus used this spectrum instead of the `CompAZ` spectrum for the calculation of the cross section predictions specified in Fig. 4.7. The deviation of the two results for the NLO prediction is again obvious.
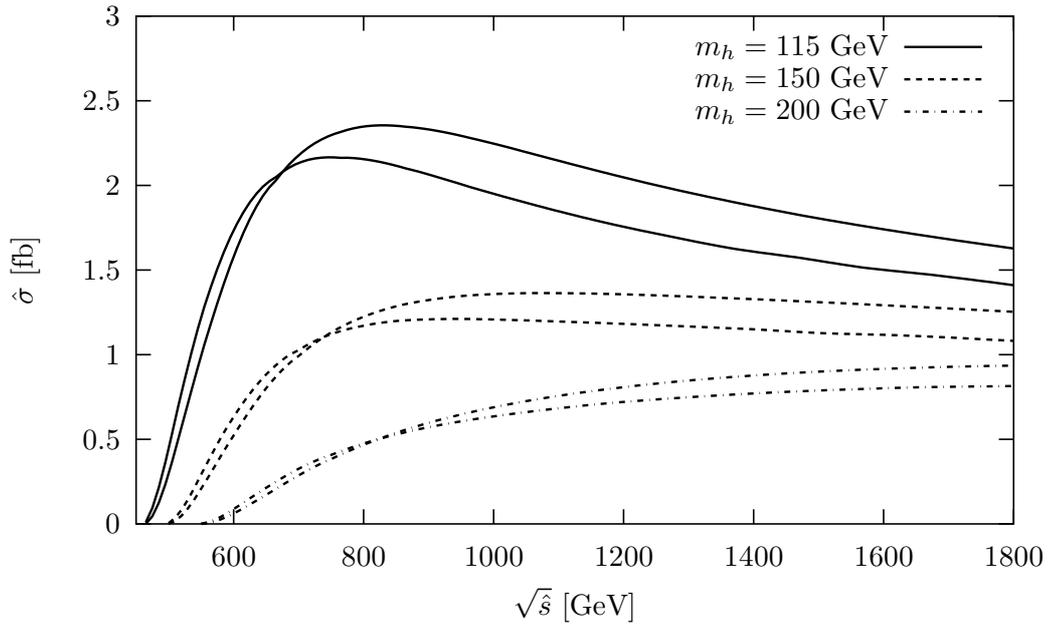
Figure 4.6: Cross section of the subprocess $\gamma\gamma \rightarrow t\bar{t}H$ in dependence of its CMS energy as obtained in Ref.[13]; the dashed curves correspond to a Higgs mass of 150 GeV; the upper curve for CMS energies above 1000 GeV belongs to the Born level while the lower shows the NLO result. The Figure has been taken from Ref.[13].
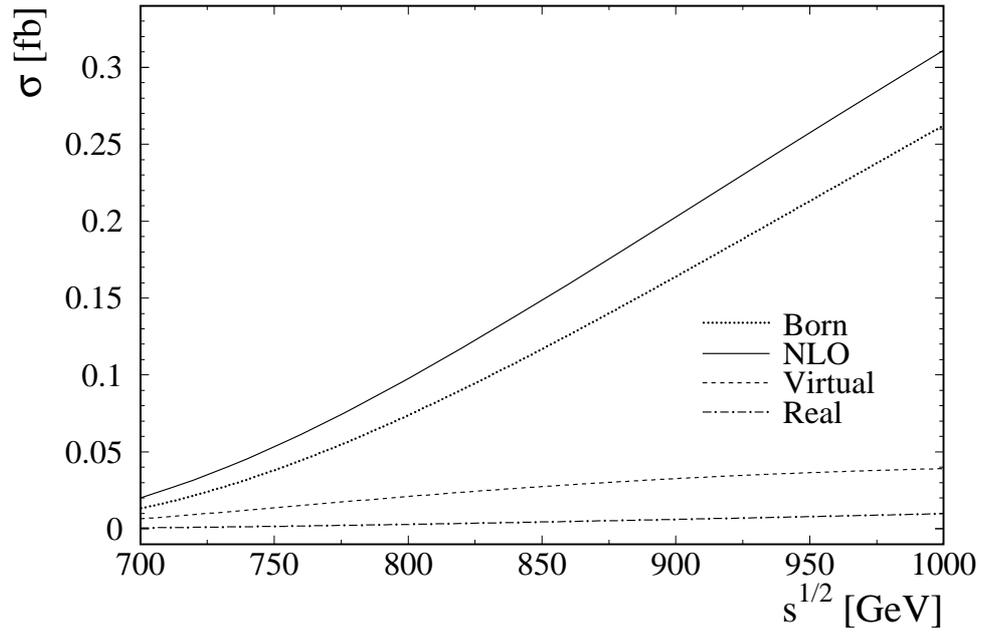
Figure 4.7: Cross section of the parent process $e^+e^- \to \gamma\gamma \to t\bar{t}H$ in dependence of its CMS energy; the Higgs mass is 150 GeV; the numerical values for the remaining parameters as well as the photon spectrum are chosen as in [13].
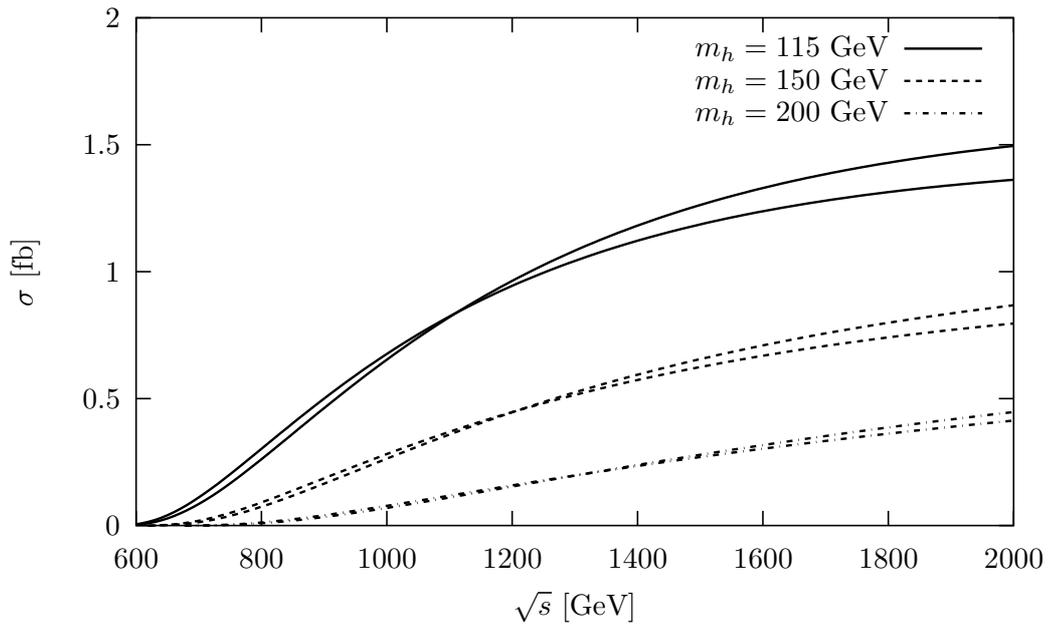
Figure 4.8: Cross section of the parent process $e^+e^- \to \gamma\gamma \to t\bar{t}H$ in dependence of its CMS energy as obtained in Ref.[13]; the dashed curves correspond to a Higgs mass of 150 GeV; the upper curve for CMS energies above 1400 GeV belongs to the Born level while the lower shows the NLO result. The Figure has been taken from Ref.[13].

Chapter 5

Summary

The LHC has a high probability of finding Higgs bosons since it will be capable of producing particles with masses up to 1 TeV. In a next step, the quantum numbers and couplings of the particles, which may have been found, have to be measured. However, precision measurements are left to a linear collider like the ILC. In this work, the process $\gamma\gamma \to t\bar{t}H$ is considered, which can be studied at a linear e^+e^--collider operated in the two-photon mode. The associated production of Higgs bosons and heavy quarks allows for a direct measurement of the respective Yukawa coupling.

We computed the NLO QCD correction to $\gamma\gamma \to t\bar{t}H$. Its inclusion reduces the scheme and scale dependences by about one order of magnitude. In order to assess the scheme dependence, we converted the on-shell results into those valid in a mixed scheme. Within the latter, the top-quark mass occurring in the Yukawa coupling is renormalised in the $\overline{\text{MS}}$ scheme while the propagator mass is kept on-shell. The scale dependence was assessed by varying the renormalisation scale, within the mixed scheme, from $0.5\,m_t$ to $2\,m_t$, where the top-quark mass is a typical hard scale of the process. The NLO QCD correction for the subprocess $\gamma\gamma \to t\bar{t}H$ is of the order of 10%. Only near threshold, it reaches several tenths of percent.

However, not the subprocess is measured at a linear collider but the parent process $e^+e^- \to \gamma\gamma \to t\bar{t}H$. In order to get a prediction for the parent process, the subprocess has to be integrated over the spectra of the incoming photons. We used the spectrum given in Ref. [6]. The NLO QCD correction for the parent process varies between roughly 10% at high CMS energies and several tenths of percent for low ones. This can obviously be explained through the increase of the relative correction for the subprocess towards

energies near threshold.

Results for $\gamma\gamma \to t\bar{t}H$ and $e^+e^- \to \gamma\gamma \to t\bar{t}H$ already exist in the literature [13]. Our results deviate from those which necessitates a further independent calculation. Such a calculation is also desirable in order to check the achieved precision for the cross section prediction.

In order to reduce the tensor integrals, we applied the method recently developed in Refs. [20]. The method seems to work reasonably well for non-exceptional phase space configurations for the process under consideration. For the calculation of more complex processes, an advanced implementation of the recursion relations could be necessary. Or the reduction method could even be inapplicable. However, it did not give reliable results for those points in phase space where the determinant of the kinematical matrix becomes small. In our actual calculation, such exceptional cases did not occur very often. It was therefore possible to set the integrand equal to zero for such cases, without affecting the desired numerical accuracy of our final results. Actually, we could also set the integrand to zero for exceptional configurations where only the Gram determinant becomes small. However, we chose to include the exceptional recursion relations pertaining to this case in our numerical analysis.

A subtraction method [32] was used for the treatment of the IR singularities. This led to effective cross sections for the virtual and the real part, respectively. In case of the virtual cross section, the cancellation of the IR singularities was shown in a semi-analytic way. The divergent part of the subtraction term was added to the IR-divergent part of the virtual correction and to the one stemming from the renormalisation of the wave functions of the external quarks. For the IR-divergent part of the virtual correction, we used the compact expression which was obtained by directly reading off the singularity structure from the original tensor integrals. This way, it was possible to show analytically that the IR poles cancel in the sum. Then it was checked numerically that the compact expression for the singularities indeed agrees with the one obtained through the reduction procedure applied to the tensor integrals. The phase space integration of the effective cross section for the real part converged fast towards a finite value.

The UV singularities could be demonstrated to cancel upon the common renormalisation procedure. Here, the mass of the top quark as well as the wave functions of the external quarks had to be renormalised.

Apart from the cancellation of the divergences, several additional checks have been performed. In particular, we implemented the tensor reduction

procedure, for non-exceptional phase space configurations, in two independent ways and checked the Bose symmetry as well as the Gauge invariance property of the virtual amplitude.

In future extensions of this work, the missing NLO corrections for the associated production of MSSM-Higgs bosons and heavy quarks could be considered. One could also investigate the case of polarised incoming photons. Finally, a detailed study of the possibility to measure the top-quark Yukawa coupling, including the relevant backgrounds, could be performed.

Bibliography

[1] R. Barate *et al.* [LEP Working Group for Higgs boson searches], Phys. Lett. B **565** (2003) 61 [arXiv:hep-ex/0306033].

[2] J. Alcaraz *et al.* [ALEPH Collaboration], arXiv:hep-ex/0612034; see also URL: `http://lepewwg.web.cern.ch/LEPEWWG/`.

[3] B. A. Kniehl, Int. J. Mod. Phys. A **17** (2002) 1457 [arXiv:hep-ph/0112023].

[4] A. Djouadi, arXiv:hep-ph/0503172.

[5] J. Brau *et al.*, "International Linear Collider reference design report. 1: Executive summary. 2: Physics at the ILC. 3: Accelerator. 4: Detectors."

[6] A. F. Zarnecki, Acta Phys. Polon. B **34** (2003) 2741 [arXiv:hep-ex/0207021].

[7] G. Weiglein *et al.* [LHC/LC Study Group], Phys. Rept. **426** (2006) 47 [arXiv:hep-ph/0410364].

[8] H. Baer, S. Dawson and L. Reina, Phys. Rev. D **61** (2000) 013002 [arXiv:hep-ph/9906419]; A. Juste and G. Merino, arXiv:hep-ph/9910301; A. Gay, Eur. Phys. J. C **49** (2007) 489 [arXiv:hep-ph/0604034].

[9] E. Boos, I. Ginzburg, K. Melnikov, T. Sack and S. Shichanin, Z. Phys. C **56** (1992) 487; K. m. Cheung, Phys. Rev. D **47** (1993) 3750 [arXiv:hep-ph/9211262].

[10] J. Y. Guo, Y. Liao and Y. P. Kuang, Phys. Rev. D **62** (2000) 035007.

[11] H. J. He, S. Kanemura and C. P. Yuan, Phys. Rev. Lett. **89** (2002) 101803 [arXiv:hep-ph/0203090]; S. Moretti and S. Kanemura, Eur. Phys. J. C **29** (2003) 19 [arXiv:hep-ph/0211055].

[12] K. J. F. Gaemers and G. J. Gounaris, Phys. Lett. B **77** (1978) 379; A. Djouadi, J. Kalinowski and P. M. Zerwas, Mod. Phys. Lett. A **7** (1992) 1765, Z. Phys. C **54** (1992) 255.

[13] H. Chen, W. G. Ma, R. Y. Zhang, P. J. Zhou, H. S. Hou and Y. B. Sun, Nucl. Phys. B **683** (2004) 196 [arXiv:hep-ph/0309106].

[14] S. Dittmaier, M. Kramer, Y. Liao, M. Spira and P. M. Zerwas, Phys. Lett. B **441** (1998) 383 [arXiv:hep-ph/9808433]; S. Dawson and L. Reina, Phys. Rev. D **57** (1998) 5851 [arXiv:hep-ph/9712400]; S. Dawson and L. Reina, Phys. Rev. D **59** (1999) 054012 [arXiv:hep-ph/9808443].

[15] S. Dawson and L. Reina, Phys. Rev. D **60** (1999) 015003 [arXiv:hep-ph/9812488]; S. Dittmaier, M. Kramer, Y. Liao, M. Spira and P. M. Zerwas, Phys. Lett. B **478** (2000) 247 [arXiv:hep-ph/0002035].

[16] S. h. Zhu, arXiv:hep-ph/0212273; P. Hafliger and M. Spira, Nucl. Phys. B **719** (2005) 35 [arXiv:hep-ph/0501164].

[17] B. A. Kniehl, F. Madricardo and M. Steinhauser, Phys. Rev. D **66** (2002) 054016 [arXiv:hep-ph/0205312].

[18] G. Belanger *et al.*, Phys. Lett. B **571** (2003) 163 [arXiv:hep-ph/0307029]; A. Denner, S. Dittmaier, M. Roth and M. M. Weber, Phys. Lett. B **575** (2003) 290 [arXiv:hep-ph/0307193]; Y. You, W. G. Ma, H. Chen, R. Y. Zhang, S. Yan-Bin and H. S. Hou, Phys. Lett. B **571** (2003) 85 [arXiv:hep-ph/0306036].

[19] A. Djouadi, arXiv:hep-ph/0503173.

[20] W. T. Giele and E. W. N. Glover, JHEP **0404** (2004) 029 [arXiv:hep-ph/0402152]; W. Giele, E. W. N. Glover and G. Zanderighi, Nucl. Phys. Proc. Suppl. **135** (2004) 275 [arXiv:hep-ph/0407016]; R. K. Ellis, W. T. Giele and G. Zanderighi, Phys. Rev. D **73** (2006) 014027 [arXiv:hep-ph/0508308].

[21] S. Dittmaier, Nucl. Phys. B **675** (2003) 447 [arXiv:hep-ph/0308246].

[22] A. Denner and S. Dittmaier, Nucl. Phys. B **734** (2006) 62 [arXiv:hep-ph/0509141].

[23] A. I. Davydychev, Phys. Lett. B **263** (1991) 107.

[24] K. G. Chetyrkin, A. L. Kataev and F. V. Tkachov, Nucl. Phys. B **174** (1980) 345; K. G. Chetyrkin and F. V. Tkachov, Nucl. Phys. B **192** (1981) 159.

[25] T. Binoth, J. P. Guillet, G. Heinrich, E. Pilon and C. Schubert, JHEP **0510** (2005) 015 [arXiv:hep-ph/0504267].

[26] R. K. Ellis, W. T. Giele and G. Zanderighi, Phys. Rev. D **72** (2005) 054018 [Erratum-ibid. D **74** (2006) 079902] [arXiv:hep-ph/0506196]; R. K. Ellis, W. T. Giele and G. Zanderighi, JHEP **0605** (2006) 027 [arXiv:hep-ph/0602185].

[27] S. Dittmaier, P. Uwer and S. Weinzierl, Phys. Rev. Lett. **98** (2007) 262002 [arXiv:hep-ph/0703120].

[28] B. W. Harris and J. F. Owens, Phys. Rev. D **65** (2002) 094032 [arXiv:hep-ph/0102128].

[29] S. Catani and M. H. Seymour, Nucl. Phys. B **485** (1997) 291 [Erratum-ibid. B **510** (1998) 503] [arXiv:hep-ph/9605323].

[30] S. Dittmaier, Nucl. Phys. B **565** (2000) 69 [arXiv:hep-ph/9904440].

[31] L. Phaf and S. Weinzierl, JHEP **0104** (2001) 006 [arXiv:hep-ph/0102207].

[32] S. Catani, S. Dittmaier, M. H. Seymour and Z. Trocsanyi, Nucl. Phys. B **627** (2002) 189 [arXiv:hep-ph/0201036].

[33] A. Daleo, T. Gehrmann and D. Maitre, JHEP **0704** (2007) 016 [arXiv:hep-ph/ 0612257].

[34] B. Badelek *et al.* [ECFA/DESY Photon Collider Working Group], Int. J. Mod. Phys. A **19** (2004) 5097 [arXiv:hep-ex/0108012].

[35] T. Hahn, Comput. Phys. Commun. **140** (2001) 418 [arXiv:hep-ph/0012260].

[36] T. Hahn and M. Perez-Victoria, Comput. Phys. Commun. **118** (1999) 153 [arXiv:hep-ph/9807565].

[37] J. A. M. Vermaseren, Symbolic Manipulation with FORM, Computer Algebra Netherlands, Amsterdam, 1991; J. A. M. Vermaseren, arXiv:math-ph/0010025.

[38] T. Hahn and M. Rauch, Nucl. Phys. Proc. Suppl. **157** (2006) 236 [arXiv:hep-ph/0601248].

[39] T. Hahn, Comput. Phys. Commun. **168** (2005) 78 [arXiv:hep-ph/0404043].

[40] G. J. van Oldenborgh, Comput. Phys. Commun. **66** (1991) 1.

[41] W. Beenakker and A. Denner, Nucl. Phys. B **338** (1990) 349.

[42] G. Rodrigo, A. Santamaria and M. S. Bilenky, J. Phys. G **25** (1999) 1593 [arXiv:hep-ph/9703360].

[43] C. Anastasiou and A. Lazopoulos, JHEP **0407** (2004) 046 [arXiv:hep-ph/0404258].

[44] A. Denner, Fortsch. Phys. **41** (1993) 307 [arXiv:0709.1075 [hep-ph]].

[45] B. A. Kniehl and A. Sirlin, Phys. Rev. Lett. **81** (1998) 1373 [arXiv:hep-ph/9805390]; B. A. Kniehl and A. Sirlin, Phys. Lett. B **440** (1998) 136 [arXiv:hep-ph/9807545]; B. A. Kniehl, C. P. Palisoc and A. Sirlin, Nucl. Phys. B **591** (2000) 296 [arXiv:hep-ph/0007002]; B. A. Kniehl and A. Sirlin, Phys. Lett. B **530** (2002) 129 [arXiv:hep-ph/0110296].

[46] B. A. Kniehl, Z. Phys. C **72** (1996) 437 [arXiv:hep-ph/9403386].

[47] F. Bloch and A. Nordsieck, Phys. Rev. **52** (1937) 54.

[48] Numerical Recipes: The Art of Scientific Computing, University of Cambridge (`http://www.nr.com`).

[49] G. Lei, M. Wen-Gan, H. Liang, Z. Ren-You and J. Yi, arXiv:0708.2951 [hep-ph].

[50] C. Farrell and A. H. Hoang, Phys. Rev. D **72** (2005) 014007 [arXiv:hep-ph/0504220]; C. Farrell and A. H. Hoang, Phys. Rev. D **74** (2006) 014008 [arXiv:hep-ph/0604166].

[51] W. M. Yao *et al.* [Particle Data Group], J. Phys. G **33** (2006) 1.

[52] [CDF Collaboration], arXiv:hep-ex/0604053.

[53] A. Djouadi, J. Lykken, K. Monig, Y. Okada, M. J. Oreglia and S. Yamashita, arXiv:0709.1893 [hep-ph].

[54] K. G. Chetyrkin, J. H. Kuhn and M. Steinhauser, Comput. Phys. Commun. **133** (2000) 43 [arXiv:hep-ph/0004189].

Acknowledgements

I would like to thank my supervisor Prof. Dr. Bernd A. Kniehl for the interesting topic. Furthermore, I am very grateful to Dr. Gudrun Heinrich for her advice and many fruitful discussions. Moreover, I am thankful to all the people of the II. Institute and the DESY theory group for the nice atmosphere and, of course, helpful discussions about physics. I refrain from a listing because of the obvious problems which come along with it. Finally, I would like to thank my parents for their support throughout the study time and the PhD work.